The little engine that could:
Characterization of noncanonical components in the speed-variable flagellar motor of the symbiotic soil bacterium *Sinorhizobium meliloti*

Richard Charles Sobe

Dissertation submitted to the faculty of the Virginia Polytechnic Institute and State University
in partial fulfillment of the requirements for the degree of
Doctor of Philosophy
in
Biological Sciences

Birgit Scharf, Chair
Clayton C. Caswell
Florian D. Schubot
Zhaomin Yang

May 9, 2022
Blacksburg, Virginia

Keywords: chemotaxis, flagellar basal body, proton channel plug, swimming motility, torque generation

The little engine that could:
Characterization of noncanonical components in the speed-variable flagellar motor of the symbiotic soil bacterium *Sinorhizobium meliloti*

Richard Charles Sobe

ABSTRACT

The bacterial flagellum is a fascinating corkscrew-shaped macromolecular rotary machine used primarily to propel bacterial cells through their environment via the conversion of chemical potential energy into rotational power and thrust. Flagella are the principal targets of complex chemotaxis systems, which allow microbes to navigate their habitats to locate favorable conditions and avoid harmful ones by continuous sampling of environmental compounds and cues. Flagella serve as surface and temperature sensors, mediators of host cell adherence by bacterial pathogens and symbionts alike, and important virulence factors for disease-causing microbes. They play several essential roles in accelerating the foundational stages of biofilm formation, during which bacteria build highly intricate microbial communities with increased resistance to predation and environmental assaults. Flagellum-mediated chemotaxis has broad and impactful implications in fields of bioremediation, targeted drug delivery, bacterial-mediated cancer therapy and diagnostics, and cross-kingdom horizontal gene transfer.

While the core structural and functional components of flagella have been well characterized in the closely related enteric bacteria, *Escherichia coli* and *Salmonella typhimurium*, major departures from this paradigm have been identified in other diverse species that merit further investigation. Many bacteria employ additional reinforcement modules to surround and stabilize their more powerful flagellar motors and provide increased contact points in the inner membrane, the peptidoglycan sacculus, and, in Gram-negative bacteria, the outer membrane. Additionally, the soil-dwelling bacterium *Sinorhizobium meliloti* exhibits marked distinctions in the regulation, structure, and function of its navigation systems. *S. meliloti* is a nitrogen-fixing symbiont of the agronomically valuable leguminous plant, *Medicago sativa* Lucerne, and uses its coupled chemotaxis and flagellar motility systems to search for host plant roots to colonize. Following

root colonization, the bacterium converts to a nitrogen-fixing factory for the plant and the combined influences of this symbiosis can quadruple the yields of the host.

This dissertation is aimed at delivering a thorough representative overview of the processes facilitating bacterial flagellum-mediated chemotaxis and motility. Chapter 1 describes the interplay between chemotaxis and flagellar motility pathways as well as the structure, function, and regulation of these systems in several model bacteria. Particular emphasis is placed on the comparison of flagellar systems from the soil-dwelling legume symbiont, *Sinorhizobium meliloti* with other model systems, and a brief introduction is provided for its primary counterpart, the agronomically valuable legume, *Medicago sativa*, more commonly referred to as alfalfa.

Chapter 2 embodies the first report of a flagellar system to require two copies of a protein known as FliL for its function. FliL is found in all bacterial flagellar systems reported to date but is only essential for some to drive motility. The more conserved copy of the protein has retained the title of FliL and several experiments to assay the proficiency of flagellar motor function revealed that in the absence of FliL swimming is essentially abolished as is the presence of flagella on the cell body. Flagellar motor activity and swimming proficiency of mutants lacking the FliL-paralog MotF was nearly as abysmal as those without FliL but flagellation was essentially normal indicating distinct roles for the two proteins. FliL is implicated in initial stator recruitment to the motor while MotF was found to serve as a power or speed modulator. A model to accommodate and explain the roles of these proteins in the flagellar motor of *S. meliloti* is provided.

Chapter 3 links a never-before characterized flagellar protein, currently named Orf23, to a role in promoting maximum swimming velocity and perhaps stator alignment with the rotor in a peptidoglycan-dependent manner. The loss of LdtR, a transcriptional regulator of peptidoglycan-modification genes, caused defects in swimming motility that are restored only by removal of Orf23 or by replacing a nonpolar glycine with a polar serine in the periphery of stator units. Bioinformatics analyses, immunoblotting, and membrane topology reporter assays revealed that Orf23 is likely embedded in the inner membrane and that the remainder of the protein extends into the periplasm. Building on findings from Chapter 2, Orf23 is anticipated to influence stator positioning through interactions with MotF, FliL, and/or stator units directly. The chapter is

concluded with the description of future experiments aimed to more thoroughly characterize Orf23.

Altogether, this work increases the depth and breadth of knowledge regarding the composition and function of the speed-variable bacterial flagellar motor. We have identified several components required for stator incorporation and function, as well as an accessory component that improves stator performance. A wise society will draw inspiration from these fascinating and powerful machines to inform new technologies to achieve modern goals including targeted drug delivery, bioremediation, and perhaps one day our own exploration.

The little engine that could:
Characterization of noncanonical components in the speed-variable flagellar motor of the symbiotic soil bacterium *Sinorhizobium meliloti*

Richard Charles Sobe

GENERAL AUDIENCE ABSTRACT

Bacteria are small autonomous single-celled organisms capable of existing and thriving in highly diverse environments. Motility is achieved by these organisms in various ways, but the most common approach is to produce one or more corkscrew-shaped propeller systems known as flagella that are constructed upon and anchored within the wall of the bacterial cell. Rotation of these propellers relies on power converters known as stators to transform the flow of ions down self-produced gradients into useful rotational energy. This process can be likened to the way that the stored energy of water behind a dam can be harnessed and used to power hydroelectric generators. While the core components of flagellar motors are well conserved and understood among distantly related bacteria, billions of years of evolution and refinement of additional structures have allowed bacteria to accommodate swimming in diverse habitats with *e.g.* low nutrient availability or high viscosity.

Here we describe the discovery and characterization of additional components in the flagellar motor system of the soil-dwelling bacterium *Sinorhizobium meliloti* to navigate soil environments. We report the first identification of a flagellar motor that requires two copies of a pervasive flagellar motor protein known as FliL and have named the more distinct version of the protein MotF. We found that FliL is required for the power converter components to install into the motor and that MotF is necessary to activate them. Next, we identify another motor component, Orf23, that is dispensible for motility but appears to be required to achieve maximum swimming velocity and may serve to shift the motor into a "higher gear". We find that disruption of a regulator of cell wall modification systems leads to defects in motility that are only restored when Orf23 is removed or when the power converter is modified. Ideas are

proposed for how FliL, MotF, and Orf23 are integrated into the motor and may contribute to stator function.

An advanced understanding of the mechanisms governing flagellar motor structure and function will provide avenues for the improvement of bacteria-based agricultural improvements, development of optimized bacteria-mediated drug delivery systems, bioremediation techniques, and more.

DEDICATION

I dedicate this work to my son, Yusef Matthew Sobe. You can achieve anything you desire if you put your mind to it. Challenges may seem insurmountable at times but willpower, resolution and determination will help you to achieve your dreams. Remember to always be grateful for what you have and be willing to work hard for what you need, and even moreso for what you want. I love you dearly.

ACKNOWLEDGEMENTS

The journey through my Ph.D. was certainly not an easy one and I am very grateful to a massive support group that consists of friends, family, and colleagues whose relationships with me tend to overlap more than one of those categories. The cost of this degree included missing out on numerous life events for many of the following people (listed with some degree of order but certainly not dictated by "importance" as such delineations would not be possible) and yet I am fortunate to still have you all in my life showing your love and support through it all.

It is hard to proclaim who I am most grateful to as such comparisons are likened to that of "apples and oranges." However, I feel quite confident that for the duration of my Ph.D. program, my loving wife Hiba Baaziz has helped me the most deeply and directly through her resolute and unwavering moral and emotional support. Hiba, you helped me to remember to refocus my energy on the metaphorical bounties to come when the trials to attain them were most burdensome and trying. Thank you for your confidence in me to overcome these various obstacles and burdens, self-imposed or otherwise, and for remaining by my side as I made some of the most important but difficult decisions in my life. Words cannot accurately convey how much you have done for me and I vow to show you my appreciation for your love until the end of my days. Nhabak Bezef, Habibi.

To my sweet Baaziz family, Nacera, Nasser, Souha and Lina, thank you so much for welcoming me into your family and accepting mine and Hiba's union every step of the way. You are such incredible people and I look forward to journeying through life with you.

Amy Irene Engle A.K.A Mom, you're short in stature but so very tall in your love and personality. You've always said your children were your best work and I have to agree that you've done so remarkably at showing your children love and helping each of us to carry that forward in our own lives. Thank you for all of your sacrifices and for always being available to us with unconditional love and support.

My remarkable brothers (Steven and Devin) and sisters (Katie and Sonni), I love each of you so much. You are all such wonderful people in your own special ways. Thank you for your unique but true personalities and for always being such great siblings and outstanding people in general. I must also give a shout out to the relevant spouses and wee babes, Jessica and Winter, Tyler and Ben, and Kevin. I am glad to call each of your family and hope for all the very best for each of you as you navigate your own paths to success and happiness.

Grandma, Grandpa and Sharon, Aunt Jen and Uncle Mike Brunner, Miranda, Jason-the-man, Sawyer, and Paxton Rozamus, Tim and Valerie Dey, Emily and Philip Chaltis, and Hannah Brunner – I love you all so much. Thank you for understanding why I have been so far away for so long and unavailable for much more than the occasional call or brief visit. It has been truly remarkable to watch as our family has grown through the years and I look forward to being much more present in your adventures moving forward.

To my Ph.D. mentor, Dr. Birgit Scharf, thank you for guiding me through this degree even if it meant I had to figure out how to make the behavioral assays work. Joking aside, your commitment and dedication to producing high-quality work with each of your students, colleagues, and associates is clearly evident and exemplified by every representation that comes from the Scharf lab (and collaborations) and into public view. Thank you for providing me opportunities to work on several very exciting projects through my Ph.D. and for helping me get back on track in several cases where I was drawn away from focusing on the big picture. Thank you additionally for helping me to redirect my good ideas into our great approaches in efforts to answer a variety of exciting research questions. I pledge to uphold your high standards of scientific quality as I venture out into the subsequent stages of my scientific career.

My gratitude to Dr. Scharf is extended to Earl Sheehan who has been so welcoming through the years and has made himself available to have deep and meaningful discussions about the way of the world and complex matters therein. Your and Dr. Scharf's mentality of nurturing the development of employees at both professional and personal levels is one I have always aligned with and appreciated, and I aim to implement these critical mentorship ideals into my own as I assume leading roles in future employment positions and in life in general.

I am very grateful to each of my committee members, whom I have named in alphabetical order, Dr. Clay Caswell, Dr. Florian Schubot, and Dr. Zhaomin Yang. I was well-aware of the “fierce” committee I had formed about four and a half years ago and am very thankful to each of you for your support and guidance and for always pushing me to reach my potential through my pursuit of this Ph.D.

I am grateful to a number of Scharf lab members, past and present, with whom I have worked in the lab and in various mentorship capacities. Special shout-outs go to Alfred Agbekudzi, my main man in protein purification and manipulation (“eh dey go on!”); to Rafael Castaneda-Saldana who helped show me the Scharf lab way of doing things when I first joined the lab; to Dr. Karl Compton, who provided invaluable training with the FPLC systems; to Djelika Kabore, my main undergraduate trainee; to Sahitya Biswas who helped me get some great work done during his two-month rotation in the Scharf lab; to Claire Yuan who joined the lab under supervision of another Scharf lab member but with whom I have had the unique privilege to establish a beautiful and long-lasting friendship through the years; and several others with whom I worked in some capacity or another as I have traversed the path through my Ph.D.

To the current Hsu lab members with whom I have worked and laughed, Hollyn Franklin, Zac Baker, Rita Makhlouf, Roger Bataglioli, and, of course, Bryan Hsu, thank you all for being such kind and supportive neighbors through the last few years.

To Ece Karatan and Ted Zerucha, thank you for motivating and believing in me when I was new to science and naïve to its possibilities. I appreciate your mentorship during my undergraduate and Master’s degree years and for being there ever since with your kindness, wisdom, and support.

To my AppState crew: Melissa Bone, Derek Mazzetti, Timbo and Tiffany Covington, Margo James, Kelly Giglio, Dakota Goad, Gary Walker, Mara Cloutier, Christina Daly, Jennie Flowers and Elin Swank, Laurel Carter, Andrew George, Curt Stacy, Anthony Phillips, and Liz Thomas, thank you so much for your continued friendship through the years despite distance and the

constant chaos of life. Our infrequent phone calls in recent years have been so deeply appreciated and have helped me to stay grounded, and my memories with each of your bring me great joy.

To Pam and Matt Stolte, I am so grateful for your love through the years. Your emotional support has been so very helpful to me at times when I needed it most. Our periodic gatherings have helped me and Hiba both feel so refreshed when work was unforgiving and we were beginning to feel burnt out. I am privileged to call you my Blacksburg parents and forever grateful to you both.

As I compile the list of people to whom I owe acknowledgements and gratitude, I realize that there is really no end or a point at which I can call this section of my dissertation truly "complete." According to Isaac Newton's third law of physics, for every action, there is an equal and opposite reaction. This law clearly does not apply to all forms of energy as time and time again I find that love begets love and kindnesses are perpetuated despite the occasional push-back. Thank you to everyone who has shown me love and kindness to this point in my life and As-salamu alaikum.

TABLE OF CONTENTS

Chapter 1: Main Introduction

Sinorhizobium meliloti and its symbiosis with *Medicago sativa*

The leguminous plant *Medicago sativa*, better known as alfalfa, is a highly valuable forage and cover crop and is therefore very important for supply of beef and dairy products as well as for preventing soil erosion (1). Alfalfa also serves as a green alternative to synthetic nitrogenous fertilizers, which tend to: leech into water supplies and promote high nitrate accumulation in leafy vegetables causing health risks, disrupt the soil microbiome balance by repressing the growth of nitrogen-fixing bacteria, and cause the physical structure of the soil to degrade as the soil microbiome structure changes and valuable nutrients are consumed (2).

Sinorhizobium meliloti is a Gram-negative rod-shaped bacterium and member of the soil-dwelling order of *Rhizobiales*, within the alphaproteobacterial class. In nature, *S. meliloti* may exist in a free-living form or in a symbiotic relationships with leguminous hosts of the *Medicago* genera through formation of root nodules, where it serves to fix atmospheric nitrogen into usable reduced forms (3). The *S. meliloti* RU11/001 genome is comprised of a ~4 Mbp circular chromosome, two large plasmids (pSymA and pSymB) of approximately 1.6-1.7 Mbp each, and four smaller plasmids ranging in size from between 55 and 170 kbp (Genbank assembly accession number: GCF_001050915.2). The chromosome encodes housekeeping genes for various metabolic processes, stress response, motility, chemotaxis, and plant interactions. pSymA encodes genes necessary for converting atmospheric nitrogen to ammonia while pSymB is required for host invasion and nutrient acquisition (4, 5). Little is known regarding the roles of the accessory plasmids. In the soil environment, *S. meliloti* may be commonly found in a motile form making use of 4-8 peritrichous flagella: corkscrew-shaped helical propellers comprised of a cytoplasmic C-ring that responds to chemotactic signals, a stabilizing rings embedded in the cell wall, and a long thin helical filament that rotates rapidly to provide propulsive thrust (6). Alternatively, they may be found as bacteroids, non-reproducing nitrogen-fixing factories, within root nodules following root hair colonization of their symbiotic hosts (5, 7-9).

Plant root colonization by *S. meliloti* is a multi-step process initiated by sensing of plant-derived compounds secreted into the soil from the site of the plant root (10). Specific plant-derived sugars, organic acids, and amino acids exuded by the plant into the soil have been shown to promote chemotaxis and draw bacteria towards host plant roots (10-12). In addition, host-

specific flavonoids in the environment are sensed by *S. meliloti*, and drive the synthesis and secretion of lipopolysaccharide-based Nod factors into the soil (13, 14). These Nod factors are in turn sensed by the host to induce vascular modifications at the plant root to promote efficient colonization by the microbe (8, 15). Once colonized, *S. meliloti* undergoes major morphological changes from the motile independent form to a nitrogen-fixing factory known as a bacteroid (7). Under appropriate conditions, addition of *S. meliloti* to the soil of leguminous hosts such as *M. sativa* (alfalfa) can lead to increased growth of the latter by up to four-fold as compared to plants grown in the absence of their microbial symbiont (16).

Chemotaxis signaling

Although not absolutely necessary for colonization, the coupled action of chemotaxis and motility employed by *S. meliloti* vastly improves colonization efficiency of host plant roots (17). This advantage is likely due to the enhanced ability of motile and chemotactically-proficient cells to reorient themselves and approach potential colonization sites in response to gradients of plant-derived chemical stimuli (18). Such compounds, including sugars, quaternary ammonium compounds, carboxylates, and amino and organic acids are recognized by a polarized cluster of small molecule sensors known as chemoreceptors, which influence a series of phosphotransfer events resulting in modulation of flagellar motor rotation (12, 18-21).

Chemotaxis is best studied in the gammaproteobacterium *Escherichia coli* (22-24). In this and other Gram-negative organisms, chemotaxis begins with diffusion of environmental compounds through the outer membrane into the periplasm where they are bound by a highly organized array of chemoreceptors localized to the cell pole (Figure 1.1) (25-27). Chemoreceptors typically contain a variable periplasmic sensor or ligand-binding domain (LBD) flanked by two transmembrane regions, one of which serves as a linker to a highly conserved cytoplasmic signaling domain (22, 25). Most chemoreceptors characterized to date are methyl-accepting chemotaxis proteins (MCPs), which bind small molecules in the periplasm via the LBD and transmit signals through the membrane causing conformational changes in the signaling domain (28, 29). MCPs relay changes in signal concentration and have thus been referred to as biological gradient sensors (30). MCPs influence the activity of a specialized two-component system composed of the histidine kinase, CheA, and the response regulator, CheY (22). CheA interacts with and senses conformational changes in MCP signaling domains to control its own

autophosphorylation (22). The coupling protein CheW stabilizes interactions between MCPs and CheA, presumably by linking the two proteins and aiding in signal transmission from the chemoreceptor to CheA (31, 32). In the absence of an attractant or presence of a repellent, CheA autophosphorylates at a conserved histidine residue in its C-terminal domain (22, 33). Activated CheA-P in turn transfers its phosphate group to a conserved aspartate residue in the response regulator, CheY, which diffuses through the cytoplasm to interact with the C-ring components of the flagellar motor, FliM and FliN (22, 34). Therefore, in contrast to typical two-component systems, which target promoters to control gene expression, this specialized two-component system targets the flagellar motor to directly modulate motility (35, 36).

In *E. coli*, the interaction between CheY-P and the C-ring results in a switch from counterclockwise (CCW) to clockwise (CW) flagellar rotation (37, 38). The asynchrony of flagellar filament rotation within the flagellar bundle causes dissociation of one or more flagella from the bundle to promote a brief tumbling behavior by the cell, thus reorienting the cell in a new random direction (39). CheY spontaneously dephosphorylates to terminate the signal, a process accelerated by the phosphatase CheZ (22). In the presence of an attractant, conformational changes in corresponding MCPs hinder autophosphorylation of CheA leaving CheY in an unphosphorylated state. Thus, flagellar motor rotation is uninhibited and the cell engages in extended runs or a "biased random walk" up the attractant gradient or down a repellant gradient (40).

MCPs additionally undergo methylation and demethylation events at conserved aspartate residues to alter the ligand sensitivity of chemoreceptors, which serves to expand the dynamic range of MCP-ligand sensitivity and serve as a temporal memory system (22). The methyltransferase CheR constitutively adds methyl groups to MCPs while the antagonistic protein CheB is responsible for the demethylation of MCPs and is only active following phosphorylation by CheA-P (40-42). In this way, the concerted action of the chemical sensors, methylation-modifying memory proteins, phospho-relay mediators, and flagellar motor effectors allows bacteria to make informed decisions to navigate towards environments most favorable for the cell.

Distinctions of chemotaxis signaling in *S. meliloti*

S. meliloti exhibits several important departures from the chemotaxis pathway of *E. coli* including an increased chemoreceptor repertoire (eight in *S. meliloti* compared to five in *E. coli*) (19, 43, 44). These include the broad range carboxylate sensor McpT, amino acid sensor McpU, the short-chain carboxylate sensor McpV, and the quaternary ammonium compound sensor McpX, which are thought to play direct roles in sensing these compounds released into the soil by host plant roots (12, 19-21). An additional adaptation protein, CheD, is also present (45). Although not experimentally verified in *S. meliloti*, a CheD homolog from *Bacillus subtilis* serves as a deamidase, which alters the number of methylation sites in chemoreceptor signaling domains to expand the dynamic range of chemoattractant concentrations sensed by the modified receptors (46). *S. meliloti* encodes two CheY homologs, CheY1 and CheY2 (47). CheY2 functions as the primary response regulator (47). Importantly and in contrast to that of *E. coli*, the flagellar motors of *S. meliloti* rotate strictly CW and are speed variable (48-51). Therefore, instead of switching rotary direction of flagellar motors to cause cell tumbling, phosphorylated CheY2-P is thought to interact with flagellar motor components to slow the rotary speed of individual motors causing asynchrony of bundle filament rotation (49). For signal termination, CheY2-P is dephosphorylated by CheA via retrophosphorylation events and CheY1 functionally replaces *E. coli* CheZ as a phosphatase to facilitate dephosphorylation of CheA-P (49, 52). This activity is further enhanced by yet another soluble protein, CheS, which promotes rapid phosphate transfer from CheA to CheY1 by promoting the CheA/CheY1 interaction and accelerates phosphate drainage from the latter (53). Another protein, CheT, remains to be thoroughly characterized but is required for taxis toward chemoattractants and on soft-agar plates (unpublished data).

Regulation of chemotaxis and flagellar gene expression in *S. meliloti*

Bacterial flagella are composed of three main components: the basal body embedded in the cell envelope, a flexible hook extending from the basal body outward from the cell, and a helical filament, which extends from and rotates rapidly with the hook and basal body core to provide thrust (32, 37, 38, 54, 55). The basal body is comprised of the rotary motor that rotates the flagellum, protein secretion machinery necessary to export many components of the flagellar structure, and a rod structure extending from the core of the basal body to the hook through a series of rings embedded in the cell wall (37, 38, 54). The P-ring is embedded in the

peptidoglycan layer and the L-ring is in the outer membrane/lipopolysaccharide layer (38, 54). These rings act as bushings and allow for smooth rotation of the rod through the cell wall (38, 54).

The motility and chemotaxis system of *S. meliloti* relies on activity and/or production of over 50 different protein products, all encoded by genes of the flagellar regulon located in a contiguous region of the *S. meliloti* chromosome (56). The final flagellar product consists of approximately 20,000 proteins, and thus the corresponding genes are tightly regulated in a hierarchical fashion (54). These are broken up into four distinct classes: class IA, class IB, class II, and class III (Figure 1.2) (57). The class IA genes, *visN* and *visR*, encode the LuxR-type global transcriptional regulators, VisN and VisR, named for being vital for swimming (58). VisN and VisR are suggested to form heterodimers and are produced throughout growth (58). VisNR acts at the top of the transcriptional hierarchy to control expression of the class IB gene, *rem*, by binding both of its promoters, P1 and P2 (57). The *rem* gene encodes the regulator of exponential growth motility (Rem), an OmpR-like master regulator that directly influences its own transcription from the P1 promoter in addition to directly activating class II genes during the logarithmic phase of growth (57).

Class II genes include components of the basal body (class IIA: *flg*, *flh*, and *fli*) and motor (class IIB: *mot*) genes, while class III genes include flagellin (*fla*) genes and those involved in chemotaxis (*che*) (57). Rem directly binds Class II promoters such as those for *flgB*, *fliF*, and *orf38*, and perhaps those of *motA* and *orf20*, all of which share consensus promoter binding regions for Rem activation (57). It has been speculated that the products of class IIA genes *fliM* and *orf38* regulate expression of class III genes, as promoters for the latter lack Rem binding sequences (18, 57). Class III genes include those encoding flagellin and components of the chemotaxis signaling system. In contrast, activation of class III genes in *E. coli* requires the σ-factor FliA whose activity is repressed by the anti-σ factor FlgM prior to completion of basal body-hook complex assembly (38, 59, 60). Neither *fliA* nor *flgM* homologs have been identified in *S. meliloti*. However, the flagellin gene regulator encoded by *flbT* is predicted to control of flagellin gene regulation (45, 57). As *S. meliloti* reaches high cell densities, the quorum sensing system master regulators Sin/ExpR repress motility and chemotaxis through suppression of *visNR* gene expression (45, 61).

Flagellum biosynthesis

Flagellum assembly, which is best characterized in *E. coli*, occurs in a proximal to distal fashion and is initiated by insertion of the MS-ring of the basal body into the cytoplasmic membrane (Figure 1.3) (55, 62-64). The flagellar type-three secretion machinery (fT3SS) comprised of FlhAB, FliOPQR, and FliI, assembles within a cavity of the MS-ring, where proton motive force drives secretion of the axial components of the rod, hook, and filament (65).The MS-ring is comprised of 26 copies of FliF and acts as a scaffold onto which remaining components of the basal body are built. The C-ring is assembled on the cytoplasmic face of the MS-ring and is comprised of FliG (26 copies), FliM (34-45 copies), and FliN (34-45 tetramers) (66, 67). Together, the C-ring components act as a switch to control direction (in *E. coli*) or speed (*S. meliloti*) of flagellar rotation. The rod contains a proximal region comprised of FliE, FlgB, FlgC and FlgF and is interlinked with the fT3SS through interactions between FliP and FliR with FliE and FlgB. A distal region is formed by FlgG (65). During rod assembly, the lytic transglycosylase FlgJ aids in degradation of the peptidoglycan layer to permit rod passage through the sacculus (68-70). Notably, FlgJ exhibits diverse domain architecture across the bacterial kingdom. FlgJ homologs in alphaproteobacterial including *S. meliloti* and *Rhodobacter sphaeroides* possess only the rod-binding domain $FlgJ_N$ domain, which acts as a cap to stabilize the distal end of the rod structure (71, 72). Peptidoglycan hydrolysis required for flagellar rod formation in these organisms is thought to be performed by alternative lytic transglycosylases such as the *R. sphaeroides* soluble lytic transglycosylase SltF, *S. meliloti* hypothetical protein SMc03045, and *Caulobacter crescentus* PleA. Notably, Gram positive bacteria use an alternative enzyme class, the β-N-acetylglucosaminidases (73, 74). Following rod construction, the P-ring (FlgI) is inserted into the peptidoglycan layer with the aid of a periplasmic chaperone, FlgA, and the L-ring lipoprotein, FlgH, is inserted into the outer membrane (75, 76). The L- and P-ring structures form a fused bushing in the cell envelope during rod rotation and the rod extends just past the outermembrane where the hook is synthesized next (77). A representation of the solved cryo-EM structure of MS-ring-rod-PL-ring assembly reported by Johnson *et al.* is shown in Figure 1.4.

The flagellar hook is a ~55 nm long flexible polymer of repeating FlgE subunits comprised of 11 parallel rows arranged in rings of approximately 11 subunits each (37, 38, 55, 63, 78). The hook assembles at the distal end of the rod with the hook-cap protein, FlgD, stabilizing the tip of the

growing hook as additional FlgE subunits are incorporated (54). During hook assembly, an infrequent molecular ruler, FliK, is secreted until the hook reaches an appropriate length and polymerization is terminated (79). This occurs as a result of interactions between FliK with the substrate-specificity determinant of the flagellar secretion system, FlhB (79). FliK is periodically secreted along with hook monomers and upon reaching an appropriate hook length, decreased velocity of FliK secretion increases the probability of productive interactions between the FliK C-terminal domain which facilitates autoproteolysis of FlhB (80). FlhB cleavage changes the specificity of substrate secretion to favor flagellin monomer export and promote filament synthesis (80). Concurrently, the hook-cap protein, FlgD, is eliminated and replaced by the hook-associated proteins (HAP), FlgK and FlgL, which form the hook-filament junction rings, and FliD, the filament-cap protein (54). FliD forms a stool-shaped homopentamer, each monomer contributing one of five legs buried within FlgL and part of a pentameric plate at the distal end (54). Unfolded flagellin monomers are then secreted through a hollow cavity within the growing axial structure to a space accommodated between two legs of the FliD cap such that just one flagellin monomer may be inserted at a time (54). Sequential helical addition of many thousands of flagellin monomers at the end of the growing filament leads to the formation of a long corkscrew-like structure (54). Flagellum-length control is diffusion-dependent with an exponential decrease of flagellin export occurring with increased filament length (81). Recent models describing the injection-diffusion control of filament growth have been proposed whereby proton motive force is used to drive secretion of unfolded flagellin monomers through a 2 nm channel within the filament (82, 83). Addition of new unfolded monomers to the growing filament is limited by two-dimensional diffusion and monomers are prohibited from passing through the occupied channel until the previous monomer is incorporated into the growing filament (82). Therefore, shorter filaments grow very quickly but exhibit an exponential decay in growth rate with increased filament length.

Similar to the hook, the mature flagellar filament possesses 11 parallel rows of protofilaments engaged in varying degrees of twist within the filament, which contributes to the helical nature of the structure (38). In *E. coli*, the helical twist of the filament is left-handed and conformational changes in interflagellin bonds during CCW to CW switching can result in a transition to right-handed helicity (38). The surface of *E. coli* filaments appears smooth or “plain” as determined by electron microscopy (84). In contrast, the flagellar filaments of *S. meliloti* exhibit a ridged or

screw thread-like surface appearance and are referred to as “complex” filaments (84-87). In addition, *S. meliloti* filaments are rigidly locked into right-handed helicity without the freedom to switch to left-handedness (84, 86). These characteristics, which distinguish the complex flagella from their plain counterparts, are attributed to the production of filament subunits that are composed of flagellin dimers. Variations in the basal flagellin protein structure are also known to be quite substantial. Some organisms such as *B. subtilis* and *Kurthia sp.* produce flagellin composed only of the highly conserved flagellin core domains (D_0 and D_1) found in all known flagellated bacteria, while other organisms such as *C. jejuni* and *S. meliloti* have been reported to produce up to three additional highly variable domains (D_2-D_4) (84, 86-88). It is hypothesized that the physical properties of complex flagella, in addition to strictly CW and speed-variable rotation, arose as adaptations to the variably viscous environment of the soil (49, 87, 89). An additional distinction from the *E. coli* paradigm is the presence of multiple flagellin homologs in the *S. meliloti* filament (86). While *E. coli* encodes just one type of flagellin, FliC, *S. meliloti* produces four closely related types: FlaA, FlaB, FlaC, and FlaD. FlaA is the most abundant (comprising at least 50% of the filament) and is absolutely required for production of a filament in addition to at least one other homolog (86).

Mechanisms powering flagellar motor function

Rotation of the bacterial flagellum is driven by circumferentially-placed stator units comprised of MotA and MotB proteins for H^+-type stators or PomA and PomB for Na^+-type stators (38, 90). MotA contains four transmembrane α-helix domains, one large cytoplasmic loop between TM2 and TM3, and a short C-terminal tail (54, 91, 92). MotB possesses an N-terminal transmembrane domain, a short proton plug region, a linker region, and a peptidoglycan binding domain in the periplasm, the latter of which serves to securely anchor MotA-MotB complexes to the cell wall following stator incorporation into the motor (93, 94). During stator assembly, a ring of five MotA monomers assemble around a dimer of MotB in the inner membrane to form two proton channels between the TM domains of the stator components (38, 91, 95, 96). The proton channels of free stators in the inner membrane are maintained in an inactive state by MotB proton plug regions trapped between short periplasmic loops in MotA until contact is made between the rotor and free stators (97, 98). Subsequent conformational changes in MotB result in extension of the flexible linker region such that the proton plug is released from blocking the proton channels and the peptidoglycan-binding domains of MotB dimerize and secure

interactions with the sugar moieties of the sacculus (94, 99). As protons (or Na^+ ions) flow down their electrochemical gradient from the periplasm into the cytoplasm through open stator channels, the MotA pentamer rotates clockwise around MotB driving counterclockwise rotation of the entire rotor-hook-filament assembly through charged residue interactions between MotA and FliG (38, 100). When phosphorylated CheY binds to the C-ring, dramatic conformational changes result in expansion of the C-ring diameter and repositioning of FliG such that contact is now made with MotA on the distal side of the stator units. This rearrangement drives opposite (clockwise) rotation of the rotor (54, 101-104).

An additional component of the flagellar motor, FliL, plays multifaceted roles in the function of bacterial flagella. In-frame *fliL* deletion mutants in enteric bacteria tend to exhibit minor defects in swimming motility but suffer a rod breakage phenotype and marked losses in a social motility known as swarming whereby bacteria migrate in a coordinated fashion in a thin fluid over surfaces (105, 106). In contrast, alphaproteobacteria suffer more pronounced swimming defects indicating that FliL plays a more essential role in flagellar motility of these organisms (107, 108). FliL is an inner membrane protein largely localized in the periplasm and has been found to associate with stators in several distantly related species (109, 110). Additionally, FliL localization at the flagellar motor is influenced by the presence of stators and mutations that disrupt the MotB plug region tend to improve flagellar motility of *S. enterica* and *R. sphaeroides fliL* deletion mutants (110-113). In *V. alginolyticus* and *B. burgdorferi*, FliL forms partial rings of about 4 monomers adjacent to the basal body where they recruit incoming stators into the motor. Additional FliL oligomers are thought to further enclose the stators to form a cage around the stator units with a central cavity through which the MotB linker regions extend to contact the sacculus (112, 114).

Variations on the flagellar theme

Flagella are truly fascinating organelles and are found in impressive varieties with regards to flagellation patterns, motor operations and motor accessory structures (115). The flagellar motors of *S. meliloti*, *Agrobacterium spp.*, and *R. sphaeroides* are locked into unidirectional clockwise rotation, which suggests that the C-ring is likely locked in the extended conformation in these organisms (48, 116-118). Monotrichously flagellated bacteria, which employ switch-type motors but are unable to form a flagellar bundle, would only run forward and reverse upon simple rotational switching as it tends to occur in peritrichous bacteria. As such, *Vibrio spp.* and

Shewanella putrefaciens have adapted a run-reverse-flick mechanism to promote redirection, in which forward motion imposes forward momentum in the flagellum and a quick reverse-flick of the motors induces a kink-push on the flagellum. In this way, the filament is said to be used as a rudder rather than a propeller (119, 120), although we suggest it is more accurately likened to a hybrid propeller and oar. Some bacteria can alternate between polar and peritrichous flagellar systems and others can adapt their flagellar motors to run on alternative fuel types including calcium, magnesium, and potassium (121-123). The planar waveshape of *B. burgdorferi* cells is caused by several periplasmic flagella that are wound around and attached at both ends of its long thin cell body (124, 125).

The maximum number of stator positions accommodated by a single motor ranges from 11 to 18 depending of the diameter of the C-ring, which correlates well with the maximum torque achieved by a given motor. For example, the C-ring diameter of *S. enterica* is 44 nm, accommodates 11 stators and achieves a torque of about 1,260 pN·nm. This pales in comparison to the 52 nm-wide *C. jejuni* C-ring around which 17 stators can be recruited to achieve about 3,600 pN·nm of torque (126). *Borrelia burgdorferi* boasts an impressive 80 nm-wide stator ring diameter, a 16 stator limit, and 4,000 pN·nm of torque with additional accommodations to provide increased torque described below (127).

Additional structures in high-torque motors

Over the last decade, several distantly related bacteria have been shown to recruit additional structures to their flagellar motors. The purpose of these extra features is to provide reinforcement through additional contacts within the cell wall to withstand greater forces than those required to navigate enteric bacteria habitats (115, 121, 126-129). Importantly, the stator dwell time in the flagellar motor of enteric bacteria is only about 30 seconds after which it is exchanged back into pool of inactive stators in the inner membrane (130-133). In contrast, additional structures found in non-enteric bacateria stabilize stator association within the motor (134), representatives of which are shown in Figure 1.5. *Vibrio* and *Shewanella spp.* incorporate a T-ring (comprised of MotXY proteins) adjacent to the peptidoglycan-associated P-ring that aids in stator recruitment and stabilization. Further stabilization is provided to *Shewanella*, *Vibrio,* and *R. sphaeroides* motors by the H-ring (comprised of FlgOPT proteins), which is recruited to the lipopolysaccharide associated L-ring just below the outer membrane. Together, PL-ring associated H- and T-rings form a flagellar outer membrane complex (FOMC) that

reinforce the flagellar motor at several points in the cell envelope. *Pseudomonas aeruginosa* and *Legionella pneumophila* also exhibit P-rings decorated with additional structures for which a protein entity has yet to be assigned and *P. aeruginosa* recruits additional stator amenities, MotC and MotD, when more torque is necessary for example in higher viscosity conditions (129). Additionally, *Helicobacter pylori* harbors a basal disk beneath the outer membranous flagellar sheath. The outer perimeter of the basal disc associates with a cage that surrounds the stator units and spans the distance of the periplasm. *B. burgdorferi* uses a collar similar to the cage in *H. pylori* (127-129). Finally, transient cytoplasmic rings of unknown composition were recently reported to assemble around FliG in the C-ring in a manner dependent on transmembrane components of the fT3SS, FliO and FliQ. These periplasmic rings were reported to facilitate stator assembly in flagellar motors known to produce higher torque than enteric bacteria and appear to dissociate from the motor once synthesis is complete. Notably, these were identified in various beta-, gamma-, and epsilonproteobacteria suggesting that transient periplasmic rings are a common tool used for stator recruitment in flagellated bacteria (134).

Additional flagellar motor components in the *S. meliloti*

No structural information is currently available for the *S. meliloti* flagellar motor. Prior to this study, *S. meliloti* was known to produce two noncanonical periplasmic Mot proteins, MotC and MotE, that are essential for flagellar motor function. MotC appears to stabilize the periplasmic region of MotB and MotE is a chaperone for MotC, supporting its proper folding and stabilization in the periplasm (135, 136). However, the precise roles of MotC in motor function are unknown. It has been proposed that stabilization of MotB by MotC may be required for efficient motor rotation in the viscous soil environment. Importantly, *S. meliloti* MotB contains a stretch of about 90 amino acid residues in its periplasmic region, which is predicted to mediate interactions with MotC as well as previously unidentified flagellar motor components (135).

Objectives of this work

Chapter 2 recounts the first reported instance of a flagellar system using dual FliL paralogs in alpha-proteobacteria, which we have demonstrated in *S. meliloti*. The less conserved paralog was named MotF. Motility defects of deletion mutants lacking either FliL or MotF were thoroughly characterized. FliL is absolutely required for swimming motility and normal flagellation, and we hypothesize that it may serve as a scaffold for stator recruitment. In contrast, the *motF* deletion mutant exhibits jerky and low-speed motility, and we provide evidence that MotF plays a role in

MotB proton plug modulation. We identified additional alterations in the flagellar motor that compensate for the loss of MotF and propose a model for the incorporation of MotF and FliL into the *S. meliloti* flagellar motor.

Chapter 3 describes ongoing work characterizing the relationship between the peptidoglycan modification gene regulator, LdtR, and a previously uncharacterized protein, currently referred to as Orf23, in *S. meliloti* flagellar motility. We determined that LdtR does not control motility gene transcription but that the presence of Orf23 in mutants lacking LdtR drastically reduces swimming motility. An amino acid substitution was identified in stator components that restores the motility when LdtR is absent from the cell. Bioinformatics analysis, structure predictions, and homology modeling revealed putative domains of Orf23 and provided some insights into possible quaternary structures that Orf23 may assume in the flagellar assembly. Drawing on a model proposed in Chapter 2, a possible arrangement for Orf23 placement around the motor is proposed. The combined evidence points to a role for Orf23 in providing maximum torque to *S. meliloti* flagellar motors and implicates its function in speed variability. Further investigation of *S. meliloti* flagellar motor composition and interaction dynamics will answer remaining questions regarding the mechanistic functions of unidirectional speed-variable flagellar motors.

Altogether, the results of these endeavors provide several important answers regarding the distinctions of speed-variable flagellar motor composition from that of other bacteria. Further characterization of flagellar and chemotaxis from diverse bacteria including *S. meliloti* will permit the future development of bioengineering objectives aimed at *e. g.* fine-tuning bacterial chemotactic abilities for recognition of and migration towards specific signals or structure-based selection of bacterial vehicles (and corresponding flagellar systems) to deliver therapeutics or bioremediation payloads to desired targets depending on the anticipated medium to be traveled.

REFERENCES

1. Bacenetti J, Lovarelli D, Tedesco D, Pretolani R, Ferrante V. 2018. Environmental impact assessment of alfalfa (*Medicago sativa* L.) hay production. Science of The Total Environment 635:551-558.
2. Liu C-W, Sung Y, Chen B-C, Lai H-Y. 2014. Effects of nitrogen fertilizers on the growth and nitrate content of lettuce (*Lactuca sativa* L.). International Journal of Environmental Research and Public Health 11:4427-4440.
3. Paau AS, Bloch CB, Brill WJ. 1980. Developmental fate of Rhizobium meliloti bacteroids in alfalfa nodules. Journal of bacteriology 143:1480-1490.
4. Barnett MJ, Fisher RF, Jones T, Komp C, Abola AP, Barloy-Hubler F, Bowser L, Capela D, Galibert F, Gouzy J. 2001. Nucleotide sequence and predicted functions of the entire Sinorhizobium meliloti pSymA megaplasmid. Proceedings of the National Academy of Sciences 98:9883-9888.
5. Finan TM, Weidner S, Wong K, Buhrmester J, Chain P, Vorhölter FJ, Hernandez-Lucas I, Becker A, Cowie A, Gouzy J. 2001. The complete sequence of the 1,683-kb pSymB megaplasmid from the N2-fixing endosymbiont Sinorhizobium meliloti. Proceedings of the National Academy of Sciences 98:9889-9894.
6. Berg HC. 2003. The rotary motor of bacterial flagella. Annu Rev Biochem 72:19-54.
7. Haag AF, Wehmeier S, Beck S, Marlow VL, Fletcher V, James EK, Ferguson GP. 2009. The Sinorhizobium meliloti LpxXL and AcpXL proteins play important roles in bacteroid development within alfalfa. Journal of bacteriology 191:4681-4686.
8. Schultze M, Kondorosi A. 1998. Regulation of symbiotic root nodule development. Annual review of genetics 32:33-57.
9. Poole P, Ramachandran V, Terpolilli J. 2018. Rhizobia: from saprophytes to endosymbionts. Nature Reviews Microbiology 16:291-303.
10. Webb BA, Helm RF, Scharf BE. 2016. Contribution of individual chemoreceptors to Sinorhizobium meliloti chemotaxis towards amino acids of host and nonhost seed exudates. Molecular Plant-Microbe Interactions 29:231-239.
11. Meier VM, Muschler P, Scharf BE. 2007. Functional analysis of nine putative chemoreceptor proteins in Sinorhizobium meliloti. Journal of bacteriology 189:1816-1826.
12. Webb BA, Karl Compton K, Castañeda Saldaña R, Arapov TD, Keith Ray W, Helm RF, Scharf BE. 2017. Sinorhizobium meliloti chemotaxis to quaternary ammonium compounds is mediated by the chemoreceptor McpX. Molecular microbiology 103:333-346.
13. Maxwell CA, Hartwig UA, Joseph CM, Phillips DA. 1989. A chalcone and two related flavonoids released from alfalfa roots induce nod genes of Rhizobium meliloti. Plant physiology 91:842-847.
14. Bensmihen S, de Billy F, Gough C. 2011. Contribution of NFP LysM domains to the recognition of Nod factors during the Medicago truncatula/Sinorhizobium meliloti symbiosis. PLoS One 6:e26114.
15. Denarie J, Debelle F, Prome J-C. 1996. Rhizobium lipo-chitooligosaccharide nodulation factors: signaling molecules mediating recognition and morphogenesis. Annual review of biochemistry 65:503-535.

16. Luo L, Yao S-Y, Becker A, Rüberg S, Yu G-Q, Zhu J-B, Cheng H-P. 2005. Two new Sinorhizobium meliloti LysR-type transcriptional regulators required for nodulation. Journal of bacteriology 187:4562-4572.
17. Caetano-Anollés G, Wrobel-Boerner E, Bauer WD. 1992. Growth and movement of spot inoculated Rhizobium meliloti on the root surface of alfalfa. Plant physiology 98:1181-1189.
18. Tambalo DD, Yost CK, Hynes MF. 2015. Motility and Chemotaxis in the Rhizobia. Biological Nitrogen Fixation:337-348.
19. Webb BA, Compton KK, del Campo JSM, Taylor D, Sobrado P, Scharf BE. 2017. Sinorhizobium meliloti Chemotaxis to Multiple Amino Acids Is Mediated by the Chemoreceptor McpU. Molecular Plant-Microbe Interactions 30:770-777.
20. Baaziz H, Compton KK, Hildreth SB, Helm RF, Scharf BE. 2021. McpT, a broad range carboxylate chemoreceptor in *Sinorhizobium meliloti*. Journal of Bacteriology:JB. 00216-21.
21. Compton KK, Hildreth SB, Helm RF, Scharf BE. 2018. Sinorhizobium meliloti chemoreceptor McpV senses short-chain carboxylates via direct binding. Journal of bacteriology 200:e00519-18.
22. Parkinson JS, Hazelbauer GL, Falke JJ. 2015. Signaling and sensory adaptation in Escherichia coli chemoreceptors: 2015 update. Trends in microbiology 23:257-266.
23. Wadhams GH, Armitage JP. 2004. Making sense of it all: bacterial chemotaxis. Nature Reviews Molecular Cell Biology 5:1024.
24. Karmakar R. 2021. State of the art of bacterial chemotaxis. Journal of Basic Microbiology 61:366-379.
25. Maddock J, Alley M, Shapiro L. 1993. Polarized cells, polar actions. Journal of bacteriology 175:7125-7129.
26. Shapiro L. 1993. Polar location of the chemoreceptor complex in the Escherichia coli cell. Science 259:1717-1723.
27. Yang W, Briegel A. 2020. Diversity of bacterial chemosensory arrays. Trends in microbiology 28:68-80.
28. Williams SB, Stewart V. 1999. MicroReview: Functional similarities among two-component sensors and methyl-accepting chemotaxis proteins suggest a role for linker region amphipathic helices in transmembrane signal transduction. Molecular microbiology 33:1093-1102.
29. Krell T, Lacal J, Muñoz-Martínez F, Reyes-Darias JA, Cadirci BH, García-Fontana C, Ramos JL. 2011. Diversity at its best: bacterial taxis. Environmental microbiology 13:1115-1124.
30. Micali G, Endres RG. 2016. Bacterial chemotaxis: information processing, thermodynamics, and behavior. Current opinion in microbiology 30:8-15.
31. Gegner JA, Graham DR, Roth AF, Dahlquist FW. 1992. Assembly of an MCP receptor, CheW, and kinase CheA complex in the bacterial chemotaxis signal transduction pathway. Cell 70:975-982.
32. Delalez NJ. 2014. Bacterial flagella: Flagellar motor. eLS.
33. Bilwes AM, Alex LA, Crane BR, Simon MI. 1999. Structure of CheA, a signal-transducing histidine kinase. Cell 96:131-141.

34. Sarkar MK, Paul K, Blair D. 2010. Chemotaxis signaling protein CheY binds to the rotor protein FliN to control the direction of flagellar rotation in *Escherichia coli*. Proceedings of the National Academy of Sciences 107:9370-9375.
35. Mitrophanov AY, Groisman EA. 2008. Signal integration in bacterial two-component regulatory systems. Genes & development 22:2601-2611.
36. Lai R-Z, Parkinson JS. 2018. Monitoring Two-Component Sensor Kinases with a Chemotaxis Signal Readout, p 127-135, Bacterial Chemosensing. Springer.
37. Silverman M, Simon M. 1974. Flagellar rotation and the mechanism of bacterial motility. Nature 249:73.
38. Berg HC. 2003. The rotary motor of bacterial flagella. Annual Review of Biochemistry 72.
39. Reigh SY, Winkler RG, Gompper G. 2013. Synchronization, slippage, and unbundling of driven helical flagella. PloS one 8:e70868.
40. Sourjik V, Wingreen NS. 2012. Responding to chemical gradients: bacterial chemotaxis. Current opinion in cell biology 24:262-268.
41. Stock JB, Zhang S. 2013. The biochemistry of memory. Current Biology 23:R741-R745.
42. Clausznitzer D, Oleksiuk O, Løvdok L, Sourjik V, Endres RG. 2010. Chemotactic response and adaptation dynamics in Escherichia coli. PLoS computational biology 6:e1000784.
43. Greenfield D, McEvoy AL, Shroff H, Crooks GE, Wingreen NS, Betzig E, Liphardt J. 2009. Self-organization of the Escherichia coli chemotaxis network imaged with super-resolution light microscopy. PLoS biology 7:e1000137.
44. Greek M, Platzer J, Sourjik V, Schmitt R. 1995. Analysis of a chemotaxis operon in Rhizobium meliloti. Molecular microbiology 15:989-1000.
45. Scharf BE, Hynes MF, Alexandre GM. 2016. Chemotaxis signaling systems in model beneficial plant–bacteria associations. Plant molecular biology 90:549-559.
46. Glekas GD, Plutz MJ, Walukiewicz HE, Allen GM, Rao CV, Ordal GW. 2012. Elucidation of the multiple roles of CheD in Bacillus subtilis chemotaxis. Molecular microbiology 86:743-756.
47. Riepl H, Maurer T, Kalbitzer HR, Meier VM, Haslbeck M, Schmitt R, Scharf B. 2008. Interaction of CheY2 and CheY2-P with the cognate CheA kinase in the chemosensory-signalling chain of *Sinorhizobium meliloti*. Molecular Microbiology 69:1373-1384.
48. Götz R, Schmitt R. 1987. *Rhizobium meliloti* swims by unidirectional, intermittent rotation of right-handed flagellar helices. Journal of Bacteriology 169:3146-3150.
49. Scharf B, Schmitt R. 2002. Sensory transduction to the flagellar motor of *Sinorhizobium meliloti*. Journal of Molecular Microbiology and Biotechnology 4:183-186.
50. Attmannspacher U, Scharf B, Schmitt R. 2005. Control of speed modulation (chemokinesis) in the unidirectional rotary motor of *Sinorhizobium meliloti*. Molecular Microbiology 56:708-718.
51. Armitage JP, Schmitt R. 1997. Bacterial chemotaxis: Rhodobacter sphaeroide and Sinorhizobium meliloti-variations on a theme? Microbiology 143:3671-3682.
52. Amin M, Kothamachu VB, Feliu E, Scharf BE, Porter SL, Soyer OS. 2014. Phosphate sink containing two-component signaling systems as tunable threshold devices. PLoS computational biology 10:e1003890.

53. Dogra G, Purschke FG, Wagner V, Haslbeck M, Kriehuber T, Hughes JG, Van Tassell ML, Gilbert C, Niemeyer M, Ray WK. 2012. *Sinorhizobium meliloti* CheA complexed with CheS exhibits enhanced binding to CheY1, resulting in accelerated CheY1 dephosphorylation. Journal of Bacteriology 194:1075-1087.
54. Morimoto YV, Minamino T. 2014. Structure and function of the bi-directional bacterial flagellar motor. Biomolecules 4:217-234.
55. Namba K, Vonderviszt F. 1997. Molecular architecture of bacterial flagellum. Quarterly reviews of biophysics 30:1-65.
56. Galibert F, Finan TM, Long SR, Pühler A, Abola P, Ampe F, Barloy-Hubler F, Barnett MJ, Becker A, Boistard P. 2001. The composite genome of the legume symbiont Sinorhizobium meliloti. Science 293:668-672.
57. Rotter C, Mühlbacher S, Salamon D, Schmitt R, Scharf B. 2006. Rem, a new transcriptional activator of motility and chemotaxis in *Sinorhizobium meliloti*. Journal of Bacteriology 188:6932-6942.
58. Sourjik V, Muschler P, Scharf B, Schmitt R. 2000. VisN and VisR are global regulators of chemotaxis, flagellar, and motility genes in *Sinorhizobium* (*Rhizobium*) *meliloti*. Journal of Bacteriology 182:782-788.
59. Ohnishi K, Kutsukake K, Suzuki H, Lino T. 1992. A novel transcriptional regulation mechanism in the flagellar regulon of Salmonella typhimurium: an anti-sigma factor inhibits the activity of the flagellum-specific Sigma factor, σF. Molecular microbiology 6:3149-3157.
60. Apel D, Surette MG. 2008. Bringing order to a complex molecular machine: the assembly of the bacterial flagella. Biochimica et Biophysica Acta (BBA)-Biomembranes 1778:1851-1858.
61. Hoang HH, Gurich N, González JE. 2008. Regulation of motility by the ExpR/Sin quorum-sensing system in *Sinorhizobium meliloti*. Journal of Bacteriology 190:861-871.
62. Ueno T, Oosawa K, Aizawa S-I. 1994. Domain structures of the MS ring component protein (FliF) of the flagellar basal body of Salmonella typhimurium. Journal of molecular biology 236:546-555.
63. Chevance FF, Hughes KT. 2008. Coordinating assembly of a bacterial macromolecular machine. Nature Reviews Microbiology 6:455.
64. Li H, Sourjik V. 2011. Assembly and stability of flagellar motor in Escherichia coli. Molecular microbiology 80:886-899.
65. Johnson S, Furlong EJ, Deme JC, Nord AL, Caesar JJ, Chevance FF, Berry RM, Hughes KT, Lea SM. 2021. Molecular structure of the intact bacterial flagellar basal body. Nature Microbiology 6:712-721.
66. Francis NR, Irikura VM, Yamaguchi S, DeRosier DJ, Macnab RM. 1992. Localization of the Salmonella typhimurium flagellar switch protein FliG to the cytoplasmic M-ring face of the basal body. Proceedings of the National Academy of Sciences 89:6304-6308.
67. Hosu BG, Nathan VS, Berg HC. 2016. Internal and external components of the bacterial flagellar motor rotate as a unit. Proceedings of the National Academy of Sciences 113:4783-4787.
68. Nambu T, Minamino T, Macnab RM, Kutsukake K. 1999. Peptidoglycan-Hydrolyzing Activity of the FlgJ Protein, Essential for Flagellar Rod Formation inSalmonella typhimurium. Journal of bacteriology 181:1555-1561.

69. Herlihey FA, Clarke AJ. 2016. Controlling autolysis during flagella insertion in Gram-negative bacteria, p 41-56, Protein Reviews. Springer.
70. Herlihey FA, Moynihan PJ, Clarke AJ. 2014. The essential protein for bacterial flagella formation FlgJ functions as a β-N-acetylglucosaminidase. Journal of biological chemistry 289:31029-31042.
71. Nambu T, Inagaki Y, Kutsukake K. 2006. Plasticity of the domain structure in FlgJ, a bacterial protein involved in flagellar rod formation. Genes & genetic systems 81:381-389.
72. de la Mora J, Osorio-Valeriano M, González-Pedrajo B, Ballado T, Camarena L, Dreyfus G. 2012. The C terminus of the flagellar muramidase SltF modulates the interaction with FlgJ in Rhodobacter sphaeroides. Journal of bacteriology 194:4513-4520.
73. García-Ramos M, de la Mora J, Ballado T, Camarena L, Dreyfus G. 2021. Modulation of the enzymatic activity of the flagellar lytic transglycosylase SltF by rod components and the scaffolding protein FlgJ in *Rhodobacter sphaeroides*. Journal of Bacteriology 203:e00372-21.
74. Herlihey FA, Clarke AJ. 2017. Controlling Autolysis During Flagella Insertion in Gram-Negative Bacteria. Adv Exp Med Biol 925:41-56.
75. Schoenhals GJ, Macnab RM. 1996. Physiological and biochemical analyses of FlgH, a lipoprotein forming the outer membrane L ring of the flagellar basal body of Salmonella typhimurium. Journal of bacteriology 178:4200-4207.
76. Macnab RM. 2004. Type III flagellar protein export and flagellar assembly. Biochimica et Biophysica Acta (BBA)-Molecular Cell Research 1694:207-217.
77. Karlinsey JE, Pease AJ, Winkler ME, Bailey JL, Hughes KT. 1997. The flk gene of Salmonella typhimurium couples flagellar P-and L-ring assembly to flagellar morphogenesis. Journal of bacteriology 179:2389-2400.
78. Aldridge P, Hughes KT. 2002. Regulation of flagellar assembly. Current opinion in microbiology 5:160-165.
79. Erhardt M, Singer HM, Wee DH, Keener JP, Hughes KT. 2011. An infrequent molecular ruler controls flagellar hook length in Salmonella enterica. The EMBO journal 30:2948-2961.
80. Minamino T, Ferris HU, Moriya N, Kihara M, Namba K. 2006. Two parts of the T3S4 domain of the hook-length control protein FliK are essential for the substrate specificity switching of the flagellar type III export apparatus. Journal of molecular biology 362:1148-1158.
81. Yonekura K, Maki-Yonekura S, Namba K. 2002. Growth mechanism of the bacterial flagellar filament. Research in microbiology 153:191-197.
82. Renault TT, Abraham AO, Bergmiller T, Paradis G, Rainville S, Charpentier E, Guet CC, Tu Y, Namba K, Keener JP. 2017. Bacterial flagella grow through an injection-diffusion mechanism. Elife 6.
83. Shaikh TR, Thomas DR, Chen JZ, Samatey FA, Matsunami H, Imada K, Namba K, DeRosier DJ. 2005. A partial atomic structure for the flagellar hook of Salmonella typhimurium. Proceedings of the National Academy of Sciences of the United States of America 102:1023-1028.
84. Trachtenberg S, DeRosier DJ, Aizawa S-I, Macnab RM. 1986. Pairwise perturbation of flagellin subunits: The structural basis for the differences between plain and complex bacterial flagellar filaments. Journal of molecular biology 190:569-576.

85. Krupski G, Götz R, Ober K, Pleier E, Schmitt R. 1985. Structure of complex flagellar filaments in Rhizobium meliloti. Journal of bacteriology 162:361-366.
86. Scharf B, Schuster-Wolff-Bühring H, Rachel R, Schmitt R. 2001. Mutational Analysis of the Rhizobium lupini H13-3 andSinorhizobium meliloti Flagellin Genes: Importance of Flagellin A for Flagellar Filament Structure and Transcriptional Regulation. Journal of bacteriology 183:5334-5342.
87. Kreutzberger MA, Sobe RC, Sauder AB, Chatterjee S, Peña A, Wang F, Giron JA, Kiessling V, Costa TR, Conticello VP. 2022. Flagellin outer domain dimerization modulates motility in pathogenic and soil bacteria from viscous environments. Nature Communications 13:1-14.
88. Kreutzberger MA, Ewing C, Poly F, Wang F, Egelman EH. 2020. Atomic structure of the Campylobacter jejuni flagellar filament reveals how ε Proteobacteria escaped Toll-like receptor 5 surveillance. Proceedings of the National Academy of Sciences 117:16985-16991.
89. Götz R, Limmer N, Ober K, Schmitt R. 1982. Motility and chemotaxis in two strains of Rhizobium with complex flagella. Microbiology 128:789-798.
90. Minamino T, Imada K. 2015. The bacterial flagellar motor and its structural diversity. Trends in Microbiology 23:267-274.
91. Blair DF, Berg HC. 1990. The MotA protein of *E. coli* is a proton-conducting component of the flagellar motor. Cell 60:439-449.
92. Zhou J, Fazzio RT, Blair DF. 1995. Membrane Topology of the MotA Protein ofEscherichia coil. Journal of molecular biology 251:237-242.
93. Chun SY, Parkinson JS. 1988. Bacterial motility: membrane topology of the Escherichia coli MotB protein. Science 239:276-278.
94. Roujeinikova A. 2008. Crystal structure of the cell wall anchor domain of MotB, a stator component of the bacterial flagellar motor: implications for peptidoglycan recognition. Proceedings of the National Academy of Sciences 105:10348-10353.
95. Stolz B, Berg HC. 1991. Evidence for interactions between MotA and MotB, torque-generating elements of the flagellar motor of Escherichia coli. Journal of bacteriology 173:7033-7037.
96. Braun TF, Blair DF. 2001. Targeted disulfide cross-linking of the MotB protein of *Escherichia coli*: evidence for two H^+ channels in the stator complex. Biochemistry 40:13051-13059.
97. Deme JC, Johnson S, Vickery O, Aron A, Monkhouse H, Griffiths T, James RH, Berks BC, Coulton JW, Stansfeld PJ. 2020. Structures of the stator complex that drives rotation of the bacterial flagellum. Nature Microbiology 5:1553-1564.
98. Santiveri M, Roa-Eguiara A, Kühne C, Wadhwa N, Hu H, Berg HC, Erhardt M, Taylor NM. 2020. Structure and function of stator units of the bacterial flagellar motor. Cell 183:244-257. e16.
99. Hosking ER, Vogt C, Bakker EP, Manson MD. 2006. The *Escherichia coli* MotAB proton channel unplugged. Journal of Molecular Biology 364:921-937.
100. Zhou J, Lloyd SA, Blair DF. 1998. Electrostatic interactions between rotor and stator in the bacterial flagellar motor. Proceedings of the National Academy of Sciences 95:6436-6441.

101. Chang Y, Zhang K, Carroll BL, Zhao X, Charon NW, Norris SJ, Motaleb MA, Li C, Liu J. 2020. Molecular mechanism for rotational switching of the bacterial flagellar motor. Nature Structural Molecular Biology 27:1041-1047.
102. Lee LK, Ginsburg MA, Crovace C, Donohoe M, Stock D. 2010. Structure of the torque ring of the flagellar motor and the molecular basis for rotational switching. Nature 466:996-1000.
103. Duke T, Le Novere N, Bray D. 2001. Conformational spread in a ring of proteins: A stochastic approach to allostery1. Journal of molecular biology 308:541-553.
104. Bai F, Branch RW, Nicolau DV, Pilizota T, Steel BC, Maini PK, Berry RM. 2010. Conformational spread as a mechanism for cooperativity in the bacterial flagellar switch. Science 327:685-689.
105. Attmannspacher U, Scharf BE, Harshey RM. 2008. FliL is essential for swarming: motor rotation in absence of FliL fractures the flagellar rod in swarmer cells of Salmonella enterica. Mol Microbiol 68:328-41.
106. Partridge JD, Nieto V, Harshey RM. 2015. A new player at the flagellar motor: FliL controls both motor output and bias. mBio 6:e02367.
107. Suaste-Olmos F, Domenzain C, Mireles-Rodriguez JC, Poggio S, Osorio A, Dreyfus G, Camarena L. 2010. The flagellar protein FliL is essential for swimming in Rhodobacter sphaeroides. J Bacteriol 192:6230-9.
108. Jenal U, White J, Shapiro L. 1994. *Caulobacter* flagellar function, but not assembly, requires FliL, a non-polarly localized membrane protein present in all cell types. Journal of molecular biology 243:227-244.
109. Zhu S, Kumar A, Kojima S, Homma M. 2015. FliL associates with the stator to support torque generation of the sodium-driven polar flagellar motor of *Vibrio*. Molecular microbiology 98:101-110.
110. Lin T-S, Zhu S, Kojima S, Homma M, Lo C-J. 2018. FliL association with flagellar stator in the sodium-driven *Vibrio* motor characterized by the fluorescent microscopy. Scientific reports 8:1-12.
111. Suaste-Olmos F, Domenzain C, Mireles-Rodríguez JC, Poggio S, Osorio A, Dreyfus G, Camarena L. 2010. The flagellar protein FliL is essential for swimming in *Rhodobacter sphaeroides*. Journal of Bacteriology 192:6230-6239.
112. Takekawa N, Isumi M, Terashima H, Zhu S, Nishino Y, Sakuma M, Kojima S, Homma M, Imada K. 2019. Structure of *Vibrio* FliL, a new stomatin-like protein that assists the bacterial flagellar motor function. mBio 10:e00292-19.
113. Partridge JD, Nieto V, Harshey RM. 2015. A new player at the flagellar motor: FliL controls both motor output and bias. MBio 6:e02367-14.
114. Guo S, Xu H, Chang Y, Motaleb MA, Liu J. 2022. FliL ring enhances the function of periplasmic flagella. Proceedings of the National Academy of Sciences 119:e2117245119.
115. Carroll BL, Liu J. 2020. Structural Conservation and Adaptation of the Bacterial Flagella Motor. Biomolecules 10.
116. Shaw CH. 1991. Swimming against the tide: chemotaxis in Agrobacterium. BioEssays 13:25-29.
117. Armitage JP, Macnab RM. 1987. Unidirectional, intermittent rotation of the flagellum of Rhodobacter sphaeroides. Journal of Bacteriology 169:514-518.

118. Yen JY, Broadway KM, Scharf BE. 2012. Minimum requirements of flagellation and motility for infection of Agrobacterium sp. strain H13-3 by flagellotropic bacteriophage 7-7-1. Applied and environmental microbiology 78:7216-7222.
119. Stocker R. 2011. Reverse and flick: Hybrid locomotion in bacteria. Proceedings of the National Academy of Sciences 108:2635-2636.
120. Kühn MJ, Schmidt FK, Eckhardt B, Thormann KM. 2017. Bacteria exploit a polymorphic instability of the flagellar filament to escape from traps. Proceedings of the National Academy of Sciences 114:6340-6345.
121. Terashima H, Kawamoto A, Morimoto YV, Imada K, Minamino T. 2017. Structural differences in the bacterial flagellar motor among bacterial species. Biophysics and Physicobiology 14:191-198.
122. Onoue Y, Iwaki M, Shinobu A, Nishihara Y, Iwatsuki H, Terashima H, Kitao A, Kandori H, Homma M. 2019. Essential ion binding residues for Na+ flow in stator complex of the Vibrio flagellar motor. Scientific reports 9:1-16.
123. Asai Y, Kawagishi I, Sockett RE, Homma M. 1999. Hybrid motor with H+-and Na+-driven components can rotate Vibrio polar flagella by using sodium ions. Journal of Bacteriology 181:6332-6338.
124. Chang Y, Liu J. 2019. Architecture and assembly of periplasmic flagellum. Microbiology spectrum 7:7.4. 22.
125. Goldstein SF, Charon NW, Kreiling JA. 1994. Borrelia burgdorferi swims with a planar waveform similar to that of eukaryotic flagella. Proceedings of the National Academy of Sciences 91:3433-3437.
126. Beeby M, Ribardo DA, Brennan CA, Ruby EG, Jensen GJ, Hendrixson DR. 2016. Diverse high-torque bacterial flagellar motors assemble wider stator rings using a conserved protein scaffold. Proceedings of the National Academy of Sciences 113:E1917-E1926.
127. Rossmann FM, Beeby M. 2018. Insights into the evolution of bacterial flagellar motors from high-throughput in situ electron cryotomography and subtomogram averaging. Acta Crystallogr D Struct Biol 74:585-594.
128. Chaban B, Coleman I, Beeby M. 2018. Evolution of higher torque in Campylobacter-type bacterial flagellar motors. Scientific Reports 8:1-11.
129. Kaplan M, Ghosal D, Subramanian P, Oikonomou CM, Kjaer A, Pirbadian S, Ortega DR, Briegel A, El-Naggar MY, Jensen GJ. 2019. The presence and absence of periplasmic rings in bacterial flagellar motors correlates with stator type. Elife 8:e43487.
130. Braun TF, Al-Mawsawi LQ, Kojima S, Blair DF. 2004. Arrangement of core membrane segments in the MotA/MotB proton-channel complex of Escherichia coli. Biochemistry 43:35-45.
131. Leake MC, Chandler JH, Wadhams GH, Bai F, Berry RM, Armitage JP. 2006. Stoichiometry and turnover in single, functioning membrane protein complexes. Nature 443:355.
132. Heo M, Nord AL, Chamousset D, Rijn E, Beaumont H, Pedaci F. 2017. Impact of fluorescent protein fusions on the bacterial flagellar motor. Scientific reports 7:12583.
133. Tusk SE, Delalez NJ, Berry RM. 2018. Subunit exchange in protein complexes. Journal of molecular biology 430:4557-4579.

134. Kaplan M, Oikonomou CM, Wood CR, Chreifi G, Subramanian P, Ortega DR, Chang YW, Beeby M, Shaffer CL, Jensen GJ. 2022. Novel transient cytoplasmic rings stabilize assembling bacterial flagellar motors. The EMBO Journal:e109523.
135. Platzer J, Sterr W, Hausmann M, Schmitt R. 1997. Three genes of a motility operon and their role in flagellar rotary speed variation in *Rhizobium meliloti*. Journal of Bacteriology 179:6391-6399.
136. Eggenhofer E, Haslbeck M, Scharf B. 2004. MotE serves as a new chaperone specific for the periplasmic motility protein, MotC, in *Sinorhizobium meliloti*. Molecular Microbiology 52:701-712.
137. Parkinson JS, Ames P, Studdert CA. 2005. Collaborative signaling by bacterial chemoreceptors. Current opinion in microbiology 8:116-121.

FIGURES

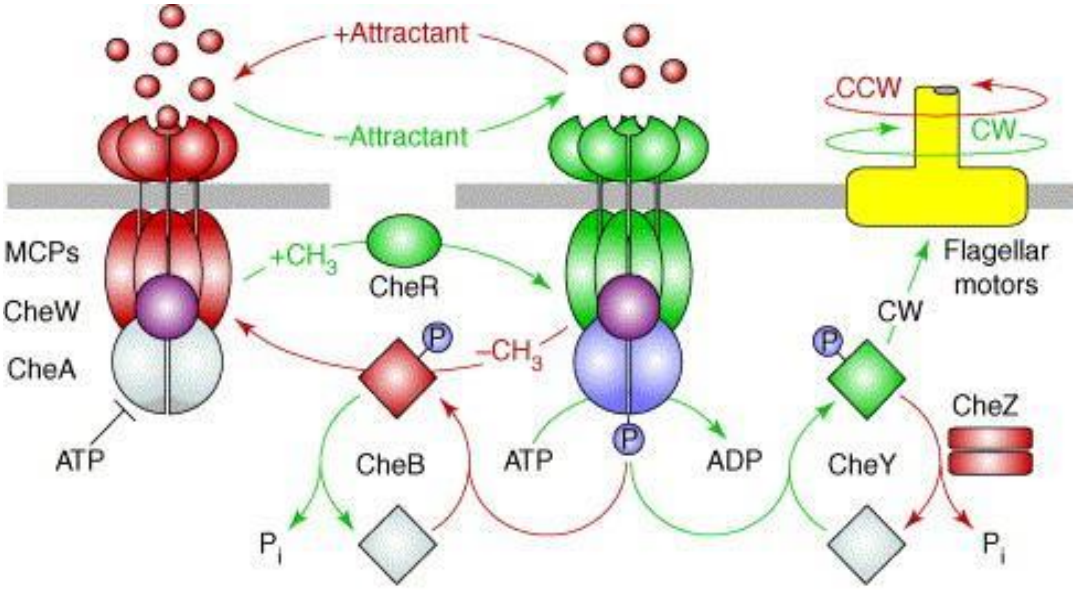

FIGURE 1.1 Chemotaxis in *E. coli*. Environmental attractants interact with the LBD of MCP-CheW-CheA complexes resulting in decreased phosphorylation by CheA and no interactions between CheY and the flagellar motor. Alternatively, loss of attractants results in increased CheA autophosphorylation leading to subsequent phosphorylation of CheY by CheA-P. CheY-P interacts with the flagellar motor to alter motor rotation form CCW to CW. CheZ dephosphorylates CheY-P to terminate the signal. CheR of the methylation adaptation system methylates MCP signaling domains while phosphorylated CheB demethylates MCPs. Image from (137). Image falls within the terms of "fair use" as determined by the Fair Use Indicator Tool (https://librarycopyright.net/resources/fairuse/howitworks.php).

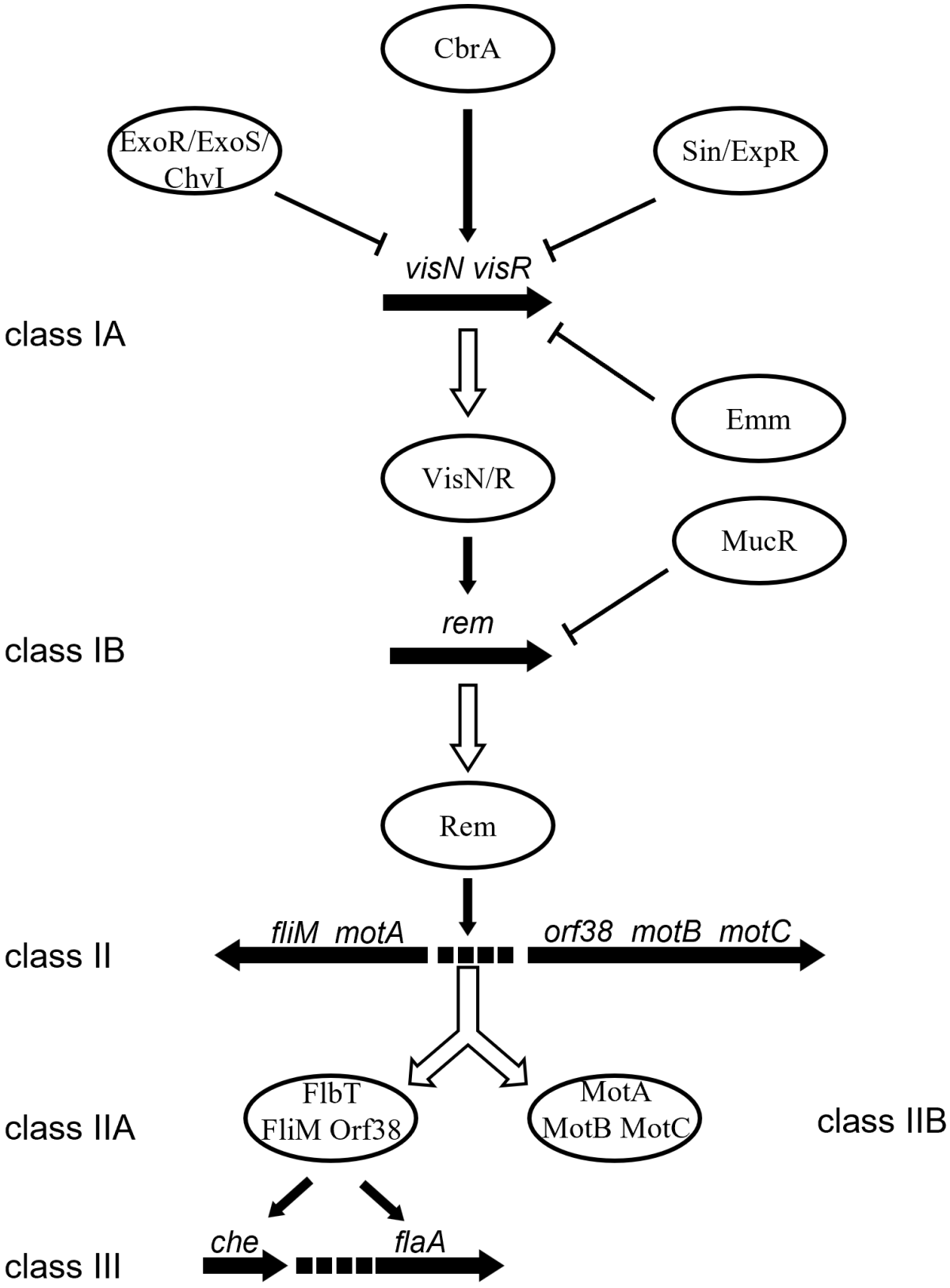
CbrA
ExoR/ExoS/
ChvI
Sin/ExpR
visN visR
class IA
Emm
VisN/R
MucR
rem
class IB
Rem
fliM motA
orf38 motB motC
class II
FlbT
FliM Orf38
MotA
MotB MotC
class IIA
class IIB
che
flaA
class III

FIGURE 1.2 Regulation of flagella and chemotaxis genes in *S. meliloti*. The class IA genes, *visN* and *visR*, are expressed throughout growth and the protein products, VisN/R, control transcription of the class IB gene, *rem*, by influencing the P1 and P2 promoters. During exponential growth, Rem positively regulates its own transcription from the P1 promoter, as well as that of class II genes. The class IIA gene products, FliM and Orf38, in turn upregulate the class III genes involved in chemotaxis (*che*) and *flaA*. Class IIB gene products, MotA, MotB, and MotC, do not influence transcription of other flagellar or chemotaxis genes. Image from (57). Image falls within the terms of "fair use" as determined by the Fair Use Indicator Tool (https://librarycopyright.net/resources/fairuse/howitworks.php).

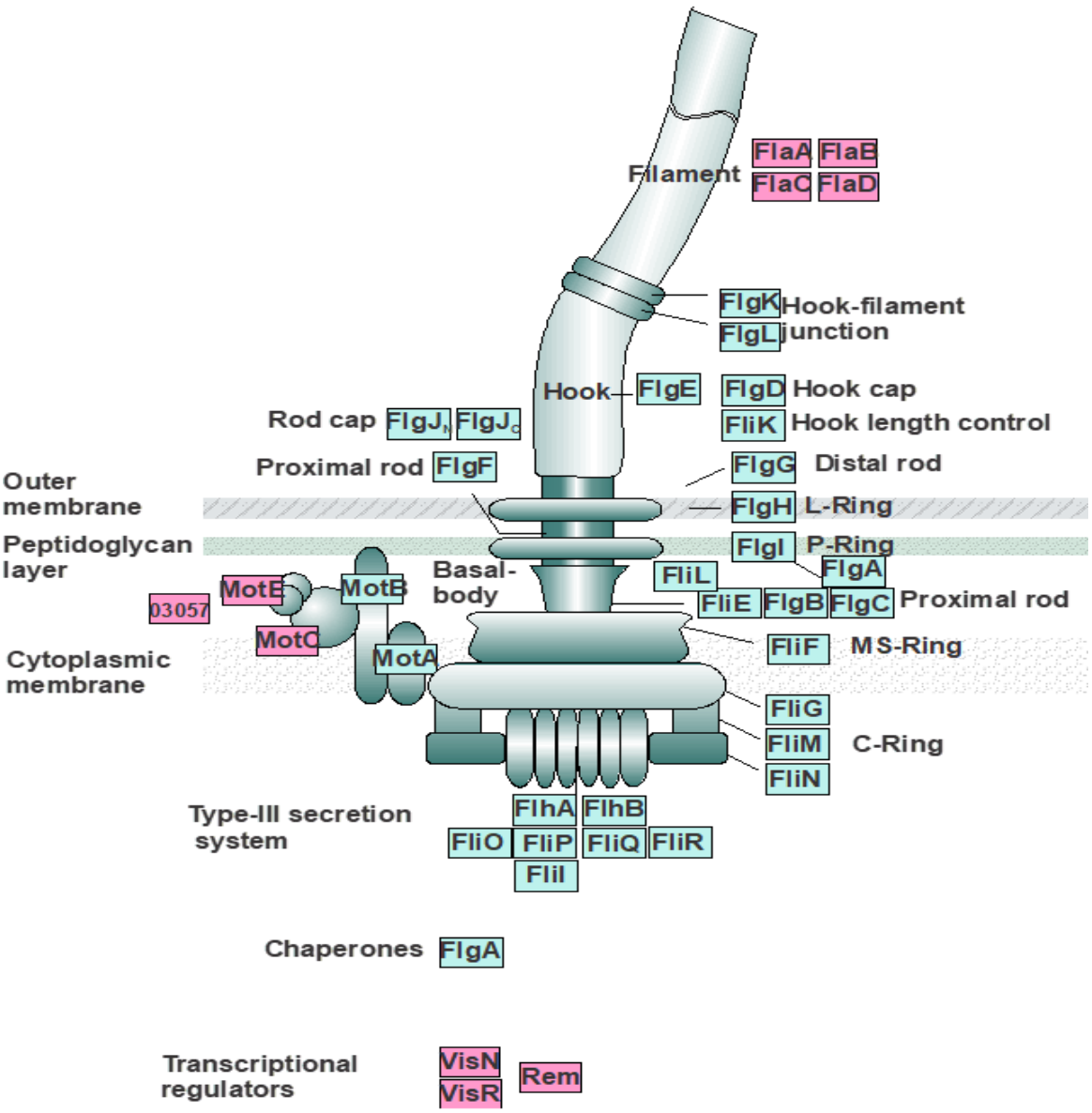
Filament
FlaA
FlaB
FlaC
FlaD
FlgK
Hook-filament
FlgL
junction
Hook
FlgE
FlgD
Hook cap
FliK
Hook length control
Rod cap
FlgJ
FlgJ
Proximal rod
FlgF
FlgG
Distal rod
Outer
membrane
FlgH
L-Ring
Peptidoglycan
layer
FlgI
P-Ring
FlgA
Basal-
body
FliL
MotB
MotE
03057
FliE
FlgB
FlgC
Proximal rod
MotC
FliF
MS-Ring
Cytoplasmic
membrane
MotA
FliG
FliM
C-Ring
FliN
FlhA
FlhB
Type-III secretion
system
FliO
FliP
FliQ
FliR
FliI
Chaperones
FlgA
Transcriptional
regulators
VisN
VisR
Rem

FIGURE 1.3 Components of the flagellum of *E. coli* (green) and additional/alternative flagellar proteins found in *S. meliloti* (pink). The flagellar basal body is composed of the stator, made up of MotA and MotB, and the rotor which is in turn comprised of the C-ring (FliG, FliM, and FliN), the MS-ring (FliF), and the rod (FlgB, FlgC, FlgF, and FlgG). In *S. meliloti*, MotC and MotE are involved in stabilization of MotB, and MotF (03057) may play a role in proper motor function. The rod runs through and rotates within the bushing-like ring proteins, FlgI (the P-ring embedded in the peptidoglycan layer) and FlgH (the L-ring embedded in the lipopolysaccharide layer). FlgA acts as a chaperone for FlgI. A type III secretion system composed of FlhA, FlhB, FliO, FliP, FliQ, FliR, and FliI sits within the basal body and exports periplasmic and extracellular components of the flagellum. The hook (comprised of FlgE) extends out from and rotates with the rod to rotate the flagellar filament. Proper assembly of the hook requires the hook cap protein, FlgD, and hook length-control protein, FliK. The hook and filament are joined by adapter proteins, FlgL and FlgK. The filament consists of thousands of copies of FliC in *E. coli* or FlaA, FlaB, FlaC, and FlaD in *S. meliloti*. A homolog or analog of filament cap of *E. coli*, called FliD (not shown), has not been identified in *S. meliloti*. VisN, VisR, and Rem functionally replace the master regulators of flagellar genes, FlhD and FlhC. Figure provided by and used with permission from Dr. Scharf.

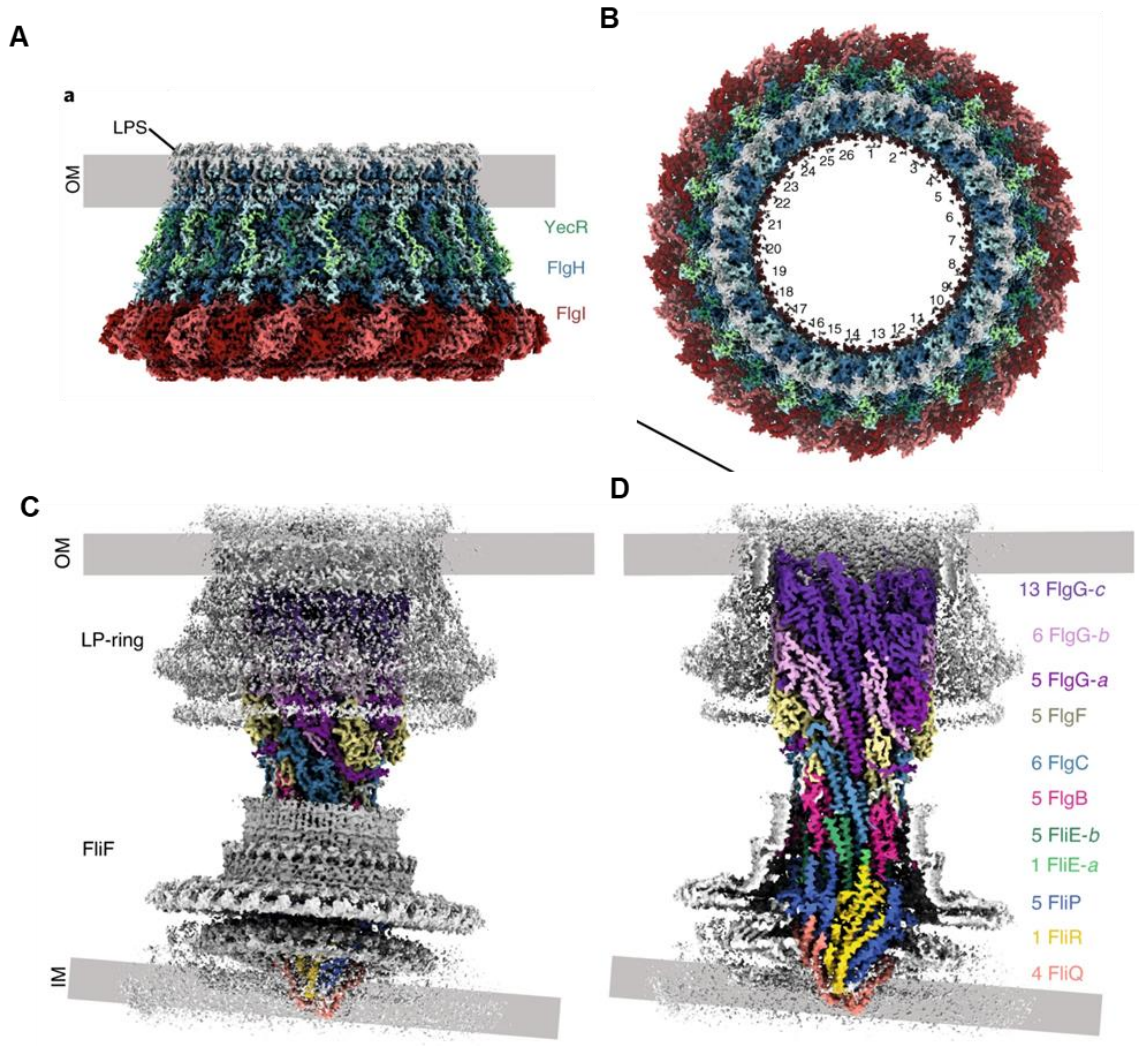

Figure 1.4 Image reconstruction of the LP-ring bushing structure (A and B) and the intact core flagellar rotor structure including most of the fT3SS components (FliPQR) and all rod components (FliE and FlgBCFG; B and C). The periplasmic region of the MS-ring (FliF) is also shown. Image adapted from (65). This is a U.S. government work and not under copyright protection in the U.S.

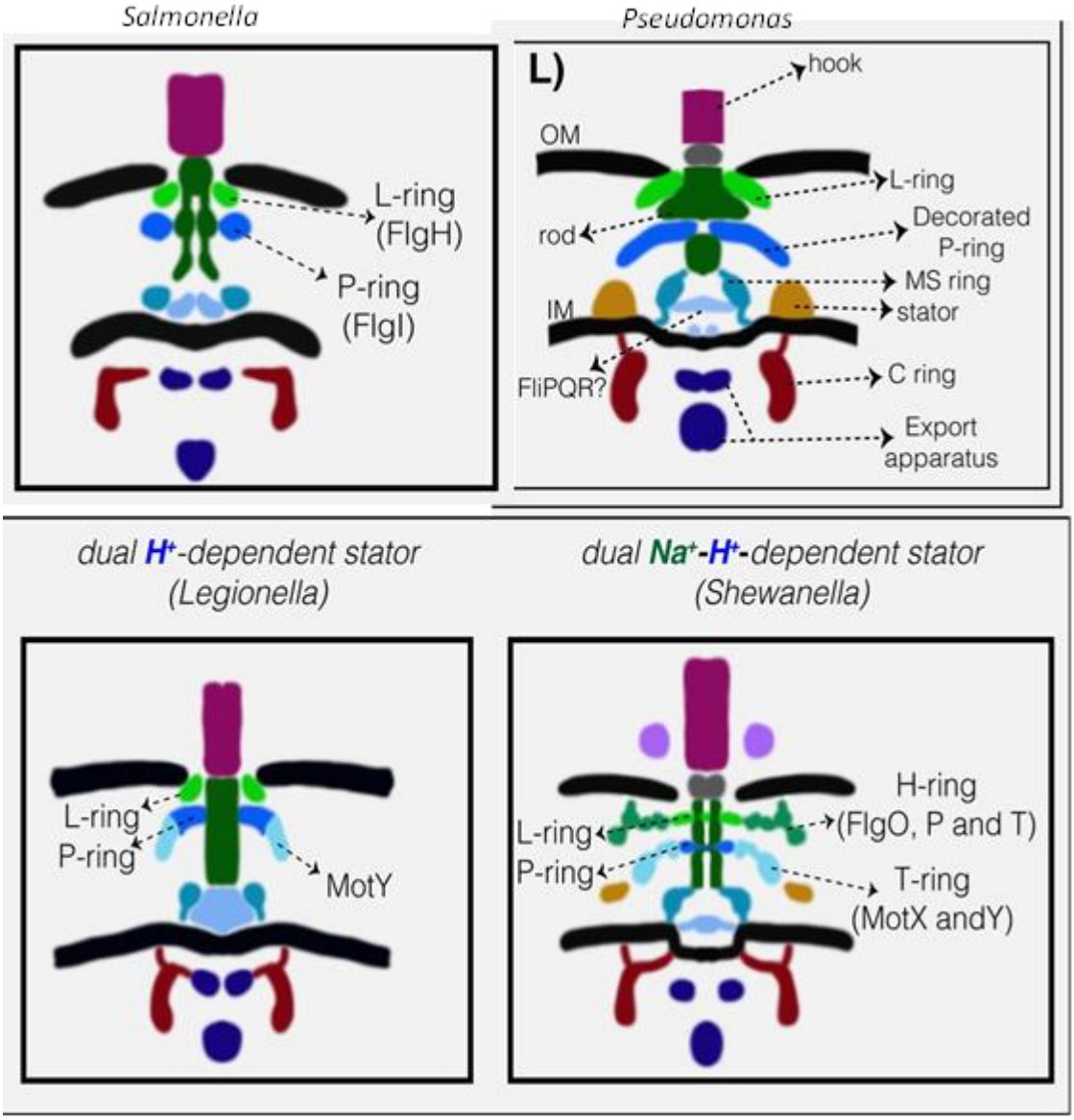

Figure 1.5 Representative images of the paradigm flagellar motor structures exemplified by (A) *Salmonella* and additional substructures found in the flagellar motors of (B) *Pseudomonas*, (C) *Legionella*, and (D) *Shewanella*. Image adapted from (129).

Chapter 2: FliL and its paralog MotF have distinct roles in the stator activity of the *Sinorhizobium meliloti* flagellar motor

Running Title: FliL and MotF have distinct roles in stator activity

RICHARD C. SOBE[a], CRYSTAL GILBERT[a], LAM VO,[b]† GLADYS ALEXANDRE[b], AND BIRGIT E. SCHARF[a]#

[a]Department of Biological Sciences, Life Sciences I, Virginia Tech, Blacksburg, VA, USA
[b]Department of Biochemistry and Cell and Molecular Biology, University of Tennessee at Knoxville, Knoxville, TN, USA

Key words: chemotaxis, flagellar basal body, proton channel plug, swimming motility, torque generation

#Address correspondence to Birgit E. Scharf, bscharf@vt.edu

†Present address: Molecular Cellular and Developmental Biology and Physics, Yale Science Building, Yale University, New Haven, CT, 06511

Attribution: RCS performed all experiments except where noted otherwise here. CG made the MotF overexpression construct, purified MotF protein for rabbit immunizations and assisted with time course β-galactosidase assays. LV developed the MATLAB tethering scripts used for tethering analysis under the supervision of GA. RCS and BS wrote the manuscript.

ABSTRACT

The bacterial flagellum is a complex macromolecular machine that drives bacteria through diverse fluid environments. Although many components of the flagellar motor are conserved across species, the roles of FliL are numerous and species-specific. Here, we have characterized an additional player required for flagellar motor function in *Sinorhizobium meliloti*, MotF, which we have identified as a FliL paralog. We performed a comparative analysis of MotF and FliL, identified interaction partners through bacterial two-hybrid and pull-down assays and investigated their roles in motility and motor rotation. Both proteins form homooligomers, interact with each other, and with the stator proteins MotA and MotB. The Δ*motF* mutant exhibits normal flagellation but its swimming behavior and flagellar motor activity is severely impaired and erratic. In contrast, the Δ*fliL* mutant is mostly aflagellate and nonmotile. Amino acid substitutions in cytoplasmic regions of MotA or disruption of the proton channel plug of MotB partially restored motor activity to the Δ*motF* but not the Δ*fliL* mutant. Altogether, our findings indicate that both, MotF and FliL, are essential for flagellar motor torque generation in *S. meliloti*. FliL may serve as a scaffold for stator integration into the motor, and MotF is required for proton channel modulation.

INTRODUCTION

Bacterial flagellar motility is a complex process whereby chemotactic signals culminate in the control of flagellar motor rotation to drive bacteria towards favorable and away from harmful conditions. The extensive evolutionary history and distinct selective pressures imparted by diverse environmental habitats correspond to the variability found in the regulation, structure, and function of the flagellar machinery from diverse bacterial species (138-143). Nonetheless, a core set of flagellar structural features are conserved across the bacterial kingdom. The basal body at the proximal end of the flagellum is anchored in the cell membrane and is comprised of a trans-envelope axial rod and connected to the MS-ring in the inner membrane and the C-ring on the cytoplasmic face of the MS-ring (144). A peptidoglycan-associated P-ring and lipopolysaccharide-associated L-ring together form a bushing between the rod and cell wall components during flagellar rotation (145). A short flexible hook is attached to the extracellular end of the rod and is followed by a rigid helical flagellar filament of up to several microns in length (38).

Rotation of the continuous basal body-hook-filament structure is mediated by conversion of ion motive force formed across the inner membrane into rotational energy by stator proteins MotA and MotB (or PomA and PomB in the Na^+-driven motors of *Vibrio* species). Between 11 to 18 stator units form studs around the rotor, with each stud consisting of five MotA and two MotB units (98, 129, 146). Each MotA monomer contains four transmembrane (TM) helices with a large cytoplasmic loop between TM2 and TM3 and a cytoplasmic C-terminal tail distal to TM4 (91). MotB contains a short cytoplasmic N-terminal domain followed by a transmembrane domain, and a large periplasmic domain comprised of a proton channel plug region and an OmpA-like peptidoglycan-binding domain near the C-terminus (99, 147, 148). Prior to assembling into the flagellar motor, inactive stator complexes form in the inner membrane with one MotB dimer surrounded by a MotA pentamer (97, 98, 141). Two proton channels formed by the transmembrane domains of MotA and MotB are locked in a closed state by the periplasmic plug regions of each MotB monomer wedged between short periplasmic stretches of MotA (149). Once contact is made between the cytoplasmic loop of MotA and the C-ring component FliG, conformational changes in the stator units cause extension of the MotB periplasmic domains such that the peptidoglycan-binding domain of MotB associates with peptidoglycan to stabilize the stators near the basal body and the proton channel plug of MotB assumes an open conformation (94, 147, 150-153). As protons flow through the now-open stator proton channels, conformational changes in the $MotA_5B_2$ complexes cause clockwise rotation of the MotA pentamer around the MotB dimer, which - through interactions between MotA and FliG - imparts opposite rotation of the axial components of the flagellum to provide thrust (141).

In the last two decades, another ubiquitous flagellar motor component, FliL, has gained considerable attention given its variable roles in flagellar motility (Figure S2.1). FliL is a membrane protein that is primarily localized in the periplasm where it is generally thought to interact with MotA and MotB. However, *fliL* mutant phenotypes differ considerably across the bacterial kingdom and a definitive role for FliL has yet to be determined. In several bacterial species, FliL has been implicated in various aspects of stator activity including stator assembly, association with the rotor, torque generation, surface sensing, and proton channel modulation as well as roles in flagellar filament (or rod) stability and orientation (108-113, 149, 154-168).

Efficient flagellar-driven movement in bacterial chemotaxis depends on the extension of run lengths in favorable directions and the decrease of tumbling events to reorient bacteria when less favorable conditions are detected. In peritrichous bacteria, runs are driven by synchronous rotation of several flagella in a propulsive flagellar bundle to provide thrust. Tumbling events are caused by disruption of the flagellar bundle when one or more flagella switch the direction of rotation from counterclockwise to clockwise or by slowing or pausing flagellar rotation (138). Tumbling mechanisms are best understood in the switch-type motors of *Escherichia coli* and *Salmonella typhimurium*, whereby the phosphorylated response regulator CheY binds to the C-ring (switch) components FliM and FliN causing conformational changes that result in a greater C-ring diameter (169). This restructuring of the C-ring causes reorganization of MotA-FliG contacts such that continued clockwise rotation of the stator units now drives clockwise rotation of the rotor (97, 146). The soil-dwelling plant symbiont *Sinorhizobium meliloti* employs a speed-variable unidirectional flagellar motor, which rotates solely in the CW direction and asynchrony of flagellar motor rotation induces bundle separation and cell tumbling (50). Molecular corollaries to these observations are found with the presence of additional motor proteins in *S. meliloti*, namely a periplasmic protein MotC and its chaperone MotE (135, 136). MotC is believed to interact with MotB; however, its role in flagellar motor function has yet to be elucidated.

Here, we describe MotF as a novel flagellar motor component and paralog of FliL in *S. meliloti*. MotF and FliL possess one transmembrane domain and reside mostly in the periplasm where both proteins engage in interactions with the stator components MotA and MotB. However, while Δ*motF* and Δ*fliL* mutants exhibit severe reductions in swimming motility and defects in flagellar motor function, a very small population of the normally flagellated Δ*motF* mutant retains poor swimming motility while the generally aflagellate Δ*fliL* mutant is nonmotile. Furthermore, we demonstrate that second-site mutations in the stator components MotA or MotB partially restore motility to the Δ*motF* but not the Δ*fliL* mutant.

RESULTS

Identification of three new flagellar genes and one new motor gene in *Sinorhizobium meliloti*

In a search of additional genes involved in *S. meliloti* motility, a mini-Tn5 transposon mutagenesis screen of the wild-type *S. meliloti* strain RU11/001 was carried out on soft agar swim plates. Upon sequencing of transposon insertion sites for 26 mutants with observed motility defects, the majority of insertions occurred within known flagellar genes. One mutant, however, contained an insertion in the gene locus *SMc03057*, which is one of four uncharacterized genes clustered immediately downstream of *fliR*, the last annotated gene of the contiguous flagellar regulon on the *S. meliloti* chromosome (Figure 2.1A). To confirm that *SMc03057* contributes to flagellar motility and to determine the role of the other three genes in motility, strains with in-frame deletions were constructed and tested for swimming proficiency on soft agar swim plates (Figure 2.1B). All four mutants exhibited a loss of motility in this assay. A BLAST search of the gene products revealed that SMc03071 shares homology with the N-terminal rod-binding domain of FlgJ ($FlgJ_N$) while SMc03072 is a homolog of the type-three secretion system chaperone FlgN involved in secretion of the hook-associated proteins FlgK and FlgL (170, 171). A search with SMc03057 resulted in matches with a FliL-like protein in *Agrobacterium tumefaciens* or hypothetical proteins in an array of alphaproteobacteria, while SMc03056 did not yield any homology or domain similarities to other characterized proteins using SignalP, TMHMM, and Pfam (Table 2.1) (172-174).

Flagellar gene transcription and biosynthesis occur in a hierarchical manner with production of flagellin and assembly of the filament taking place after completion of the basal body and hook structures (38, 57). Therefore, to determine if any of these genes are required for flagellar synthesis, we analyzed the production of flagellin proteins by immunoblot analysis. Three of the four mutants did not produce flagellin; however, the Δ*SMc03057* strain produced flagellin at levels comparable to wild type (Figure 2.1C). In agreement with these results, we found that the promoter activity of the principle flagellin gene *flaA* (P*flaA*) was markedly reduced for the three mutants lacking flagellin production throughout the motility phase of cell culture growth when compared to the wild type (Figure S2.2). Such downregulation of *flaA* transcription has been reported for mutants defective in basal body production (58). This result was expected for Δ*SMc03071* and Δ*SMc03072* considering the predicted structural roles of $FlgJ_N$ and FlgN in

basal body synthesis. These analyses also categorized the hypothetical gene *SMc03056* as flagellar assembly or structural gene. In contrast, the *flaA* promoter activity in the Δ*SMc03057* strain was mostly comparable to wild type (Figure S2.2). The finding that the deletion of *SMc03057* resulted in a non-motile (Figure 2.1B) but flagellin-producing mutant (Figure 2.1C and Figure S2.2) defined it as motility gene, and we thus named it *motF*. The Δ*motF* motility defect was complemented upon ectopic expression from a self-replicating plasmid (Figure S2.3). When the Δ*motF* strain was viewed by phase contrast microscopy, most of the cells in the population were nonmotile. Interestingly, a very small percentage of cells exhibited slow swimming motility interrupted by frequent jerking and pauses, and abrupt directional changes. Altogether, these results suggested that MotF is required for flagellar function but not synthesis, and its role in motility was further characterized.

MotF is a distantly related paralog of *S. meliloti* FliL

An NCBI BLASTP search of the nonredundant database with the MotF amino acid sequence yielded results for many hypothetical proteins from various rhizobial species as well as proteins from the FliL family in *Agrobacterium tumefaciens* (51% identity) and *Rhizobiaceae* bacterium LC148 (49% identity). FliL is described as an enigmatic protein with diverse roles in flagellar swimming and swarming in *E. coli*, *S. typhimurium*, *Vibrio alginolyticus*, *Rhodobacter sphaeroides*, *Caulobacter crescentus*, and *Bradyrhizobium diazoefficiens*, surface sensing in *Proteus mirabilis*, and flagellar orientation in *Borrelia burgdorferi* (Figure S2.1) (108-111, 113, 155, 156, 159, 161, 163, 166, 168, 175). The flagellar regulon of *S. meliloti* contains a gene annotated as *fliL* located between the L-ring encoding *flgH* and the flagellar biosynthetic gene *fliP* (Figure S2.4). However, the role of FliL in *S. meliloti* swimming motility had yet to be determined. A multiple sequence alignment of *S. meliloti* MotF and FliL with FliL sequences from diverse bacterial species revealed that *S. meliloti* FliL aligns more closely with FliL from other species than with *S. meliloti* MotF (Figure 2.2A and Table S2.1) implying that MotF is a FliL paralog with substantial evolutionary divergence from the ancestral protein. It should be noted that the genomes of *V. alginolyticus* and *R. sphaeroides* encode two *fliL* gene copies. However, each FliL functions separately in independent flagellar motor systems in these two species (112, 155).

The *V. alginolyticus* FliL structure has been determined (Figure 2.2B) (112) and was used to generate a structural model of *S. meliloti* MotF using the SWISS-MODEL server. The *V. alginolyticus* FliL segment encompassing amino acid residues 40 to 167 (PDB ID: 6AHQ) was used to model MotF residues 38-140 (Figure 2.2C). Although low QMEAN (-4.64), GMQE (0.28), and QMEANDisCo (0.45 ± 0.08) scores suggested an overall low confidence, the homology model supports a possible evolutionary link between MotF and FliL. These data indicate that MotF is a highly divergent FliL paralog in *S. meliloti* and related bacteria.

The *fliL* deletion mutant is nonmotile and exhibits reduced flagellation and *flaA* gene transcription

The evolutionary relatedness of MotF and FliL led us to an initial motility assessment of an in-frame *fliL* deletion mutant. The Δ*fliL* strain is nonmotile on soft agar swim plates (Figure 2.3A) and appeared similarly nonmotile when observed by phase contrast microscopy. We used immunoblot analysis to compare flagellin levels in the Δ*fliL* strain with wild type, the Δ*motF* strain and a Δ*flaA* strain, which has previously been shown to exhibit reduced flagellation (Figure 2.3B) (176). The Δ*fliL* strain exhibited substantially reduced flagellin levels comparable to the Δ*flaA* strain. Additionally, while the wild type and the Δ*motF* strain were similarly flagellated as determined by transmission electron microscopy, the Δ*fliL* strain was mostly aflagellate (Figure 2.3C).

To determine whether the loss of FliL causes a dysregulation of *flaA* transcription, we investigated P*flaA* activity in the Δ*fliL* strain (Figure 2.3D). Transcription of *flaA* was about 50% reduced compared to wild type or the *motF* deletion strain, which both exhibit normal flagellation. Furthermore, the reduction of P*flaA* was greater than that of the Δ*fliM* strain, which served as a measure for low P*flaA* activity due to feedback inhibition by accumulation of intracellular flagellin (58). In conclusion, the presence of FliL is required for wild-type P*flaA* gene transcription and production of flagellar filaments, whereas MotF appears more strictly linked to flagellar motor function.

MotF protein architecture resembles that of FliL

All known FliL proteins have a short (comprised of less than 15 aa) N-terminal region in the cytoplasm and a single transmembrane domain, with the remainder of the protein residing in the

periplasm. Bioinformatics analysis of *S. meliloti* FliL using the TMHMM server for transmembrane domain prediction were in good agreement with this protein organization: aa 1-12 were predicted to be localized in the cytoplasm, aa 13-35 to form a transmembrane helix, and aa 36-163 to be localized in the periplasm (Fig. 2A) (112, 113, 174). A domain prediction for *S. meliloti* MotF by TMHMM yielded similar results (174). In contrast, consensus predictions by programs such as SignalP 5.0 suggested that the hydrophobic N-terminal region in MotF serves as a signal peptide with a canonical AXA signal peptidase I cleavage site after aa 28 for secretion of the protein into the periplasm (Figure 2.2A, 2.4A). If MotF (20.5 kDa) is translated as a pre-protein, the cleavage by a signal peptidase would yield a mature MotF (MotF*) of 17.5 kDa. To investigate the size of MotF and to gain insight into its subcellular location, a series of biochemical analyses were performed. Immunoblot analysis of *S. meliloti* wild-type cell lysates detected MotF at the full-length size of 20.5 kDa compared to purified recombinant MotF* at 17.5 kDa indicating that MotF is not being cleaved (Figure 2.4A). To confirm that MotF is localized to the membrane via its N-terminal transmembrane domain, we performed cell fractionation experiments and probed for MotF in the soluble and membrane fractions (Figure 2.4B). The majority of MotF was detected in the membrane fraction. The small amount of MotF in the cytoplasm likely stems from translated protein that has yet to be inserted into the membrane.

Next, we sought to determine the orientation of the MotF transmembrane domain by employing the dual reporter plasmid system pKTop (177, 178). The pKTop system drives production of a fusion protein comprised of a protein of interest translationally fused at the C-terminus to the *E. coli* alkaline phosphatase (AP, encoded by *phoA*) and the alpha subunit of β-galactosidase (encoded by *lacZα*), which are only active in the periplasm and cytoplasm, respectively. Periplasmic AP converts the substrate X-Pho to an insoluble blue precipitate while cytoplasmic LacZα converts a substrate Red-Gal to an insoluble red precipitate. Control plasmids include the unmodified pKTop plasmid, which produces a AP-LacZα fusion protein that remains in the cytoplasm, and a periplasmic control plasmid encoding the first outward-facing transmembrane domain of *E. coli* YmgF (YmgF$_{1-39}$) fused to AP-LacZα (177, 178). When we introduced a pKTop derivative harboring the full-length *motF* coding sequence into *E. coli* DH5α and plated transformants on LB agar supplemented with X-Pho, we observed blue coloration comparable to a periplasmic control strain indicating that the C-terminus of MotF is located in the periplasm

(Figure 2.4C). To confirm that the MotF transmembrane domain alone is sufficient to place PhoA-LacZα in the periplasm, we introduced the corresponding MotF coding region (aa 1-28) into pKTop. Transformants harboring this construct also produced a blue coloration. Altogether, these data demonstrate that MotF contains an N-terminal transmembrane domain and that the majority of the protein is located in the periplasm similar to FliL homologs characterized to date.

The MotF interactome resembles the FliL interactome

FliL from *S. enterica* and *V. alginolyticus* have been reported to exhibit self-interaction, as well as interactions with the MS ring component FliF and the stator proteins MotA and MotB (112, 113). To determine how *S. meliloti* FliL and MotF compare in their respective interactomes to FliLs from other species, we performed bacterial two-hybrid (BACTH) analyses for FliL and MotF with various basal body and stator components using MacConkey plates and quantitative colorimetric β-galactosidase assays. We transformed *E. coli* BTH101 Δ*flhC* with pKT25 and pUT18C derivatives to avoid interference from the host flagellar machinery (113). Similar to previous reports with other FliLs, we determined that *S. meliloti* FliL interacts strongly with itself and moderately with both stator components MotA and MotB (Figure 2.5A and B). The BACTH data suggested that FliL interacts with FliF but not FliG while the β-galactosidase data showed the opposite. However, it should be noted that Partridge *et al.* also reported weak and inconsistent interactions between FliL and both basal body components (113). Intriguingly, FliL interacted strongly with MotF. When we performed the BACTH experiments with MotF and the various basal body and stator components, we found similar interaction as described above for FliL. MotF interacted strongly with itself and FliL, moderately with MotA, and weakly with MotB and possibly FliF, but not with FliG (Figure 2.5C and D). Control experiments with protein pairs such as MotA/MotA and MotA/MotB yielded the expected positive interactions (Table S2.2). However, interactions could not be detected between other known interacting pairs such as MotA/FliG and FliF/FliG, perhaps due to limitations of expressing functional and/or stable FliF and FliG proteins in the heterologous *E. coli* host. Altogether, these results demonstrate that *S. meliloti* FliL and its paralog MotF form homooligomers, interact with each other, and interact with both stator components.

To provide additional evidence of MotF interaction partners, we performed immobilized metal affinity chromatography (IMAC) pull-down assays. Candidate interaction partners, each fused

N-terminally to a 6xHis tag, were used as bait, coexpressed with MotF as prey, pulled down via IMAC, and assayed using anti-MotF antiserum. We also included MotC in this experiment, which is an alphaproteobacteria-specific protein that is required for flagellar motor function in *S. meliloti* (135). The cytoplasmic chemotaxis protein CheR was employed as a negative control. As seen in Figure 2.6, MotF could be detected robustly in pull-down fractions with 6xHis-FliL and 6xHis-MotA, weakly with 6xHis-MotC, and very weakly with 6xHis-MotB, but not with, -FliF, -FliG, or -CheR. Importantly, we were able to detect all our bait proteins with an anti-His-antibody in corresponding soluble and pull-down fractions except for FliF, presumably due to solubilization issues (data not shown). Altogether, these data further indicate that MotF and FliL interact with each other and that MotF interacts with MotA, MotB, and MotC.

The periplasmic domain of MotF forms multimers and interacts with MotC and the periplasmic domain of MotB

We next tested whether the periplasmic region of MotF (MotF*) alone can interact with the periplasmic regions of MotB (MotB*) and FliL (FliL*), and with MotC by BACTH analysis and *in vitro* crosslinking with purified proteins. The BACTH assay detected self-interactions for MotF*, MotB*, and FliL* but not between different proteins (Table S2.3). It is conceivable to speculate that the conditions in the cytosolic environment were unsupportive of these protein-protein interactions. However, using *in vitro* crosslinking of purified proteins with glutaraldehyde, we detected interactions of MotF* with MotB* (Figure 2.7B) and with MotC (Figure 2.7C) but not with FliL* (Figure 2.7A). MotF* was detected as a monomer at ~18 kDa without crosslinker or as a monomer, homodimer (~36 kDa), and homotrimer (~54 kDa) when glutaraldehyde was present in the reaction mixture. In addition to these signals, we discovered high molecular weight complexes of 75-250 kDa in cross-linking reactions with MotF* and MotB* or MotC suggesting that they associate with and promote higher-degree MotF* oligomerization. Taken together, we infer that the periplasmic domain of MotF is sufficient for the formation of homo-oligomers and to interact with MotB and MotC, but that MotF and FliL might associate via their transmembrane domains.

MotF and FliL stabilize each other

We have shown that MotF and FliL interact with each other as well as with the stator components MotA and MotB. Thus, we asked whether FliL and the Mot proteins promote

stability of one another (179). To investigate this possibility, we first compared cellular levels of MotF in mutants lacking individual *mot* genes or *fliL*. As presented in Figure 2.8A, MotF levels in the Δ*motA*, Δ*motB*, and Δ*motC* strains are comparable to those in wild type and in the control strain Δ*cheY1* implying that individual Mot proteins are not required for MotF stability. In contrast, MotF levels were reduced in the Δ*fliL* strain suggesting that MotF requires FliL for stability (Figure 2.8A). We also investigated whether MotB, MotC, or FliL require MotF for normal cellular abundance (Figure 2.8B-D). While MotB and MotC levels in the Δ*motF* strain were comparable to wild type, FliL levels were strongly reduced in the absence of MotF. Altogether, these results imply that the interaction between MotF and FliL promotes their stability and integration into the *S. meliloti* flagellar motor.

The *motF* and *fliL* deletion strains exhibit severely impaired but distinct motility phenotypes

An initial test of the *motF* and *fliL* deletion strains showed that neither mutant is able to spread on soft agar plates (Figure 2.1B, Figure S2.3, and Figure 2.3A). However, a quantitative analysis indicated that Δ*motF* produces swim rings that are slightly larger than those formed by Δ*fliL* (Figure S2.5). To thoroughly assess swimming motility behavior, we determined percentages of motile cells and free-swimming velocities of bacteria by phase contrast microscopy and computerized motion analysis using TumbleScore (180). The percentage of free-swimming Δ*motF* cells was reduced by nearly 20-fold to 2.1 ± 0.5% compared to 36.0 ± 8.2% for the wild-type population (Figure 2.9A and Table 2.2). For the small motile population of Δ*motF* cells, average swimming velocities were 10.9 ± 0.6 μm/s, which was about 70% lower than that of the wild type (37.7 ± 1.7 μm/s). Thus, the swimming defect exhibited by the Δ*motF* strain is due to a substantial reduction of the motile population and severely reduced swimming velocity. The Δ*fliL* strain was nonmotile, with the exception of an extremely low number of cells (<1%) that exhibited stationary rotational movement.

The decreased swimming capacity exhibited by Δ*motF* could be caused by reduced flagellar motor rotation or the inability to form a propulsive bundle due to asynchronized rotation of flagellar motors along the cell. If the swimming defects are caused by asynchronized rotation of the motors, we would expect to observe similar motor rotation rates for this mutant compared to wild type. In contrast, if motors are generally defective in their rotation, then we would expect an

overall decreased prevalence of rotating motors as well as diminished rotation rates. To distinguish between these possibilities, we performed cell tethering assays and analyzed motor behavior (Figure 2.9). Rotation rates of wild-type motors averaged approximately at 12.5 Hz, as previously documented (181), with maximal rotation rates of up to 28 Hz (Figure 2.9B). In contrast, motor rotation rates of Δ*motF* averaged at 0.8 Hz and reached a maximum rotation rate of 7.5 Hz, clearly indicating an overall diminished functional capacity. Further exemplifying this point, a representative graph depicting activity of an individual wild-type motor over a 60-second time period revealed high overall rotation rates with brief fluctuations above and below the average of about 12 Hz (representative image shown in Figure 2.9C). The Δ*motF* mutant consistently exhibited low level rotation rates around 1 Hz with brief pulses of rotation above the average rotation rate interspersed between periods of no or low activity (Figure 2.9C). Additionally, the number of rotating Δ*motF* bacterial cells was substantially reduced compared to wild type. These data demonstrate that the swimming defect exhibited by the *motF* deletion strain is caused by an inability to induce consistent motor rotation. Since a very small population of Δ*fliL* cells exhibited stationary motion, we also quantified motor rotation of this mutant in the tethered cell assay. The percentage of rotating Δ*fliL* bacteria was far smaller than for the already severely defective Δ*motF* strain but with similar average and maximum rotation rates (Figure 2.9B). In conclusion, the absence of MotF, and to an even greater degree of FliL, severely reduces the number of flagellar motors engaged in rotation. However, once motors are engaged, both deletion strains exhibit comparably abysmal rotation rates.

Mutations in the stator genes *motA* and *motB* restore motility to the *motF* but not the *fliL* deletion strain

To further investigate the mechanism by which MotF and FliL contribute to flagellar motility, we imposed selective pressure to produce second-site suppressor mutations in both deletion mutant backgrounds by extended incubation on soft agar swim plates. Under the conditions of this assay, motile bacteria exhibit a fitness advantage by swimming outward from the inoculum towards regions with higher levels of nutrients. Despite several attempts, we were unable to obtain Δ*fliL* suppressor mutants. However, we independently isolated five Δ*motF* suppressor mutants and found via whole-genome sequencing that all five strains contained single mutations in coding regions of *motA* corresponding to amino acid substitution G136S in the cytoplasmic loop connecting TM 2 and 3 (two of five mutants) or Y248H in the C-terminal, cytoplasmic tail

region (three of five mutants) (Figure 2.10A). We then performed targeted mutagenesis to generate the corresponding *motA* variants in wild type, Δ*motF*, and Δ*fliL* background strains and performed quantitative swim ring analyses. As was reported for the original suppressor mutants, the Δ*motF* $motA_{G136S}$ and Δ*motF* $motA_{Y248H}$ double mutant strains exhibited partially restored swimming on soft agar with an average swim ring diameter of about 20-25% of wild type (compared to about 5% for the Δ*motF* mutant; Figure 2.11A). The percentage of motile Δ*motF* $motA_{G136S}$ and Δ*motF* $motA_{Y248H}$ mutant cells was twice that of the Δ*motF* parental strain (from 2.1 ± 0.5% to 3.5 ± 1.8 and 5.5 ± 2.5, respectively), and the average swimming velocity was marginally improved (Table 2.2). Furthermore, both mutants exhibited increased average rotational velocity in tethered cell experiments compared to the wild type (Figure 2.12A). However, neither of the *motA* second-site mutations conferred motility to the Δ*fliL* parental strain on swim plates or in motility medium (Figure 2.11A and Table 2.2). Finally, the respective *motA* point mutations in the wild-type background elicited no effect on motility (Figure 2.11A, Table 2.2, and Figure 2.12A).

It has been previously reported that point mutations in the plug region of MotB can partially restore motility of Δ*fliL* strains in *R. sphaeroides* and *S. typhimurium*, namely F63L and A67D/E, and L56A and A60E, respectively. A multiple sequence alignment using T-Coffee identified equivalent residues in *S. meliloti* MotB as K60 and A64 (Figure 2.10B). Thus, we created similarly disruptive mutations by introducing either a neutralizing (K60A) or a negatively charged (A64E) residue in wild-type, Δ*motF*, and Δ*fliL* backgrounds. Additionally, we asked whether removal of the entire MotB plug region (corresponding to residues 58-69) would influence motility. All three strains with mutations in the plug region, specifically $motB_{K60A}$, $motB_{A64E}$, and $motB_{\Delta plug}$, referred to here as $motB_{plug}$ mutants, restored the motility of Δ*motF* on swim plates to about 20% of wild type, similar to the *motA* second-site mutants (Figure 2.11B). The percentage of motile cells (5%) and average swimming speed (13.9 mm/s) was similarly improved for Δ*motF* $motB_{K60A}$ (Table 2.2). The introduction of $motB_{A64E}$ and $motB_{\Delta plug}$ into Δ*motF* resulted in an even greater enhancement of the percentage of motile cells (~10%) and swimming velocity of the motile population (~17 μm/s). All three second-site mutations in the Δ*motF* background caused improved tethered cell rotation rates compared to the Δ*motF* parent strain (Figure 2.12B). Introduction of $motB_{\Delta plug}$ resulted in the greatest improvement with an average rotation rate of 4.1 Hz. In contrast, *motB* plug mutations in the Δ*fliL* background did not

permit swimming on soft agar plates. The Δ*fliL motB*$_{A64E}$ and Δ*fliL motB*$_{\Delta plug}$ mutants exhibited a very small degree of swimming ability (<0.5% motile and swimming velocities of <9 μm/s), albeit still inferior to the Δ*motF* mutant. It should be noted that the introduction of the *motB*$_{\Delta plug}$ mutation in the wild-type background reduced motility in all assays (Figure 2.10, Figure 2.11, and Table 2.2). Altogether, these data suggest that mutations that disrupt the MotB proton channel plug can partially bypass the requirement for MotF in flagellar motor function but not for FliL, and by extension that MotF is required for proton plug modulation.

DISCUSSION

MotF and FliL: paralogous proteins required to drive the flagellar motor

In this work, we provide the first report of a novel FliL paralog, MotF, operating in conjunction with FliL to drive motor rotation. Our motility analyses demonstrate that MotF and FliL are both essential to support flagellar motor function in *S. meliloti*. The presence of two *fliL* copies has been described for bacterial species that employ more than one type of flagellar system, such as *V. alginolyticus, Bradyrhizobium diazoefficiens,* and *Shewanella putrefaciens* (110, 154, 155). However, in all of these cases, the two FliL paralogs are part of separate flagellar systems, specifically a lateral multi-flagellar system or a single (sub)polar flagellum. In contrast, *S. meliloti* is only known to possess one flagellar system, and thus we explored the specific roles of the two FliL paralogs employed within their peritrichous flagella. Our combined experimental evidence suggests co-dependence of MotF and FliL and closely linked functions: 1) MotF and FliL levels are reduced in deletion mutants of *fliL* and *motF*, respectively; 2) both proteins interact with each other in BACTH and pull-down assays; and 3) strains lacking *motF* or *fliL* exhibit severe flagellar motor impairment.

Roles of MotF and FliL in flagellation

While the Δ*motF* mutant retained flagella at wild-type levels and quality, transmission electron microscopCy analysis showed that the Δ*fliL* mutant was mostly aflagellate, and transcriptional and immunoblot analyses revealed reduced flagellin production. The inability to produce functional filaments negatively regulates the promoter activity of the principal flagellin gene *flaA* in a feedback mechanism (176). We can only speculate how FliL contributes to production and/or stabilization of *S. meliloti* flagellar filaments. Reduced flagellation in the absence of *fliL* has been reported previously in *Pseudomonas putida* (165) and *Silicibacter* sp. strain TM1040

(162). A *Salmonella fliL* mutant exhibits a rod-breakage phenotype under swarming conditions implying a role for FliL in rod stability under high load (113, 163). Although this was not the main focus of the current work, it would be interesting to determine whether *S. meliloti* FliL is involved in anchoring the flagellum in the cell wall by stabilizing the rod.

In contrast to *Salmonella* and *E. coli*, the lack of *fliL* in *P. mirabilis* caused a more pronounced swimming defect, and swarming was only affected in a temperature-dependent manner (175). Additionally, while *P. mirabilis* wild-type cells require 1.5% agar for swarmer differentiation, Δ*fliL* mutant cells also swarm on 0.9% agar, suggesting a role of FliL in surface sensing-dependent differentiation (175). Thus, FliL in *P. mirabilis* is not a rod-reinforcement module as seen in swarming *Salmonella*. To add to the variable function of FliL, cells of *C. crescentus* (108), *R. sphaeroides* (111), as well as swimming *Salmonella* (163) exhibit normal flagellation in the absence of *fliL*. Thus, *S. meliloti* MotF would be appropriately placed in the FliL-class described above. Another phenotype has been observed in *B. burgdorferi*, in which the lack of FliL caused a decrease in swimming velocity due to misorientation of 50% of its internal flagella (161). In summary, while FliL proteins in various bacterial species exhibit some unifying characteristics as they are linked to flagellar motor performance, their functions are numerous and appear to be largely species-specific.

Importance of MotF and FliL in torque generation and MotB plug function

The *motF* and *fliL* deletion strains both exhibited very poor motor performance in tethered cell experiments. However, it was much more difficult to find examples of rotating Δ*fliL* cells, an observation which may be explained by strongly diminished flagellation and/or further impairment of motor function. In accordance with these observations, the Δ*fliL* mutant was completely nonmotile and less than 1% of cells were found to twirl in place. Although Δ*motF* cells were mostly nonmotile, about 2% of bacteria (compared to 36% motile for the wild type) retained some degree of slow and jerking swimming motility.

We isolated suppressor mutants with partially restored swimming ability after extended incubation of the Δ*motF* strain on soft agar. The two unique SNPs in *motA*, $motA_{G136S}$ and $motA_{Y248H}$, when introduced into *S. meliloti* wild type, had little effect on motility, but improved overall swimming population, swimming velocity, and tethered cell rotation rates of the Δ*motF*

strain. The same mutations were unable to restore motility of the Δ*fliL* strain, which is supporting evidence for distinct functions of MotF and FliL. Intriguingly and despite multiple attempts, we have not been able to obtain suppressor mutants for the Δ*fliL* strain, suggesting that *S. meliloti* FliL is indispensable for flagellar function and swimming motility.

Specific second-site mutations in the MotB plug region restore motility defects in *R. sphaeroides* (111) and *S. enterica* (113) Δ*fliL* mutants. Thus, we tested whether comparable mutations in *S. meliloti* $MotB_{plug}$ would similarly improve the *fliL* or *motF* deletion phenotypes. We saw no such restoration for the Δ*fliL* mutant, other than a minimal increase in the number of cells with motility reminiscent of the Δ*motF* mutant. However, disruption of the MotB proton channel plug greatly improved the swimming and flagellar motor rotation defects of the Δ*motF* mutant as did deletion of the entire MotB plug. Motility phenotype restoration was comparable to that of the *motA* second-site mutants suggesting that the latter modifications may distort the proton channel sufficiently to mimic removal of the MotB plug region.

In addition to its role in $MotB_{plug}$ modulation, FliL has been linked to the stomatin/prohibitin/flotillin/HflK/C (SPFH) family of scaffolding proteins (112). In *R. sphaeroides* and *S. enterica*, it was shown that FliL associates with basal body components (111, 113). Additionally, the localization of *V. alginolyticus* MotAB stator units at the basal body is reduced in the absence of FliL (110). From these findings, coupled with our behavioral data, we speculate that *S. meliloti* FliL may serve as an essential primary scaffold at the flagellar basal body, which stators may assemble onto and become stabilized. Then, MotF may assemble around the stators to unlock the $MotB_{plug}$ from its inactive state within the periplasmic crenelations of pentameric MotA and modulate the $MotB_{plug}$ region. This hypothesis is in line with the observations that (1) FliL is essential, (2) the absence of MotF can be overcome by removing the $MotB_{plug}$, and (3) removal of the $MotB_{plug}$ is equally detrimental as the loss of MotF.

Partridge *et al.* proposed that FliL may either increase stator occupancy or alternatively increase the dwell time of stators at the motor (113). Based on the tethering results reported here, both hypotheses are plausible for *S. meliloti* MotF and FliL. Clearly, MotF is directly and FliL directly or indirectly required for torque generation in *S. meliloti* as has been observed for FliL in other

alphaproteobacteria including *R. sphaeroides* and *C. crescentus* and the lateral flagellar system of *B. diazoefficiens* (108, 111, 155). Structural analyses have informed a model in which FliL forms a partial ring, which serves as a scaffold awaiting incoming stators, before it oligomerizes into a fully encapsulating ring structure. The FliL proteins in *C. jejuni* and *B. burgdorferi* readily form such partial rings of 4-5 monomers (114, 149). We similarly observed dimers and trimers of the periplasmic region of MotF in chemical crosslinking experiments. Additionally, the periplasmic domain of MotB or MotC were found to promote further MotF oligomerization into high molecular weight complexes reaching up to ~250 kDa, perhaps corresponding to a MotB* or MotC dimer (~80 kDa) in complex with up to a decamer of MotF* (185 kDa). In contrast, the periplasmic regions of MotF and FliL did not interact with each other implying that their transmembrane domains (directly or indirectly) are mediating their association.

S. meliloti MotB contains one large (~90 aa residue) insertion in its periplasmic domain compared to *E. coli* MotB indicating the existence of additional contacts with other components of the *S. meliloti* flagellar motor. Some preliminary data point to an interaction of *S. meliloti* MotB with the alphaproteobacteria-specific MotC protein. In addition, work presented here demonstrate interactions between MotF and FliL with MotB and MotA and provided evidence for a MotF/MotC interaction. We propose that MotF is the primary $MotB_{plug}$ modulator, while FliL and/or MotC engage with this additional MotB region.

Model and concluding remarks

Altogether, these data lead to a model where partial rings of *S. meliloti* FliL and MotF assemble at the basal body prior to stator incorporation (Figure 2.13). As stators engage the basal body/FliL/MotF complex, additional FliL and MotF proteins complete their rings to stabilize the stators and modulate the MotB plug region. In the absence of either of these proteins, stator assembly and torque generation are drastically reduced. For motors without the FliL scaffold, stator assembly is nearly abolished, whereas motors lacking MotF can achieve stator incorporation by FliL, although the MotB plug remains primarily in the inactive state resulting in slow or no motor rotation.

Why would *S. meliloti* employ two distinct proteins to do the job that one can accomplish in other bacteria? This may be driven by the distinct motility behavior of this organism: *S. meliloti*

employs unidirectional speed-variable motors whereas many other characterized bacteria use variations on the reversible switch type-motor theme. *S. meliloti* is also capable of effectively swimming in environments of higher viscosity, which is mediated by the screw-like surface structure of its flagellar filaments (84, 87, 89). These adaptations may require additional motor components, such as MotF and MotC. It would also be interesting to explore the architecture of the *S. meliloti* flagellar motor in light of the intricacy and diversity of basal body structures from distantly related organisms (65, 90, 97, 98, 112, 114, 121, 146, 147, 149, 182-184). It is intriguing to speculate how exactly MotF and FliL are arranged in the *S. meliloti* flagellar motor. Do they form stacked or concentric rings around the stators? It also remains to be determined how MotC fits into the structure and function of the *S. meliloti* flagellar motor. How is rotational speed modulated and how is the motor locked into a clockwise rotation? These questions and more will be the focus of future studies as we dissect the mechanisms driving the function of this macromolecular marvel.

MATERIALS AND METHODS

Strains and plasmids

Derivatives of *E. coli* K-12, highly motile derivatives of *S. meliloti* MVII-1, and the plasmids used in this study are described in Table S2.4.

Media and growth conditions

E. coli strains used for IMPACT protein purification, pull-down assays, or bacterial two-hybrid (BACTH) analyses were grown in lysogeny broth (LB; (185)) at 37°C or 30°C with appropriate antibiotics at the following concentrations: ampicillin (Ap) at 100 µg/ml and kanamycin (Km) at 50 µg/ml.

S. meliloti strains were routinely grown in tryptone-yeast extract-calcium chloride (TYC) medium supplemented with streptomycin (Sm; 600 µg/ml) at 30°C (20). For motility assays, stationary phase cultures were diluted to an OD_{600} of 0.01 and grown for 24 h. Cultures were diluted to an OD_{600} of 0.004 in 10 ml *Rhizobium* basal medium (RB) [6.1 mM K_2HPO_4, 3.9 mM KH_2PO_4, 1 mM $MgSO_4$, 1 mM $(NH_4)_2SO_4$, 0.1 mM $CaCl_2$, 0.1 mM NaCl, 0.01 mM Na_2MoO_4, 0.001 mM $FeSO_4$, 20 mg/l biotin, and 100 mg/l thiamine] on Bromfield plates and grown at 30°C for 16 h to an OD_{600} of 0.25 ± 0.05 (Bromfield overlay plates) (20). Antibiotics for *S.*

meliloti strains bearing plasmids were provided at the following concentrations: neomycin at 120 µg/ml and tetracycline at 10 mg/ml.

Swim plate assays

Swim plates (0.3% agar) containing Bromfield medium (0.04% Bacto tryptone, 0.01% yeast extract, 0.01% $CaCl_2$, 0.3% agar) were inoculated with 3 µl of stationary-phase cultures and incubated for 3-5 days at 30°C.

Cell fractionation

Bacterial cells from 20 Bromfield overlay plates were harvested by centrifugation at 5,000 x g for 10 min at 4°C. Samples were kept on ice/at 4°C for the remainder of the experiment. Bacteria were suspended in C-buffer (10 mM $MgCl_2$, 50 µg/ml DNase A, 50 µg/ml RNase I, 20 mM Tris/HCl, pH 8.0) and lysed by three passages through a mini-French pressure cell at 14,000 lb/in^2 (SLM Aminco, Silver Spring, MD). Unlysed cells were removed by centrifugation for 5 min at 15,000 x g and the supernatants were recovered. Membranes were pelleted at 160,000 x g for 90 min at 4°C, and the supernatants retained as soluble fractions. Membranes were washed once in C-buffer and suspended in Laemmli buffer. All samples were boiled for 10 min prior to SDS-PAGE and immunoblotting.

Purification of recombinant proteins

Periplasmic domains of MotF (MotF*), MotB (MotB*), FliL (FliL*), and mature MotC (MotC*) were expressed from pBS357, pBS56, pBS1286, and pBS54, respectively, in *E. coli* ER2566 (Table 2.4) using the Intein-Mediated Purification with an Affinity Chitin-binding Tag (IMPACT™) method as described previously (186). Briefly, cells were grown to an OD_{600} of 0.5 to 0.7 at 37°C in LB broth and expression was induced by the addition of 0.3 mM isopropyl ß-D-1-thiogalactopyranoside (IPTG) and incubation overnight at 16°C. Cells were harvested at 16,000 x g for 10 min at 4°C, suspended in IMPACT buffer (20mM Tris-HCl, 500mM NaCl, 1mM EDTA, 1 mM phenylmethylsulfonyl fluoride (PMSF), pH 8.0) and lysed by three passages through a French pressure cell at 14,000 lb/in^2. Cell debris was removed by centrifugation at 56,000 x g for 90 min at 4°C and the soluble fraction was loaded onto a gravity flow column containing a 25-ml bed of chitin-agarose that was pre-equilibrated with IMPACT buffer. Cleavage was performed by addition of IMPACT buffer supplemented with 50 mM dithiothreitol

and continued incubation at 4°C for 40 h, and cleaved proteins were eluted with IMPACT buffer. Proteins were concentrated in an Amicon ultrafiltration apparatus with a regenerated 10 kDa MWCO cellulose membrane and further purified by fast performance liquid chromatography at 1 ml/min using a HiPrep 26/60 Sephacryl S-200 HR column (Cytiva) equilibrated in crosslinking buffer (150 mM NaCl, 20 mM sodium phosphate, 5% (w/v) glycerol, pH 8.0). Fractions containing target proteins were concentrated as described above and protein concentrations determined by the Bradford protein assay (Bio-Rad) prior to use in crosslinking experiments.

***In-vitro* crosslinking experiments**

Purified proteins at a concentration of 10 µM were incubated in crosslinking buffer (150 mM NaCl, 20 mM sodium phosphate, 5% (w/v) glycerol, pH 8.0) in the presence or absence of 10 mM glutaraldehyde for 1 h prior to quenching with an equal volume of Laemmli buffer. Reaction mixtures were boiled at 100°C for 10 min and analyzed by immunoblotting.

SDS-PAGE and immunoblotting

When necessary, polyclonal antibodies were affinity-purified as described previously (176). One-ml culture aliquots grown in Bromfield overlay plates were pelleted at 15,000 x g and all but ~15 µl of the supernatants removed. Cells were suspended in the remaining supernatant and 15 µl Laemmli buffer was added prior to boiling for 10 min. For *S. meliloti* flagellin immunoblots, 15 µl of cell culture were mixed with 15 µl of Laemmli buffer and boiled for 10 min. All samples were stored frozen at -20°C until further processing. Immunoblot analysis was performed essentially as described previously (187) except that four washes were used after each antibody incubation. Primary antibodies were used in blocking buffer (PBS supplemented with 5% (w/v) skim milk) at the following concentrations: polyclonal rabbit anti-flagellin, -MotF, -FliL crude sera were used at 1:10,000; affinity-purified anti-MotB, -MotC, -MotE, and -CheR antibodies were used at 1:100, 1:67, 1:200, and 1:1,000, respectively, and monoclonal mouse anti-6x-His antibody (Santa Cruz Biotech, Santa Cruz CA) was used at 1:50. Donkey anti-rabbit HRP secondary antibody (NA-934, Cytiva) was used at 1:10,000 and anti-mouse HRP (NXA-931, Cytiva) was used at 1:1,000.

Bacterial two-hybrid analysis

Triplicate LB-Ap-Km cultures were prepared from single colonies in LB broth and grown overnight at 30°C. Four microliters of stationary-phase cultures were spot-inoculated on MacConkey/lactose agar (Difco) plates supplemented with ampicillin and kanamycin (188). Positive interactions were identified as colonies yielding red color after a 48-h incubation period at 30°C. Representative results from three independent experiments were reported.

Membrane topology reporter assay

MotF topology was investigated using a transcriptional fusion of *phoA* and *lacZα* to the 3' end of *motF* or the 3' end of the MotF transmembrane domain-encoding region in the reporter plasmid pKTop (177, 178). *E. coli* DH5α was transformed with the resulting plasmids, pBS1319 and pBS1320, and single colonies were streaked on LB agar plates supplemented with 1 mM IPTG and 80 µg/ml 5-chloro-4-bromo-3-indolyl phosphate (X-Phos) (RPI, Mt Prospect, IL, USA) and incubated overnight at 30°C. Strains harboring pKTop or pKTop encoding a C-terminal fusion of the first 39 amino acids of YmgF (178) served as negative and positive control for cytoplasmic or periplasmic localization, respectively.

β-galactosidase assays

Stationary cultures of co-transformed *E. coli* BTH101 Δ*flhC* strains were diluted 1:100 in LB broth and grown to an OD_{600} of 1.6 ± 0.2. An appropriate amount of culture was collected and stored at -20°C. Z-buffer (60 mM Na_2HPO_4, 40 mM NaH_2PO_4, 10 mM KCl, 1 mM $MgSO_4$, 50 mM β-mercaptoethanol, pH 7.0) was added to obtain a final volume of 1 ml prior to addition of 30 µl chloroform and 30 µl of 0.1% SDS. Samples were vortexed vigorously for 10 sec and incubated for five min at 28°C. Two hundred microliters of 4 mg/ml O-nitrophenyl-β-D-galactoside (ONPG) was added, reactions were continued until a faint yellow appearance was observed and stopped by addition of 500 µl 1 M Na_2CO_3. Samples were centrifuged at 21,000 x g for two min and the absorbance at 420 nm of the supernatants was recorded. Relative β-galactosidase activity was expressed in Miller units and determined using the formula: $(1000)*(A_{420})/(\Delta t*v*OD_{600})$, where Δt is the reaction duration and v is the culture volume in milliliters in the reaction. Reported values are the averages and standard deviations of three experiments each performed in triplicate. Cultures of *S. meliloti* containing p*flaA-lacZ* fusions

were sampled, diluted 1:1 in Z buffer (189), permeabilized with 30 µl chloroform and 30 µl 0.1% SDS, and assayed for β-galactosidase activity as described above.

Pull-down assays

Overnight cultures of *E. coli* BL21 (DE3) with pETDuet-1 derivatives (Table S2.4) were diluted 1:1,000 in LB broth and grown at 37°C to an OD_{600} of 0.5 to 0.7 prior to induction with 0.3 mM IPTG for four h at 25°C. Aliquots of 70 ml were harvested by centrifugation at 16,000 x g for 5 min at 4°C and stored at -20°C. Cell pellets were thawed and suspended in 2 ml Ni-NTA MagBeads prewashed with binding buffer (20 mM sodium phosphate, 500 mM NaCl, 20 mM imidazole, 0.4% CHAPS (3-[(3-cholamidopropyl)-dimethylammonio]-1-propanesulfonate), 1 mM PMSF, 1 mg/ml lysozyme, and 5 µg/ml DNase I pH 7.4) . Cells were incubated on a rotisserie incubator for 1 h at 4°C and lysed by two passages through a mini-French pressure cell at 14,000 lb/in^2 (SLM Aminco, Silver Spring, MD). Unlysed cells and insoluble debris were removed by centrifugation at 16,000 x g for 45 min at 4°C. PureCube Ni-NTA MagBeads (Cube Biotech, Monheim am Rhein, Germany) were prepared by washing 20 µl resin slurry thrice with 1 ml binding buffer. Soluble fractions were mixed with the washed resin and incubated on a rotisserie incubator for 1 h at 4°C. The unbound fraction was removed and the resin washed four times each with 200 µl binding buffer without CHAPS. Bound proteins were eluted twice by addition of 50 µl elution buffer (20 mM sodium phosphate, 500 mM NaCl, 500 mM imidazole, pH 7.4). Samples of the soluble fraction (200 ng of total protein) and elution fraction (25 ng of total protein) were analyzed by immunoblotting as described above.

Computerized swimming and cell tethering analysis

Bacteria were grown on Bromfield overlay plates to an OD_{600} of 0.25 ± 0.05, harvested by centrifugation at 4,000 x g for 8 min at room temperature, and suspended in overlay broth that was prepared by incubating Bromfield plates with a 10-ml layer of RB at 30°C for 16 h and passing the supernatant through a 0.22 mm PES filter. To assess the percentage of motile cells and determine swimming velocities, bacteria were adjusted to an OD_{600} of 0.05 and analyzed by phase contrast microscopy using a Nikon Eclipse E600 microscope with a 40x objective and a custom Nikon CMOS camera from The Imaging Source (Charlotte, NC, USA). Five-second videos were analyzed using the TumbleScore program to quantify swimming velocities (180). For quantification of percent motile bacteria, the videos were shortened to two seconds, and the

number of motile bacteria was determined. The two-second videos were reanalyzed with the "stuck distance" setting – corresponding to the distance a bacterium must move in a trajectory to be considered not stuck – was reduced to zero and the number of bacteria in the video was counted. The percentage of motile bacteria was calculated by dividing the number of motile bacteria by total bacteria in the two-second videos. For tethering analyses, chloramphenicol (Cp) was added at a final concentration of 30 µg/ml to 2 ml of cell suspension standardized to an OD_{600} of 0.20 and incubated at room temperature for 20 min. Flagella were sheared by 15 passages through syringes equipped with 26-gauge beveled needles attached by plastic tubing. Cells were pelleted by centrifugation at 3,000 x g for 6 min at room temperature and washed in one ml of overlay broth supplemented with Cp to remove sheared flagella. Cells were suspended in 500 µl overlay broth with Cp and tethering to glass coverslips was achieved by incubating 10 µl of cell suspension with 10 µl anti-flagellin antibody (176) diluted 1:1,000 in overlay broth with Cp for 30 min at room temperature. Coverslips were inverted and fixed to glass slides with three layers of tape on either side and thin strips of Apeizon M grease. Unattached cells were removed by several washes of 100 µl overlay broth with Cp through the channel between the slide-tape-coverslip assembly and visualized under a 100x objective lens using a Nikon Eclipse microscope equipped with a custom Nikon CMOS camera. Tethered cell rotation rates were quantified using custom scripts written in MATLAB.

Transmission electron microscopy

Motile cells (30 ml) were harvested at an OD_{600} of 0.25 ± 0.05 by centrifugation over Fluorolube® at 7,000 x g for 10 min at room temperature. The supernatant was removed and cells washed twice with 15 ml overlay broth over Fluorolube®. The majority of the supernatant was removed and the concentrated layer of cells (~1000 µl) on top of the Fluorolube® layer was collected. A sample was observed by phase contrast microscopy to ensure motility. Cells were fixed through the addition 4% glutaraldehyde (diluted from a 50% stock solution in overlay broth) to a final concentration of 2% and stored at 4°C until further processing. Cells were stained for two min in 1% uranyl acetate and fixed to a 200-mesh copper grid (Electron Microscopy Sciences, Hatfield, PA, USA), visualized using a JEM-1400 JEOL transmission electron microscopy equipped with a W filament at 80 kV, and imaged with a Gatan Orius SC100 CCD Camera (Gatan, Pleasonton CA, USA).

ACKNOWLEDGEMENTS

We thank Drs. Gouzel Karimova and Daniel Ladant for providing the pKTop and BACTH plasmids as well as Dr. Rasika Harshey for providing the BTH101 Δ*flhC* strain. We thank the BIOL4544 class of 2012 for performing the transposon mutagenesis screen that identified the *motF* mutant motility defect. We thank Elizabeth Denson for the construction of pBS357 and purification of the $MotF_{Peri}$ antigen used in MotF antibody production and Sahitya Biswas for assistance with some of the motility analysis. We thank Nathalie Becerra for assistance with cell fixation and staining for TEM analysis and Daniel Shickel for assisting with some of the β-galactosidase assays. We also thank Dr. Michael Galperin for helpful discussions.

CONFLICT OF INTEREST

The authors declare no conflict of interest.

AUTHOR CONTRIBUTIONS

RCS and BES conceived and designed this study. RCS, BES, and CG performed the experiments. LTV wrote tethered cell analysis scripts under the supervision of GA. RCS and BES analyzed the data and wrote the paper. All authors edited the paper.

FUNDING INFORMATION

National Science Foundation, Grant/Award Number: MCB-1253234, MCB-1817652, and MCB-2128232 to BS and MCB-1715185 and IOS-1855066 to GA.

REFERENCES

1. Subramanian S, Kearns DB. 2019. Functional regulators of bacterial flagella. Annual review of microbiology 73:225-246.
2. Imada K. 2018. Bacterial flagellar axial structure and its construction. Biophysical reviews 10:559-570.
3. Schuhmacher JS, Thormann KM, Bange G. 2015. How bacteria maintain location and number of flagella? FEMS Microbiology Reviews 39:812-822.
4. Wadhwa N, Berg HC. 2021. Bacterial motility: machinery and mechanisms. Nature Reviews Microbiology:1-13.
5. Carroll BL, Liu J. 2020. Structural conservation and adaptation of the bacterial flagella motor. Biomolecules 10:1492.
6. Rossmann FM, Beeby M. 2018. Insights into the evolution of bacterial flagellar motors from high-throughput in situ electron cryotomography and subtomogram averaging. Acta Crystallographica Section D: Structural Biology 74:585-594.
7. Kinoshita M, Furukawa Y, Uchiyama S, Imada K, Namba K, Minamino T. 2018. Insight into adaptive remodeling of the rotor ring complex of the bacterial flagellar motor. Biochemical and Biophysical Research Communications 496:12-17.
8. Kaplan M, Sweredoski MJ, Rodrigues JP, Tocheva EI, Chang Y-W, Ortega DR, Beeby M, Jensen GJ. 2020. Bacterial flagellar motor PL-ring disassembly subcomplexes are widespread and ancient. Proceedings of the National Academy of Sciences 117:8941-8947.
9. Berg HC. 2003. The rotary motor of bacterial flagella. Annual Review of Biochemistry 72.
10. Kaplan M, Ghosal D, Subramanian P, Oikonomou CM, Kjaer A, Pirbadian S, Ortega DR, Briegel A, El-Naggar MY, Jensen GJ. 2019. The presence and absence of periplasmic rings in bacterial flagellar motors correlates with stator type. Elife 8:e43487.
11. Hu H, Santiveri M, Wadhwa N, Berg HC, Erhardt M, Taylor NM. 2021. Structural basis of torque generation in the bi-directional bacterial flagellar motor. Trends in Biochemical Sciences.
12. Santiveri M, Roa-Eguiara A, Kühne C, Wadhwa N, Hu H, Berg HC, Erhardt M, Taylor NM. 2020. Structure and function of stator units of the bacterial flagellar motor. Cell 183:244-257. e16.
13. Blair DF, Berg HC. 1990. The MotA protein of *E. coli* is a proton-conducting component of the flagellar motor. Cell 60:439-449.
14. Kojima S, Takao M, Almira G, Kawahara I, Sakuma M, Homma M, Kojima C, Imada K. 2018. The helix rearrangement in the periplasmic domain of the flagellar stator B subunit activates peptidoglycan binding and ion influx. Structure 26:590-598. e5.
15. Hosking ER, Vogt C, Bakker EP, Manson MD. 2006. The *Escherichia coli* MotAB proton channel unplugged. Journal of Molecular Biology 364:921-937.
16. De Mot R, Vanderleyden J. 1994. The C-terminal sequence conservation between OmpA-related outer membrane proteins and MotB suggests a common function in both gram-positive and gram-negative bacteria, possibly in the interaction of these domains with peptidoglycan. Molecular microbiology 12:333-336.
17. Deme JC, Johnson S, Vickery O, Aron A, Monkhouse H, Griffiths T, James RH, Berks BC, Coulton JW, Stansfeld PJ. 2020. Structures of the stator complex that drives rotation of the bacterial flagellum. Nature Microbiology 5:1553-1564.

18. Tachiyama S, Chan KL, Liu X, Hathroubi S, Peterson B, Khan MF, Ottemann KM, Liu J, Roujeinikova A. 2022. The flagellar motor protein FliL forms a scaffold of circumferentially positioned rings required for stator activation. Proceedings of the National Academy of Sciences 119.
19. Morimoto YV, Nakamura S, Kami-ike N, Namba K, Minamino T. 2010. Charged residues in the cytoplasmic loop of MotA are required for stator assembly into the bacterial flagellar motor. Molecular microbiology 78:1117-1129.
20. Kojima S, Imada K, Sakuma M, Sudo Y, Kojima C, Minamino T, Homma M, Namba K. 2009. Stator assembly and activation mechanism of the flagellar motor by the periplasmic region of MotB. Molecular microbiology 73:710-718.
21. Van Way SM, Hosking ER, Braun TF, Manson MD. 2000. Mot protein assembly into the bacterial flagellum: a model based on mutational analysis of the *motB* gene. Journal of molecular biology 297:7-24.
22. Zhu S, Takao M, Li N, Sakuma M, Nishino Y, Homma M, Kojima S, Imada K. 2014. Conformational change in the periplamic region of the flagellar stator coupled with the assembly around the rotor. Proceedings of the National Academy of Sciences 111:13523-13528.
23. Roujeinikova A. 2008. Crystal structure of the cell wall anchor domain of MotB, a stator component of the bacterial flagellar motor: implications for peptidoglycan recognition. Proceedings of the National Academy of Sciences 105:10348-10353.
24. Pecina A, Schwan M, Blagotinsek V, Rick T, Klüber P, Leonhard T, Bange G, Thormann KM. 2021. The stand-alone PilZ-domain protein MotL specifically regulates the activity of the secondary lateral flagellar system in *Shewanella putrefaciens*. Frontiers in microbiology 12:1160.
25. Mengucci F, Dardis C, Mongiardini EJ, Althabegoiti MJ, Partridge JD, Kojima S, Homma M, Quelas JI, Lodeiro AR. 2020. Characterization of FliL proteins in *Bradyrhizobium diazoefficiens*: lateral FliL supports swimming motility, and subpolar FliL modulates the lateral flagellar system. Journal of bacteriology 202.
26. Takekawa N, Isumi M, Terashima H, Zhu S, Nishino Y, Sakuma M, Kojima S, Homma M, Imada K. 2019. Structure of *Vibrio* FliL, a new stomatin-like protein that assists the bacterial flagellar motor function. mBio 10:e00292-19.
27. Lin T-S, Zhu S, Kojima S, Homma M, Lo C-J. 2018. FliL association with flagellar stator in the sodium-driven *Vibrio* motor characterized by the fluorescent microscopy. Scientific reports 8:1-12.
28. Kumar A, Isumi M, Sakuma M, Zhu S, Nishino Y, Onoue Y, Kojima S, Miyanoiri Y, Imada K, Homma M. 2017. Biochemical characterization of the flagellar stator-associated inner membrane protein FliL from *Vibrio alginolyticus*. The Journal of Biochemistry 161:331-337.
29. Chawla R, Ford KM, Lele PP. 2017. Torque, but not FliL, regulates mechanosensitive flagellar motor-function. Scientific reports 7:1-9.
30. Zhu S, Kumar A, Kojima S, Homma M. 2015. FliL associates with the stator to support torque generation of the sodium-driven polar flagellar motor of *Vibrio*. Molecular microbiology 98:101-110.
31. Partridge JD, Nieto V, Harshey RM. 2015. A new player at the flagellar motor: FliL controls both motor output and bias. MBio 6:e02367-14.

32. Lee Y-Y, Patellis J, Belas R. 2013. Activity of *Proteus mirabilis* FliL is viscosity dependent and requires extragenic DNA. Journal of bacteriology 195:823-832.
33. Fabela S, Domenzain C, De la Mora J, Osorio A, Ramirez-Cabrera V, Poggio S, Dreyfus G, Camarena L. 2013. A distant homologue of the FlgT protein interacts with MotB and FliL and is essential for flagellar rotation in *Rhodobacter sphaeroides*. Journal of Bacteriology 195:5285-5296.
34. Cusick K, Lee Y-Y, Youchak B, Belas R. 2012. Perturbation of FliL interferes with *Proteus mirabilis* swarmer cell gene expression and differentiation. Journal of bacteriology 194:437-447.
35. Motaleb MA, Pitzer JE, Sultan SZ, Liu J. 2011. A novel gene inactivation system reveals altered periplasmic flagellar orientation in a *Borrelia burgdorferi fliL* mutant. Journal of bacteriology 193:3324-3331.
36. Suaste-Olmos F, Domenzain C, Mireles-Rodríguez JC, Poggio S, Osorio A, Dreyfus G, Camarena L. 2010. The flagellar protein FliL is essential for swimming in *Rhodobacter sphaeroides*. Journal of Bacteriology 192:6230-6239.
37. Belas R, Horikawa E, Aizawa S-I, Suvanasuthi R. 2009. Genetic determinants of *Silicibacter* sp. TM1040 motility. Journal of Bacteriology 191:4502-4512.
38. Attmannspacher U, Scharf BE, Harshey RM. 2008. FliL is essential for swarming: motor rotation in absence of FliL fractures the flagellar rod in swarmer cells of *Salmonella enterica*. Molecular Microbiology 68:328-341.
39. Belas R, Suvanasuthi R. 2005. The ability of *Proteus mirabilis* to sense surfaces and regulate virulence gene expression involves FliL, a flagellar basal body protein. Journal of Bacteriology 187:6789-6803.
40. Segura A, Duque E, Hurtado A, Ramos JL. 2001. Mutations in genes involved in the flagellar export apparatus of the solvent-tolerant *Pseudomonas putida* DOT-T1E strain impair motility and lead to hypersensitivity to toluene shocks. Journal of Bacteriology 183:4127-4133.
41. Schoenhals GJ, Macnab RM. 1999. FliL is a membrane-associated component of the flagellar basal body of *Salmonella*. Microbiology 145:1769-1775.
42. Aldridge P, Jenal U. 1999. Cell cycle-dependent degradation of a flagellar motor component requires a novel-type response regulator. Molecular Microbiology 32:379-391.
43. Raha M, Sockett H, Macnab RM. 1994. Characterization of the fliL gene in the flagellar regulon of *Escherichia coli* and *Salmonella typhimurium*. Journal of Bacteriology 176:2308-2311.
44. Jenal U, White J, Shapiro L. 1994. *Caulobacter* flagellar function, but not assembly, requires FliL, a non-polarly localized membrane protein present in all cell types. Journal of molecular biology 243:227-244.
45. Chang Y, Zhang K, Carroll BL, Zhao X, Charon NW, Norris SJ, Motaleb MA, Li C, Liu J. 2020. Molecular mechanism for rotational switching of the bacterial flagellar motor. Nature structural & molecular biology 27:1041-1047.
46. Attmannspacher U, Scharf B, Schmitt R. 2005. Control of speed modulation (chemokinesis) in the unidirectional rotary motor of *Sinorhizobium meliloti*. Molecular Microbiology 56:708-718.

47. Eggenhofer E, Haslbeck M, Scharf B. 2004. MotE serves as a new chaperone specific for the periplasmic motility protein, MotC, in *Sinorhizobium meliloti*. Molecular Microbiology 52:701-712.
48. Platzer J, Sterr W, Hausmann M, Schmitt R. 1997. Three genes of a motility operon and their role in flagellar rotary speed variation in *Rhizobium meliloti*. Journal of Bacteriology 179:6391-6399.
49. Hirano T, Minamino T, Macnab RM. 2001. The role in flagellar rod assembly of the N-terminal domain of *Salmonella* FlgJ, a flagellum-specific muramidase. Journal of molecular biology 312:359-369.
50. Aldridge P, Karlinsey J, Hughes KT. 2003. The type III secretion chaperone FlgN regulates flagellar assembly via a negative feedback loop containing its chaperone substrates FlgK and FlgL. Molecular Microbiology 49:1333-1345.
51. Rotter C, Mühlbacher S, Salamon D, Schmitt R, Scharf B. 2006. Rem, a new transcriptional activator of motility and chemotaxis in *Sinorhizobium meliloti*. Journal of Bacteriology 188:6932-6942.
52. Sourjik V, Muschler P, Scharf B, Schmitt R. 2000. VisN and VisR are global regulators of chemotaxis, flagellar, and motility genes in *Sinorhizobium* (*Rhizobium*) *meliloti*. Journal of Bacteriology 182:782-788.
53. Lee Y-Y, Belas R. 2015. Loss of FliL alters *Proteus mirabilis* surface sensing and temperature-dependent swarming. Journal of bacteriology 197:159-173.
54. Scharf B, Schuster-Wolff-Bühring H, Rachel R, Schmitt R. 2001. Mutational analysis of the *Rhizobium lupini* H13-3 and *Sinorhizobium meliloti* flagellin genes: Importance of flagellin A for flagellar filament structure and transcriptional regulation. Journal of Bacteriology 183:5334-5342.
55. Karimova G, Ladant D. 2017. Defining membrane protein topology using *pho-lac* reporter fusions, p 129-142, Bacterial Protein Secretion Systems. Springer.
56. Karimova G, Robichon C, Ladant D. 2009. Characterization of YmgF, a 72-residue inner membrane protein that associates with the *Escherichia coli* cell division machinery. Journal of Bacteriology 191:333-346.
57. Dixit PD, Maslov S. 2013. Evolutionary capacitance and control of protein stability in protein-protein interaction networks. PLoS Computational Biology 9:e1003023.
58. Pottash AE, McKay R, Virgile CR, Ueda H, Bentley WE. 2017. TumbleScore: run and tumble analysis for low frame-rate motility videos. BioTechniques 62:31-36.
59. Sourjik V, Schmitt R. 1996. Different roles of CheY1 and CheY2 in the chemotaxis of *Rhizobium meliloti*. Molecular Microbiology 22:427-436.
60. Guo S, Xu H, Chang Y, Motaleb MA, Liu J. 2022. FliL ring enhances the function of periplasmic flagella. Proceedings of the National Academy of Sciences 119:e2117245119.
61. Kreutzberger MA, Sobe RC, Sauder AB, Chatterjee S, Peña A, Wang F, Giron JA, Kiessling V, Costa TR, Conticello VP. 2022. Flagellin outer domain dimerization modulates motility in pathogenic and soil bacteria from viscous environments. Nature Communications 13:1-14.
62. Trachtenberg S, DeRosier DJ, Aizawa S-I, Macnab RM. 1986. Pairwise perturbation of flagellin subunits: The structural basis for the differences between plain and complex bacterial flagellar filaments. Journal of molecular biology 190:569-576.

63. Götz R, Limmer N, Ober K, Schmitt R. 1982. Motility and chemotaxis in two strains of Rhizobium with complex flagella. Microbiology 128:789-798.
64. Rossmann FM, Hug I, Sangermani M, Jenal U, Beeby M. 2020. *In situ* structure of the *Caulobacter crescentus* flagellar motor and visualization of binding of a CheY-homolog. Molecular Microbiology.
65. Ferreira JL, Gao FZ, Rossmann FM, Nans A, Brenzinger S, Hosseini R, Wilson A, Briegel A, Thormann KM, Rosenthal PB. 2019. γ-proteobacteria eject their polar flagella under nutrient depletion, retaining flagellar motor relic structures. PLoS Biology 17:e3000165.
66. Terashima H, Kawamoto A, Morimoto YV, Imada K, Minamino T. 2017. Structural differences in the bacterial flagellar motor among bacterial species. Biophysics and Physicobiology 14:191-198.
67. Minamino T, Imada K. 2015. The bacterial flagellar motor and its structural diversity. Trends in Microbiology 23:267-274.
68. Chen S, Beeby M, Murphy GE, Leadbetter JR, Hendrixson DR, Briegel A, Li Z, Shi J, Tocheva EI, Müller A. 2011. Structural diversity of bacterial flagellar motors. The EMBO Journal 30:2972-2981.
69. Johnson S, Furlong EJ, Deme JC, Nord AL, Caesar JJ, Chevance FF, Berry RM, Hughes KT, Lea SM. 2021. Molecular structure of the intact bacterial flagellar basal body. Nature Microbiology 6:712-721.
70. Bertani G. 1951. Studies on lysogenesis I: the mode of phage liberation by lysogenic *Escherichia coli*. Journal of Bacteriology 62:293-300.
71. Baaziz H, Compton KK, Hildreth SB, Helm RF, Scharf BE. 2021. McpT, a broad range carboxylate chemoreceptor in *Sinorhizobium meliloti*. Journal of Bacteriology:JB. 00216-21.
72. Mitchell SF, Lorsch JR. 2015. Protein affinity purification using intein/chitin binding protein tags, p 111-125, Methods in Enzymology, vol 559. Elsevier.
73. Zatakia HM, Arapov TD, Meier VM, Scharf BE. 2018. Cellular stoichiometry of methyl-accepting chemotaxis proteins in *Sinorhizobium meliloti*. Journal of bacteriology 200:e00614-17.
74. Battesti A, Bouveret E. 2012. The bacterial two-hybrid system based on adenylate cyclase reconstitution in *Escherichia coli*. Methods 58:325-334.
75. Miller JH. 1972. Experiments in molecular genetics.
76. Magis C, Taly J-F, Bussotti G, Chang J-M, Tommaso PD, Erb I, Espinosa-Carrasco J, Notredame C. 2014. T-Coffee: Tree-based consistency objective function for alignment evaluation, p 117-129, Multiple Sequence Alignment Methods. Springer.

TABLES

TABLE 2.1 Predicted molecular weight and function of newly discovered motility genes.

Protein	Molecular weight (kDa)	Description
SMc03056	15.3	Hypothetical protein
SMc03071	19.5	$FlgJ_N$ rod-binding protein
SMc03072	13.5	FlgN flagella synthesis protein
SMc03057†	20.5	FliL-like protein

† Renamed MotF.

TABLE 2.2 Quantification of motile populations and swimming velocities of *S. meliloti* wild type and mutant strains.

Strain	Percent motile	Swimming velocity (μm/s)
WT	36.0 ± 8.2	37.7 ± 1.7
motA$_{G136S}$	18.4 ± 1.9	37.3 ± 0.8
motA$_{Y248H}$	21.1 ± 4.0	37.4 ± 1.6
motB$_{K60A}$	25.0 ± 8.9	36.3 ± 0.7
motB$_{A64E}$	22.8 ± 10.6	38.7 ± 1.6
motB$_{\Delta plug}$	16.4 ± 6.5	19.9 ± 2.0
Δ*motF*	2.1 ± 0.5	10.9 ± 0.6
Δ*motF motA*$_{G136S}$	3.5 ± 1.8	13.1 ± 0.4
Δ*motF motA*$_{Y248H}$	5.5 ± 2.5	12.4 ± 1.3
Δ*motF motB*$_{K60A}$	5.3 ± 1.2	13.9 ± 1.6
Δ*motF motB*$_{A64E}$	9.3 ± 3.8	16.7 ± 1.1
Δ*motF motB*$_{\Delta plug}$	10.7 ± 4.9	17.4 ± 1.2
Δ*fliL*	Nonmotile	Nonmotile
Δ*fliL motA*$_{G136S}$	Nonmotile	Nonmotile
Δ*fliL motA*$_{Y248H}$	Nonmotile	Nonmotile
Δ*fliL motB*$_{K60A}$	Nonmotile	Nonmotile
Δ*fliL motB*$_{A64E}$	0.2 ± 0.2	8.8 ± 1.4
Δ*fliL motB*$_{\Delta plug}$	0.4 ± 0.2	7.7 ± 1.9

FIGURES

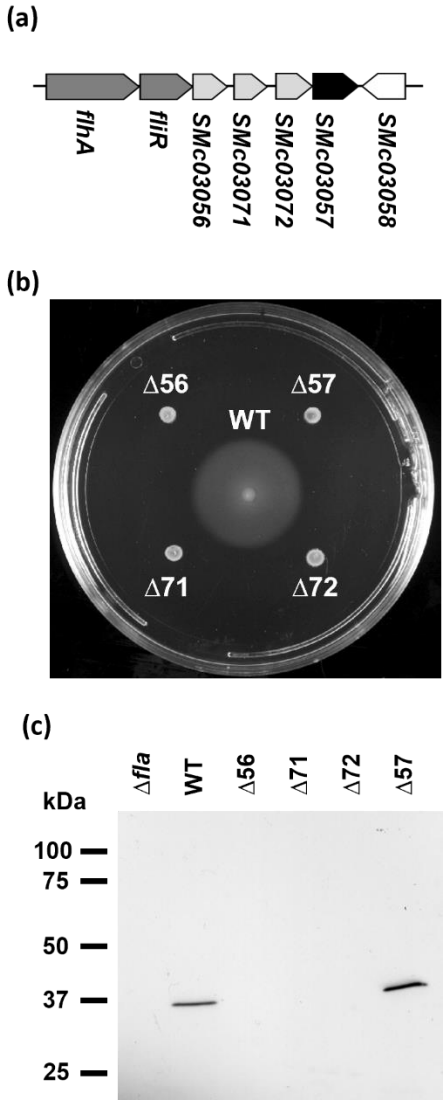
(a)
flhA
flhR
SMc03056
SMc03071
SMc03072
SMc03057
SMc03058
(b)
Δ56
Δ57
WT
Δ71
Δ72
(c)
kDa
Δfla
WT
Δ56
Δ71
Δ72
Δ57
100
75
50
37
25

FIGURE 2.1 Identification of genes required for flagellar motility in *S. meliloti*. (a) Genomic context of four uncharacterized motility genes located on the *S. meliloti* chromosome downstream of *fliR*, the last gene in the flagellar regulon. The currently annotated flagellar genes *flhA* and *fliR* are shown in dark grey, structural genes *SMc03057*, *SMc03071* and *SMc03072* are shown in light grey, *SMc03057* (renamed *motF* in this study) is shown in black, and a putative glycosyltransferase gene, SMc03058, encoded on the (-) strand, is shown in white. (b) Swim ring analysis of in-frame deletions of *SMc03056* (Δ56), *SMc03071* (Δ71), *SMc03072* (Δ72), and *SMc03057* (Δ57) compared to wild type (WT). Stationary phase cultures (3 µl) of each strain were transferred onto swim plates and incubated at 30°C for three days. (c) Anti-flagellin immunoblot analysis of wild type, Δ56, Δ71, Δ72 and Δ57. A mutant lacking all four flagellin genes (Δ*fla*) was used as a negative control.

(a)

```
MotF_S.mel   ---------- ---------- ---------- --MLKLVLTG VWVCAVTL-- GSVYFSMQHA SAPVVSDAEA DRRAS-----   41
FliL_S.mel   ---------- --MEE-IESK ETK---ATS- -RLMTIAAVA VLTLVAGGG- GWLAGMLLAP PPSEKT-ETA AE--L-----   53
FliL_A.tum   ---------- --MENEQAEG KKK---SSP- -LVMTIAGVA ILTLLGAGG- GWLVGDMIAP KIAGAE-AHA PTAAG-----   56
FliL_R.sph   ---------- --MTDASASL DTKPRRGRGL LRALVFLLLG AFLLAAGFGA GYFYFANPLS PAKDVL-RLI ERTPE-----   62
FliL_C.cre   VAKKPEKEAP APEGEEGAEG EAPAKKKPP- --ILIIAIAA GVLVLGGGGA A-AFFLLKPK PAAEAG-EHG EKKEEKKKEK   75
FliL_V.alg   ---------- --MAEEQLQG ADAPKGKSK- --LLIIIIAV VVLLLGGGAA --TFFLMGSD EPAQAE-S-- ----------   50
FliL_E.col   ---------- --MTDY---- AISKKSKRS- --LWIPILVF I-TLAACASA GYSYWHSH-Q VAA-DD-K-- ----------   45
FliL_S.typ   ---------- --MTDS---- AINKKSKRS- --IWIPLLVL I-TLAACATA GYSYWRMQ-Q QPTTNA-K-- ----------   46

MotF_S.mel   QE-------- YVPGE-MIT IPSIKDGAVQ- -----GYFLA KLSF--SA-- --SREGIAKL HAPLR----Q LVTDELYD--   94
FliL_S.mel   ---------- -PANATGEE DIPKMSAVAHG IV-------Q LDPI--TTNL AYPAENWVRL EVALQF--DG APDVALA---   108
FliL_A.tum   ---------- -GHGEKKEE GIEKISAEANG IV-------Q LDPI--TTNL AYPSTNWVRL EVALMF--KG PVEVGLA---   111
FliL_R.sph   -----ADE-- --PAADPDA PQKVPRPTPER ESFVTSYYQF KEPL--TTNL R-ASRRLLQA GIGLSTQYDQ KVMDNVARNE   130
FliL_C.cre   KKEEKGDKKD AEKGAEGAA GTPVIKEGPDG VV----FYTL PDIVVNMQTA D-GKSTFLKL KLTFELP-DE ETADELTPNL   149
FliL_V.alg   ---------- -------SQ QAQVKASDAAP IA----YVNL PQAFVFNVTG D-SRDRLVQI KAQLMVR-GA ENEELARYHS   107
FliL_E.col   ---------- -------AQ QR----VVPSP VF----Y--A LDTF--TVNL G-DADRVLYI GITLRLK-DE ATRSRLSEYL   94
FliL_S.typ   ---------- -------AE PA----PPPAP VF----F--A LDTF--TVNL G-DADRVLYI GVTLRLK-DE ATRARLNEYL   95

MotF_S.mel   MLVGSRFIDV ---------A DTATFDL--A AFKVAVKDGL NRKLGSEVIS EVLVEQLEYL TKEDVERVAN SQNRPYQKPV   163
FliL_S.mel   ETIHQDIAAY LKTVSLQQIQ GPRGFQYLRD DIQERVDLR- ----SEGRVT NVMFRTFVIQ ---------- ----------   163
FliL_A.tum   EDIHQDIMAY VRTVSLQQLE GPRGFQYLKD DIQERVDLR- ----SQGRVS KVMFRTFVIE ---------- ----------   166
FliL_R.sph   VALRSDMLAI VGTFSEEELQ DKAGRDRLAE ALRGAVNARL QQLEGFGGIE AVFFPSFILQ ---------- ----------   190
FliL_C.cre   PRLQDMFQTF LRELRPEDLN GSQGTYQLRV ELLRRVN--L VAA--PAKVN AVLIEEMLIN ---------- ----------   205
FliL_V.alg   PLIESSMLST FASAIVDQLR SPTGRVELRD RASEDIKAAL NAAVGKPVIE KVLFTDFVIQ ---------- ----------   167
FliL_E.col   PEVRSRLLLL FSRQDAAVLA TEEGKKNLIA EIKTTLSTPL VAGQPKQDVT DVLYTAFILR ---------- ----------   154
FliL_S.typ   PEVRSRLLLL FSRQNAAELS TEAGKQKLIA AIKETLAAPL VAGQPKQVVT DVLYTAFILR ---------- ----------   155

MotF_S.mel   PILDRNGQGA SDRLPESAAQ ATSTH        188
FliL_S.mel   ---------- ---------- -----        163
FliL_A.tum   ---------- ---------- -----        166
FliL_R.sph   ---------- ---------- -----        190
FliL_C.cre   ---------- ---------- -----        205
FliL_V.alg   ---------- ---------- -----        167
FliL_E.col   ---------- ---------- -----        154
FliL_S.typ   ---------- ---------- -----        155
```

(b)

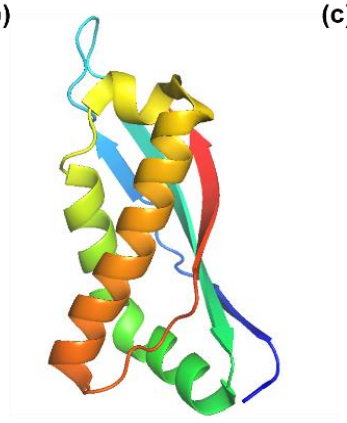

(c)

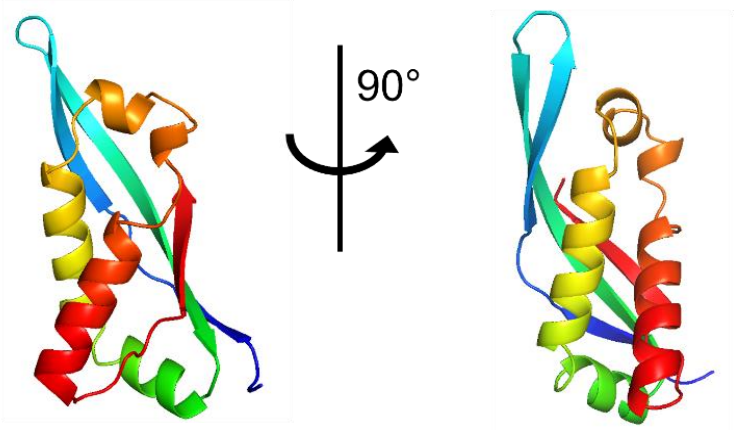

FIGURE 2.2 Comparison of MotF and FliL from different bacterial species. (a) Clustal Omega multiple sequence alignment. The light grey bar indicates the N-terminal cytoplasmic domain common to FliL but not MotF sequences, the black bar indicates the transmembrane domain, and the dark grey line indicates the C-terminal extension found only in MotF. The black arrow indicates the predicted signal peptide cleavage site in MotF, and the recognition site is highlighted in green. (b) Ribbon structure of the $FliL_{40-167}$ crystal structure from *V. alginolyticus* (PDB ID: 6AHQ). (c) Homology model of $MotF_{29-188}$ using *V. alginolyticus* $FliL_{40-167}$ as a template.

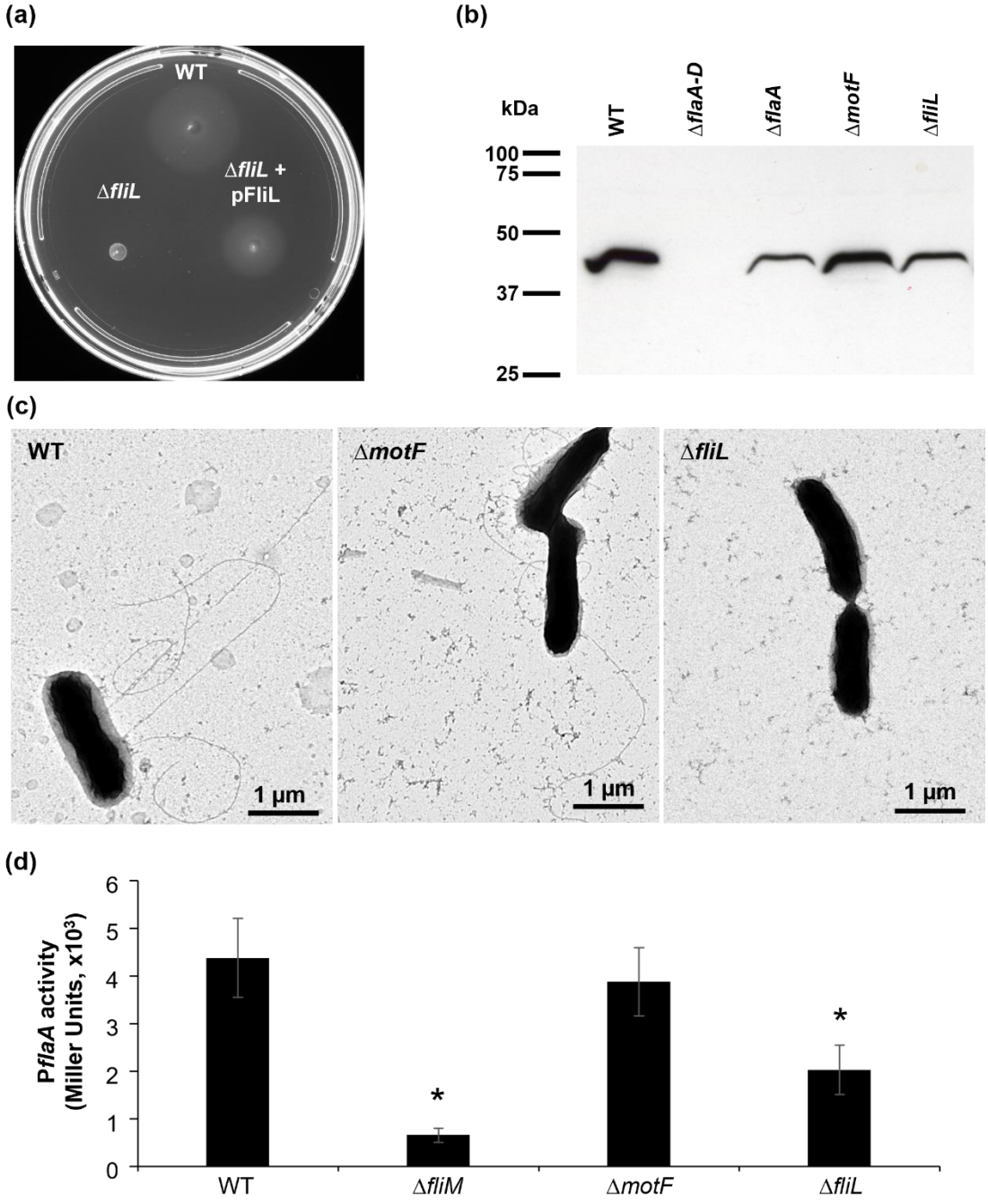
(a)
WT
ΔfliL
ΔfliL + pFliL
(b)
kDa
WT
ΔflaA-D
ΔflaA
ΔmotF
ΔfliL
100
75
50
37
25
(c)
WT
ΔmotF
ΔfliL
1 μm
1 μm
1 μm
(d)
PflaA activity (Miller Units, x10³)
0
1
2
3
4
5
6
*
*
WT
ΔfliM
ΔmotF
ΔfliL

FIGURE 2.3 Motility behavior and flagellation of the Δ*fliL* strain. (a) Swim ring analysis of wild type, Δ*fliL* and Δ*fliL* complemented *in trans*. (b) Anti-flagellin immunoblot analysis of wild type, Δ*flaA-D*, Δ*flaA*, Δ*motF*, and Δ*fliL* cell cultures. (c) Transmission electron microscopy (TEM) analysis of wild type (WT), Δ*motF,* and Δ*fliL* grown in Bromfield overlay cultures. Bacteria were fixed in 2% glutaraldehyde and stained with 1% uranyl acetate. (d) Activity of the *flaA* promoter in wild type, Δ*motF*, Δ*fliL*, and Δ*fliM* as negative control. Shown are the averages and standard deviations of β-galactosidase activity for three independent experiments with three technical replicates each. Asterisks (*) indicate significant difference from the wild type ($p<0.02$).

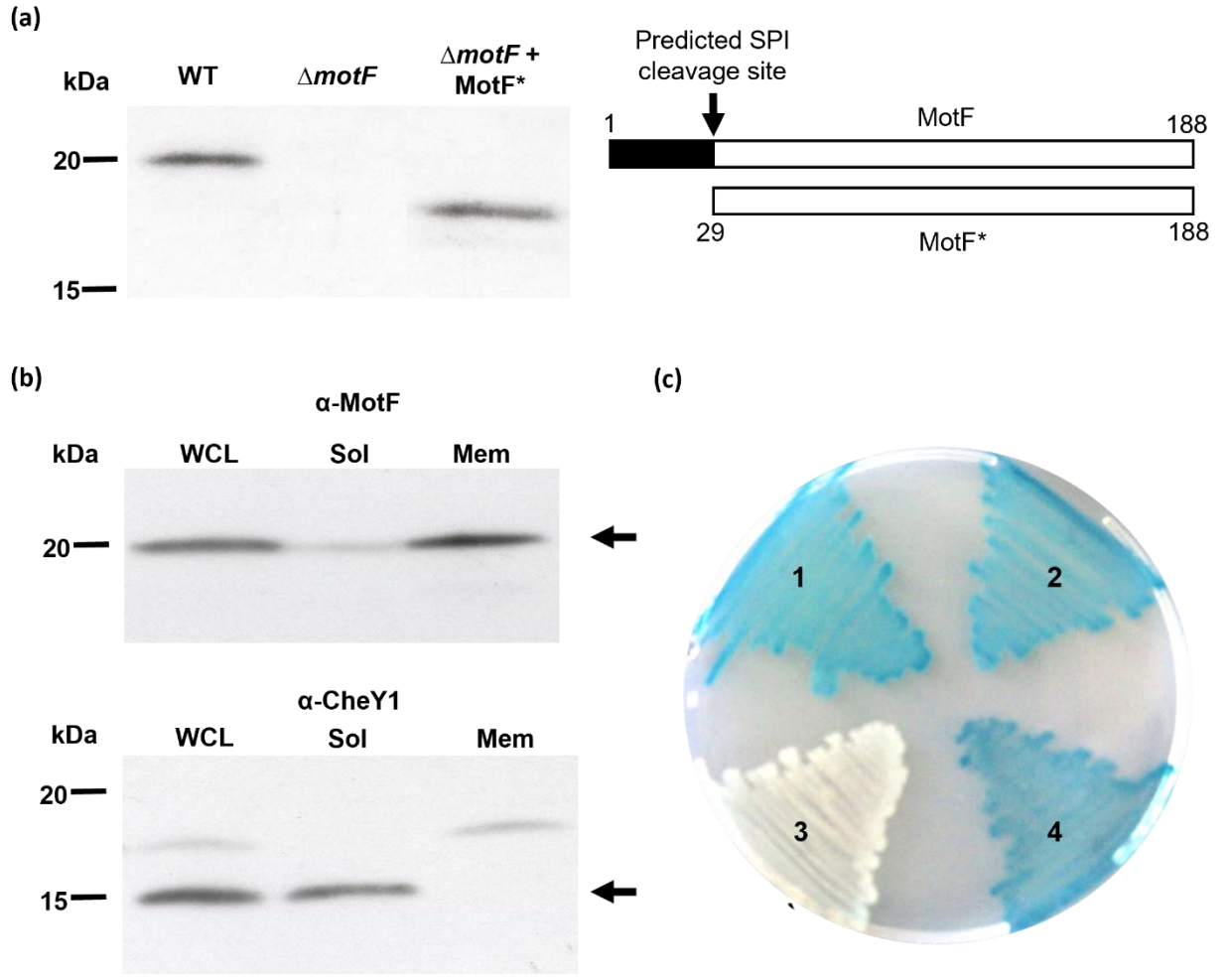

FIGURE 2.4 Subcellular localization and topology of MotF. (a) anti-MotF immunoblot analysis of wild type (WT) cell lysates compared to purified MotF lacking the predicted signal sequence (MotF*) in Δ*motF* cell lysates. The topologies of the detected proteins are illustrated to the right. (b) Immunoblot analysis of MotF (top panel) and CheY1 (bottom panel) in subcellular fractions. The MotF and CheY1 bands are indicated by arrows. Lys, whole cell lysate; Sol, soluble fraction; Mem, membrane fraction. (c) MotF topology analysis in an alkaline phosphatase (AP) reporter assay. *E. coli* DH5α with pKTop expressing AP fusion proteins with full-length MotF (1), the MotF transmembrane domain (2), unmodified AP (3), or the periplasmic control YmgF$_{1-39}$ (4) were incubated on LB agar plates supplemented with the chromogenic substrate X-Pho. Blue color indicates periplasmic localization of the C-terminus of the expressed protein.

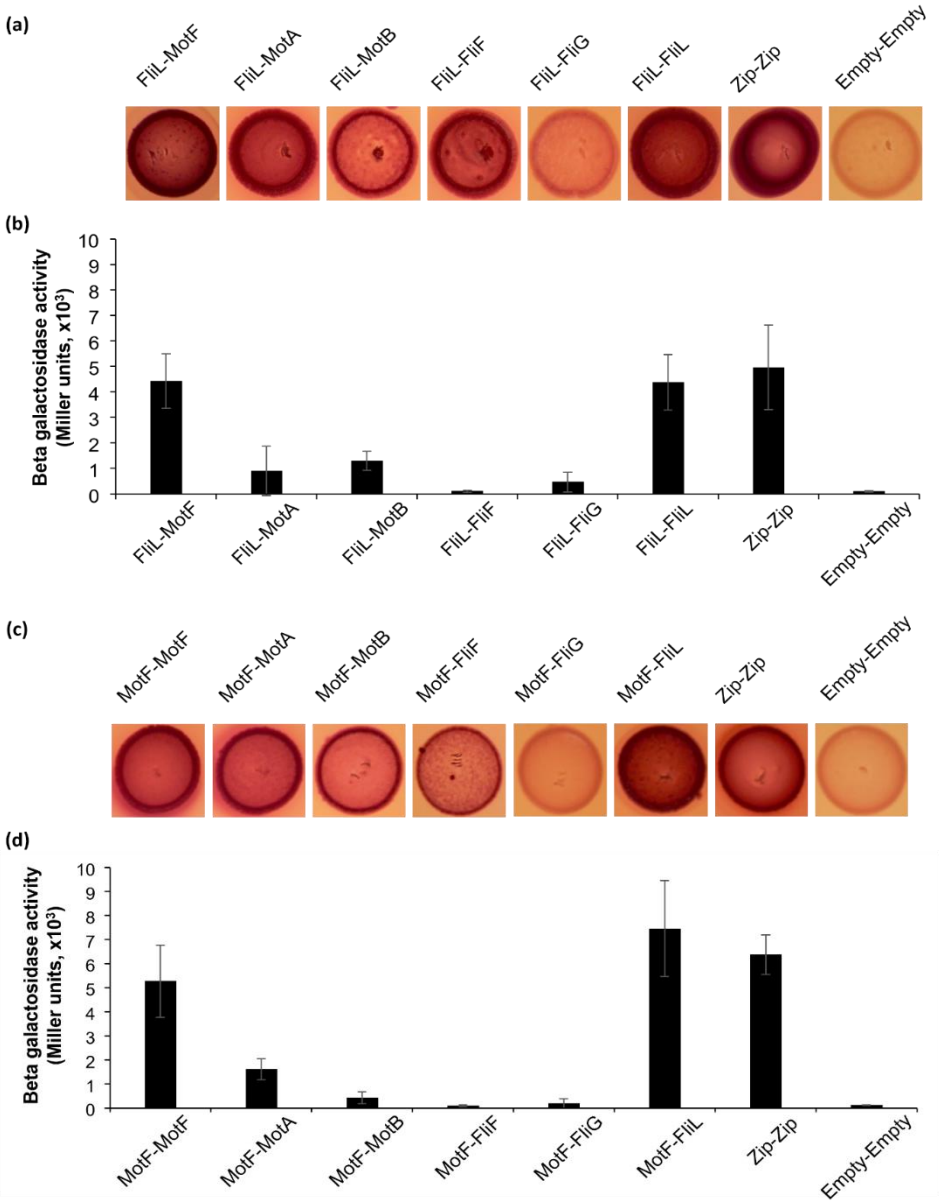

FIGURE 2.5 Bacterial two-hybrid **(**BACTH) assays of FliL and MotF interactions with basal body components. FliL and the indicated proteins were tested for interaction in *E. coli* BTH101 Δ*flhC* cells on MacConkey/lactose plates at 30°C for 48 h (a) and by β-galactosidase assays (b); MotF and the indicated proteins were tested for interaction in *E. coli* BTH101 Δ*flhC* cells on MacConkey/lactose plates at 30°C for 48 h (c) and by β-galactosidase assays (d). Interaction pair labels correspond do proteins produced from pKT25 and pUT18C, respectively.

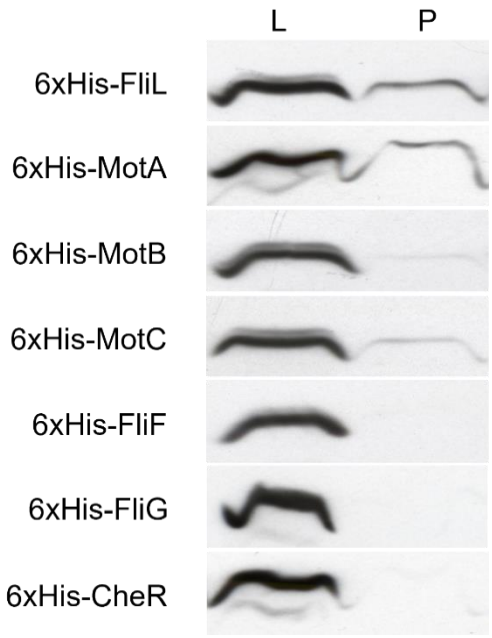

FIGURE 2.6 Pull-down assays of MotF. Genes encoding putative MotF interaction partners were cloned in MCS-1 of pETDuet-1 to yield proteins N-terminally fused with a 6x-his tag; *motF* was cloned in MCS-2. Pull-down assays using IMAC were performed as described in Materials and Methods. L, loaded fraction; P, pulled-down fraction.

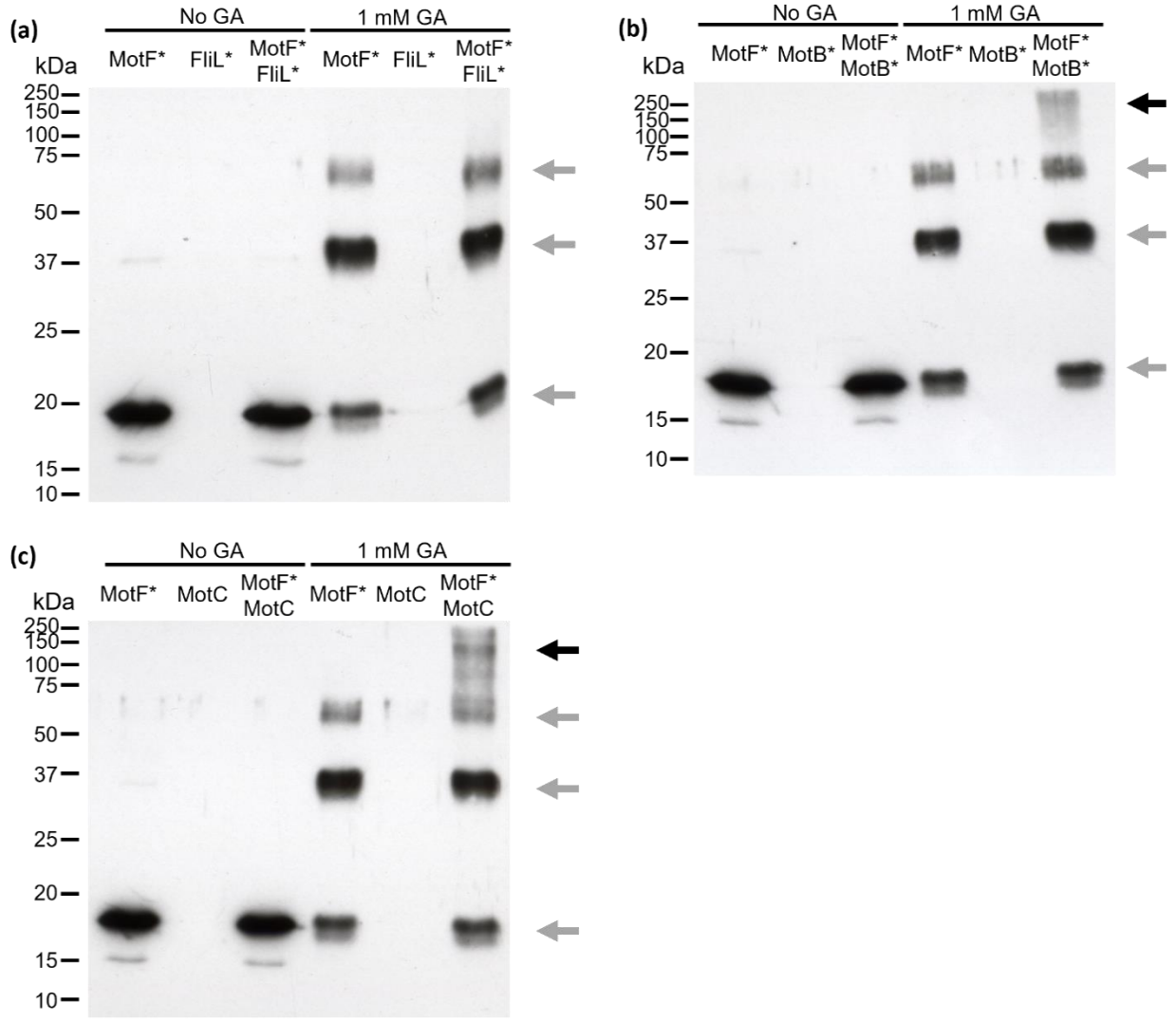

FIGURE 2.7 *In vitro* glutaraldehyde crosslinking assay of the purified periplasmic domain of MotF (MotF*) with (a) the periplasmic domain of MotB (MotB*), (b) MotC, and (c) the periplasmic domain of FliL (FliL*). Grey arrows mark different oligomeric states of MotF* and black arrows mark the heterooligomers with MotF* and MotB* or MotC. Purified proteins at 1 µM were incubated in the presence or absence of 1 mM glutaraldehyde for 1 h at room temperature prior to gel electrophoresis and immunoblot analysis with the anti-MotF antibody.

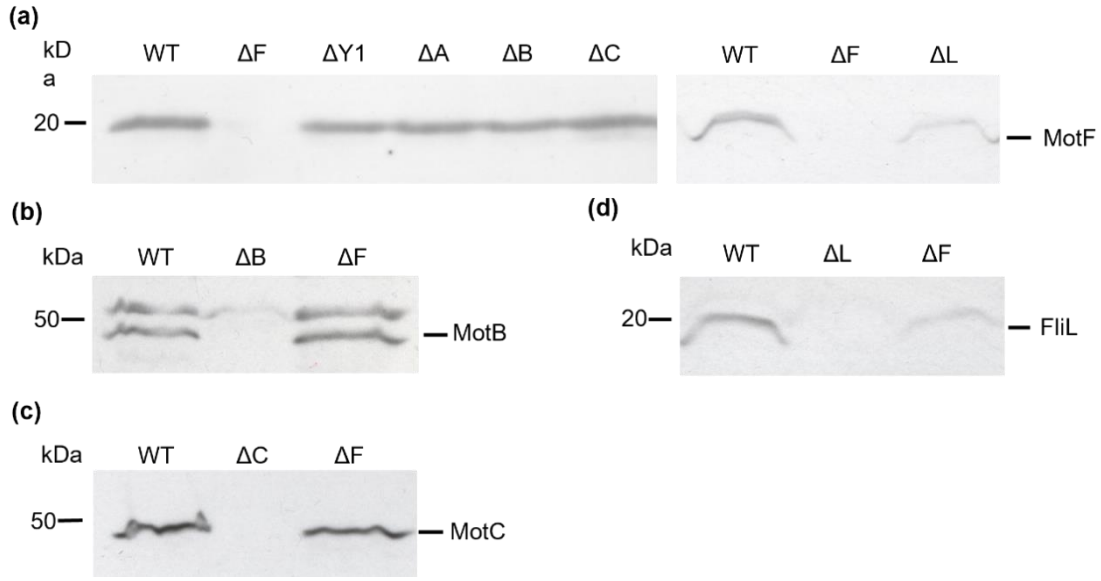

FIGURE 2.8 Immunoblot analysis of cellular protein levels in wild type and deletion strains. Levels of MotF in various deletion strains (a). Levels of MotB (b), MotC (c), and FliL (d) in Δ*motF*. Equal amounts of lysates from cells grown in Bromfield overlay cultures were analyzed using polyclonal antibodies raised against the specified protein.

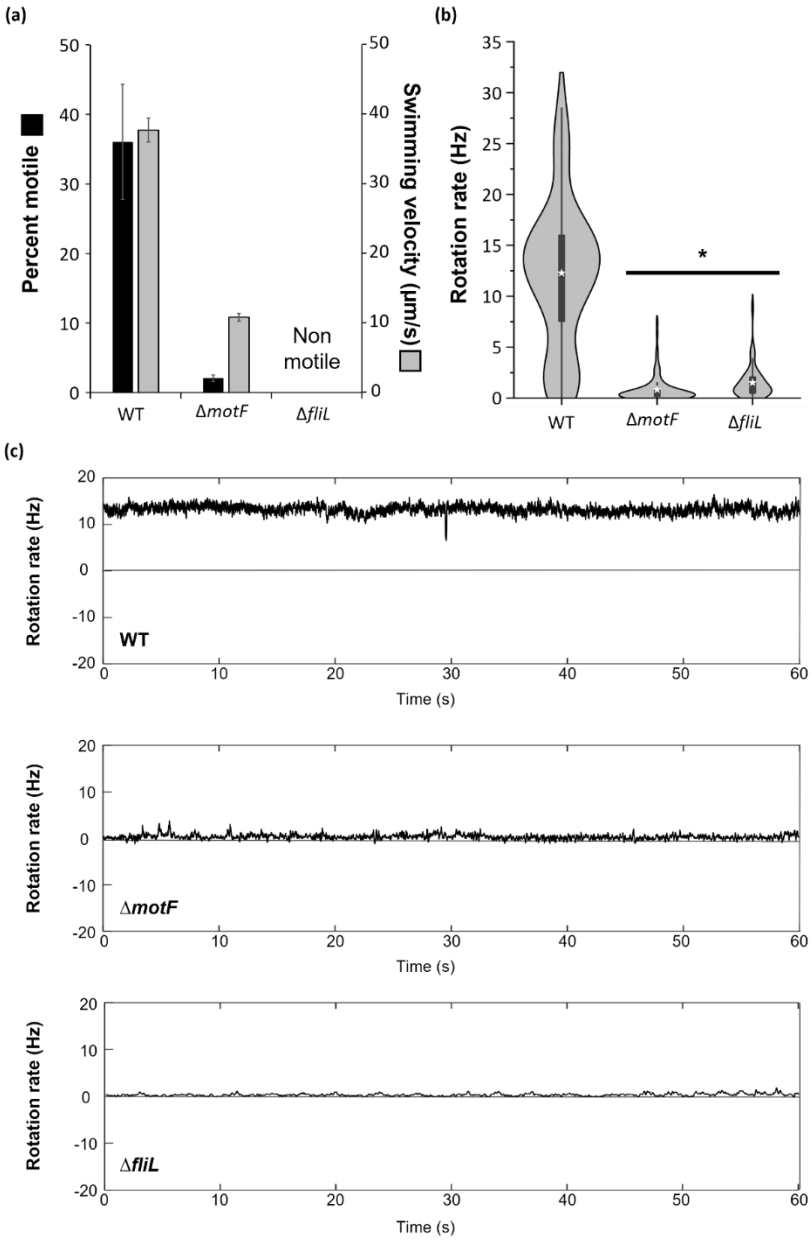

FIGURE 2.9 Swimming and flagellar motor behavior of *S. meliloti* wild type, Δ*motF* and Δ*fliL* in the tethered-cell assay. (a) Swimming velocity and percentage of motile bacteria. (b) Average rotation rates of single flagellar motors (n=100 for wild type and Δ*motF*, and n=40 for Δ*fliL*). Asterisks mark average rotation rates and boxes correspond to the interquartile ranges. (c) Traces of representative rotation rates for each strain.

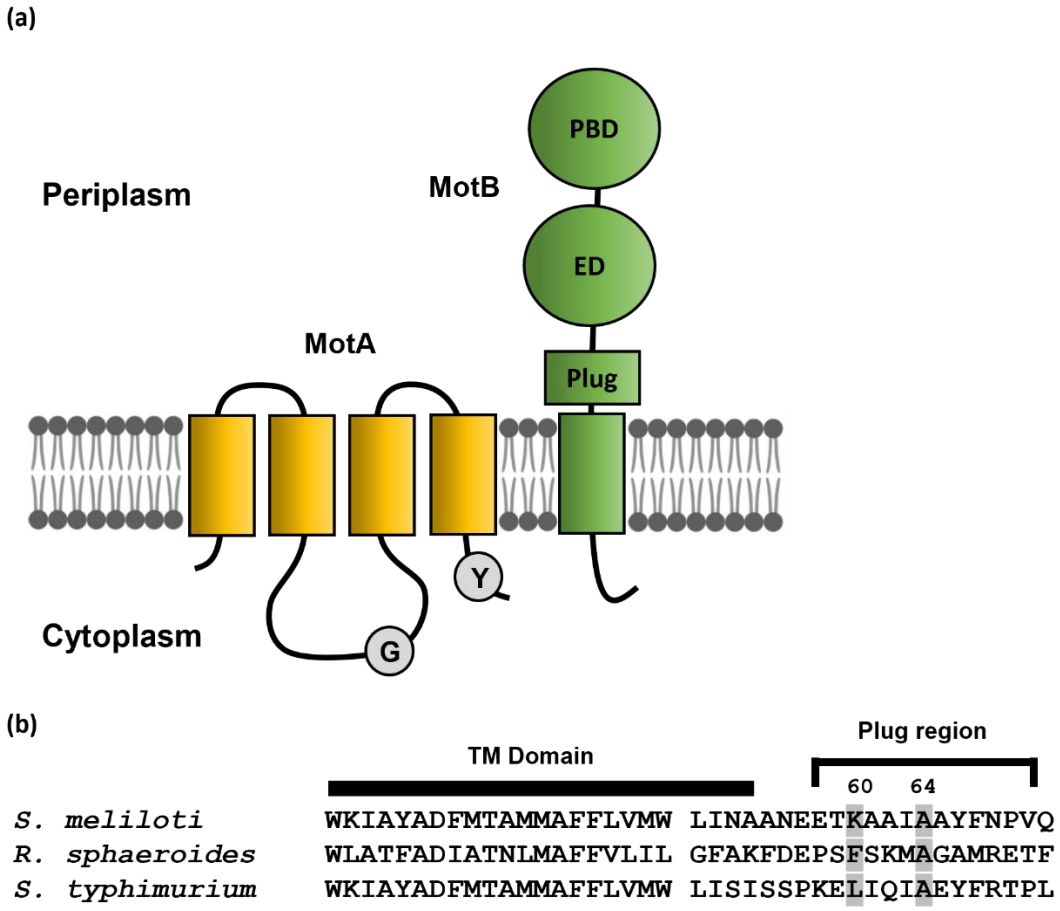

FIGURE 2.10 Topology and sequence alignment of stator proteins. (a) Topology of MotA and MotB marking the position of mutated residues. G, Gly136; Y, Tyr248; PBD, peptidoglycan binding domain; ED, *S. meliloti* extra domain; Plug, MotB plug region (aa 58-69) (b) Multiple sequence alignment of the N-terminal region of *S. meliloti*, *R. sphaeroides*, and *S. typhimurium* MotB using the T-Coffee server (190). MotB TM domains are indicated by a black line and the plug regions are bracketed. The position of mutated residues is labeled with the corresponding *S. meliloti* MotB amino acid residue number.

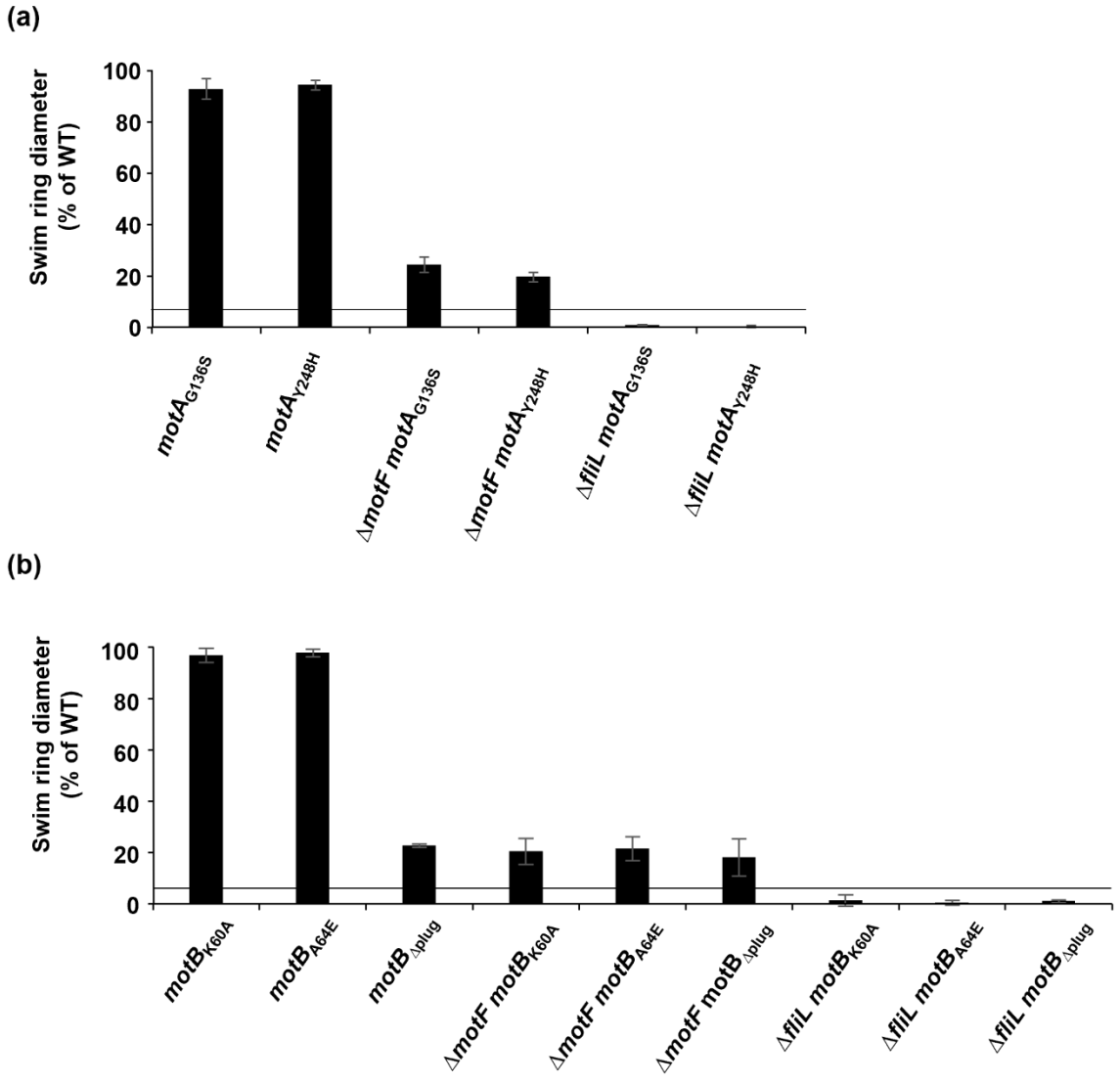

FIGURE 2.11 Swim ring analysis of Δ*motF* and Δ*fliL* strains with second-site mutations in *motA* (a) and *motB* (b). Horizontal black lines serve as reference of the Δ*motF* swim ring diameter. Data are averages and standard deviations for at least three independent experiments with three technical replicates.

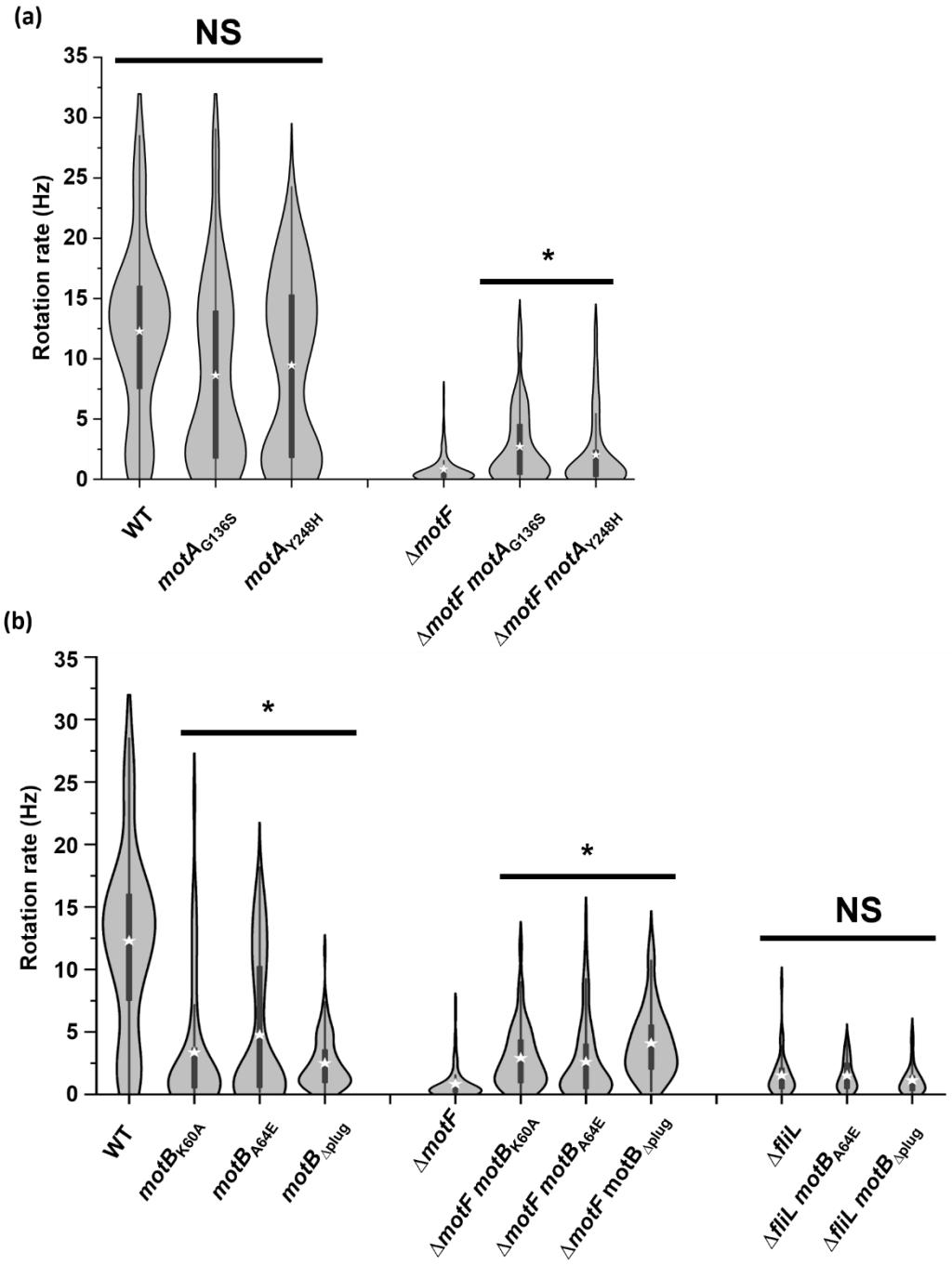
(a)
NS
*
Rotation rate (Hz)
0
5
10
15
20
25
30
35
WT
motA G136S
motA Y248H
ΔmotF
ΔmotF motA G136S
ΔmotF motA Y248H
(b)
*
*
NS
Rotation rate (Hz)
WT
motB K60A
motB A64E
motB Δplug
ΔmotF
ΔmotF motB K60A
ΔmotF motB A64E
ΔmotF motB Δplug
ΔfliL
ΔfliL motB A64E
ΔfliL motB Δplug

FIGURE 2.12 Flagellar motor behavior of Δ*motF* and Δ*fliL* strains with mutations in *motA* (a) and *motB* (b) in the tethered-cell assay. Tethered cell rotation rates of wild type (WT) and *mot* mutants (n=100 each for wild-type and Δ*motF* background strains and n=40 for Δ*fliL* background strains). Dots indicate average rotation rates and boxes correspond to the interquartile ranges. Asterisks indicate significant difference of the means (P>0.02) from the corresponding parental strain as determined by the Kruskal-Wallis and Dunn's multiple comparison post-hoc tests. NS, not significant.

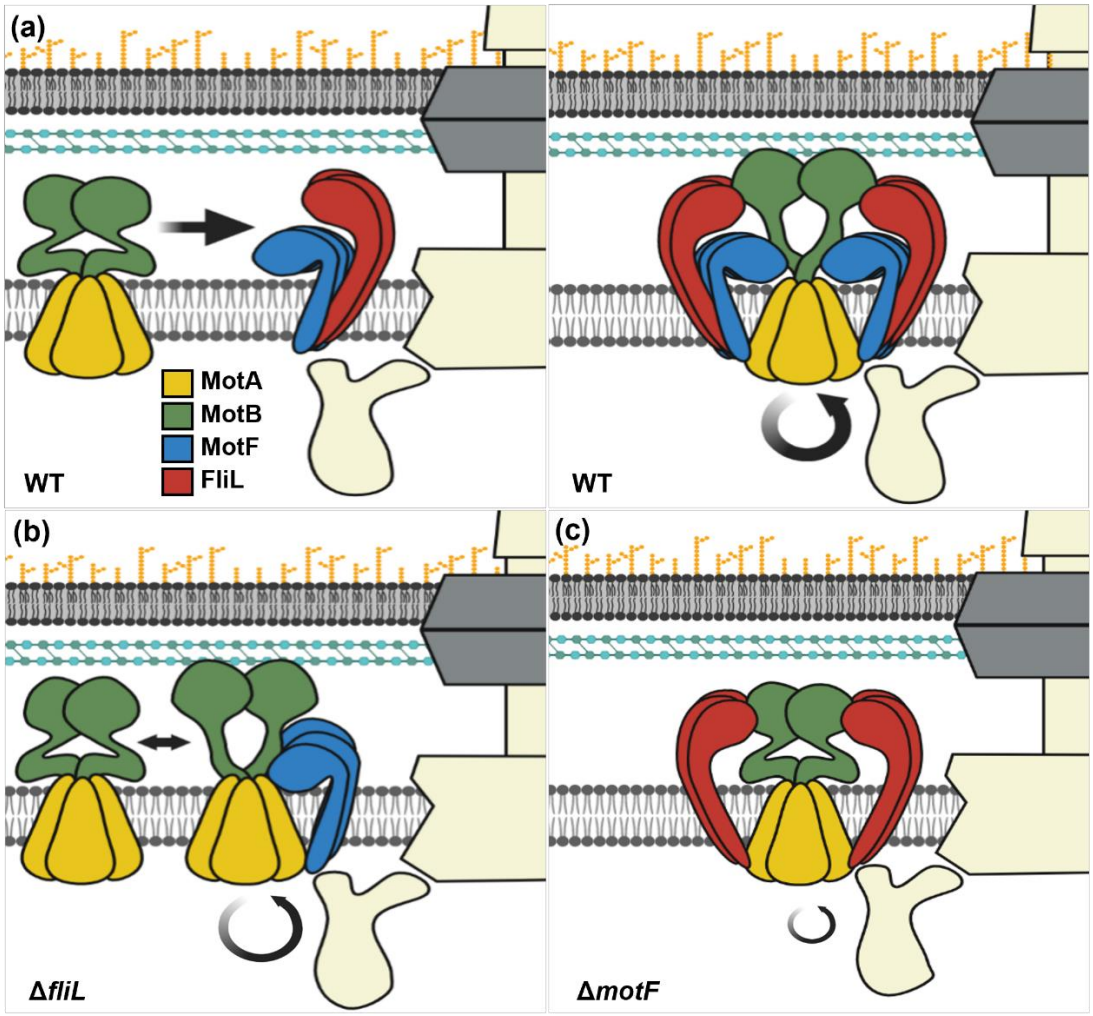

FIGURE 2.13 Model describing the roles of MotF and FliL and effects of their absence on flagellar motility in *S. meliloti*. (a) In the wild type, stator units are recruited to basal bodies by partial rings of FliL and MotF (top left panel), which recruit additional FliL and MotF proteins to form a cage around the stators. MotF modulates the $MotB_{plug}$ to promote motor rotation (top right panel). (b) In the absence of MotF, stators are stabilized by FliL near the basal body but are unable to release $MotB_{plug}$ resulting in overall low torque generation. (c) In motors without FliL, stators associate with MotF but remain unable to securely integrate into the basal body leading to low torque generation.

Chapter 3: Identification and characterization of Orf23 required for optimal flagellar motor function in *Sinorhizobium meliloti*

Identification and characterization of Orf23 required for optimal flagellar motor function in *Sinorhizobium meliloti*

Running Title: Orf23 is required for optimal flagellar motor function

RICHARD C. SOBE, DJELIKA KABORE†, and BIRGIT E. SCHARF[#]

[a]Department of Biological Sciences, Life Sciences I, Virginia Tech, Blacksburg, VA, USA

Key words: chemotaxis, flagellar basal body, proton channel plug, swimming motility, torque generation

#Address correspondence to Birgit E. Scharf, bscharf@vt.edu
Tel (+1) 540 231 0757
Fax (+1) 540 231 4043
Biological Sciences, Life Sciences I
Virginia Tech
Blacksburg, VA, 24061, USA

†Present address: NIH Clinical Center, Bethesda, MD 20892

Attribution: RCS performed all experiments except where noted otherwise. DK performed osmotic stress assays and swim plate assays in Figure 3.1 and 3.2. RCS and BES wrote the mansucript.

ABSTRACT

Stabilization of the bacterial flagellar motor in the peptidoglycan sacculus is a critical prerequisite for proper flagellar motor function in bacteria. Among the proteins with known roles in peptidoglycan regulation that impact motility is the transcriptional regulator LdtR, a MarR-type regulator known to regulate peptidoglycan synthesis genes in *Sinorhizobium meliloti* and *Liberibacter spp.* Here, we report that the loss of LdtR nearly abolishes *S. meliloti* motility but not production of flagella and that deletion of a previously uncharacterized gene in the flagellar regulon, *orf23*, mostly restores the motility defect. Immunoblot analysis with protein-specific antibodies revealed that LdtR does not regulate motility genes including *orf23*. Furthermore, the osmotic stress defect of a Δ*ldtR* mutant is not restored upon deletion of *orf23*. Intriguingly, suppressor mutant and homology modeling analyses revealed that a mutation in *motA* causing a G12S amino acid substitution at the periphery of MotAB stator units restores motility to the Δ*ldtR* strain similar to removal of Orf23. Our combined work suggests that Orf23 may serve an accessory role to improve stator performance but is not critical for function. Furthermore, Orf23 may engage in peptidoglycan-dependent alignment of flagellar stators that becomes detrimental when peptidoglycan crosslinking is disrupted.

INTRODUCTION

The bacterial flagellum is a highly complex rotary machine that requires the activity of about 50 different protein products for its regulation, synthesis, and function. (1). Each flagellum consists of a staggering number of 20,000 proteins and thus the genes encoding these are tightly regulated in a hierarchical fashion (2). In the soil bacterium *Sinorhizobium meliloti* the regulation of motility genes occurs in a three-tiered system. At the apex of the motility regulatory cascade are the class IA genes, *visN* and *visR*, which encode the LuxR-type global transcriptional regulators, VisNR, named for being vital for swimming (3). VisNR are produced throughout the growth phases but only activate the class IB gene, *rem*, during exponential growth (3, 4). *rem* encodes the regulator of exponential growth motility (Rem), an OmpR-like master regulator that directly influences its own transcription in addition to activating class IIA (flagellar basal body) and class IIB (motor) genes. Following proper assembly of the basal body, rod, and hook structures, class III genes including those coding for flagellin and chemotaxis proteins are activated in a manner

dependent on the uncharacterized protein Orf38, the flagellin regulator FlbT, and the flagellar C-ring component FliM (4, 5).

Flagellum biosynthesis is initiated by construction of the flagellar type-three secretion system (fT3SS) and the MS-ring, which surrounds the secretion system in the inner membrane (6). The fT3SS is a portal for secretion of the main axial components, namely the rod, hook, and filament structures and associated adaptor proteins (6). The MS-ring serves as a scaffold onto which the cytoplasmic C-ring assembles as well as an adapter for the transmission of torque from the C-ring to the flagellar rod in the periplasm. The C-ring, comprised of FliG, FliM, and FliN, influences flagellar rotation in response to chemotactic signals (7, 8). The flagellar rod is built atop the MS-ring and protrudes through the periplasm, peptidoglycan layer, and the outer membrane. During rod formation, the peptidoglycan-associated P-ring component FlgI and lipopolysaccharide-associated L-ring component FlgH are secreted through the SEC pathway and assemble to form a fused bushing structure through which the rod rotates (9). The flexible hook (FlgE) is produced next and serves as a universal joint to permit the smooth transmission of rotary torque from the rod to the long (two to several micrometer) rigid flagellar filament as the motor rotates (10).

Flagellar rotation is driven by the conversion of ion motive force into rotary motion by stator units comprised of MotA and MotB for proton-driven stators or PomA and PomB for Na^+-driven stators (*e.g.* in *Vibrio spp.*), which are positioned as 11-18 studs in the inner membrane at the periphery of the basal body (11-13). MotA consists of four transmembrane (TM) helices with a large cytoplasmic domain between TM2 and TM3, and a cytoplasmic C-terminal domain distal to TM4 (14). MotB consists of a short N-terminal stretch of amino acids in the cytoplasm followed by a TM domain and a periplasmic domain comprised of a proton channel plug region, a linker region, and a peptidoglycan-binding domain (15-17). Inactive stator complexes form in the inner membrane as a MotA pentamer surrounding a dimer of MotB (11, 12, 18). Two proton channels formed between the TM helices of MotA and MotB are maintained in an inactive state by the MotB plug regions, which remain wedged within the crenelations formed between short periplasmic sections of MotA (19). This arrangement prevents unnecessary proton flow until the stators are activated by contact between MotA in free stators and the C-ring component FliG in the cytoplasm. Upon stator-rotor contact, the periplasmic regions of the MotB dimer extend

upward to secure interactions between their peptidoglycan-binding domains and the rigid sacculus (15, 20-24). Consequently, the MotB proton plugs are released, the proton channels are opened, and proton flow through the stator units drives rotation of the MotA ring around MotB (11). This rotational energy is transmitted from MotA through interactions between MotA and FliG in the cytoplmasmic C-ring, which drives rotation of the entire basal body-hook-filament superstructure.

Peptidoglycan remodeling is a critical process in flagellum biosynthesis (25). The rod, consisting of proximal rod (FliE, FlgB, FlgC, and FlgF) and distal rod (FlgG) substructures, spans the periplasm and must therefore pass through the peptidoglycan and outer membrane layers of the cell envelope (6). As the average pore-size of the peptidoglycan meshwork is about 2-4 nm and the rod diameter boasts about 10-20 nm, peptidoglycan remodeling is a necessary phase of rod synthesis. In some bacteria including *Escherichia coli* and *Salmonella enterica*, peptidoglycan deconstruction required for rod insertion is catalyzed by the rod-associated FlgJ hydrolase, which caps the growing rod structure via its N-terminal rod-binding domain and contains a β-N-acetylglucosaminidase domain in its C-terminal region (26). Interestingly, in *Rhodobacter sphaeroides*, the functional components of FlgJ are accomplished by two separate proteins: a $FlgJ_N$-like rod-binding protein and a lytic transglycosylase enzyme, SltF (25, 27). In *S. meliloti*, $FlgJ_N$ is encoded by *SMc03071* and the peptidoglycan hydrolytic domain is predicted to be encoded by *SMc03045* (https://iant.toulouse.inra.fr/bacteria/annotation/cgi/rhime.cgi). Specific peptidoglycan architecture is required for stator association with the peptidoglycan (28), which serves as a chassis within the cell envelope to stabilize the motor against the substantial forces required to drive flagellar filament rotation. It has been proposed that proteins with an OmpA-like domain such as MotB bind to the peptidoglycan by a flexible clamp, which allows for dynamic associations of stators with the sacculus (29). Additionally, MotB has been shown to bind the NAM component of peptidoglycan directly (24).

Here, we have determined that a transcriptional regulator of peptidoglycan-modification genes, LdtR, is required for robust motility on soft agar swim plates. We found that spontaneous suppressor mutations in the previously uncharacterized flagellar gene *orf23* readily arise in the Δ*ldtR* background strain resulting in restored motility on soft agar swim plates from 25% to about 75% of those produced by the wild type. The Δ*orf23* strain produces swim rings with a

25%-reduced diameter compared to the wild type suggesting that the Δ*orf23* phenotype is dominant over that of the Δ*ldtR* mutant. Additionally, alteration of the transmembrane domain 1 (amino acid substitution G12S) of the flagellar stator component MotA greatly restores motility to the Δ*ldtR* strain. Orf23 possesses a single transmembrane domain and is localized mainly in the periplasm. Homology modeling revealed that Orf23 may form a β-sandwich domain in the C-terminal region, and mutational analysis suggests that this region is critical for Orf23 function. Possible implications of the $MotA_{G12S}$ mutation in stator function are discussed. Our data suggest that Orf23 may be involved in fine-tuning of peptidoglycan-dependent stator placement and high velocity swimming in the flagellar motor of *S. meliloti*.

RESULTS

LdtR is required for motility but not synthesis of flagella in *S. meliloti*

We performed a mini-Tn5 transposon mutagenesis screen to identify genes required for swimming motility in the wild-type *S. meliloti* strain RU11/001. Whole genome sequencing revealed that out of 32 mutants sequenced, one mutant harbored a disruption of *SMc01768* causing reduced swimming capacity on soft-agar swim plates to about 20% of the wild type. Similar results were obtained for an in-frame deletion mutant of *SMc01768* and the phenotype was complemented to about 65% of wild type levels by ectopic expression (Figure 3.1A). Notably, a small population of ~5-10% of bacteria appeared motile when samples of liquid culture were observed by phase contrast microscopy.

SMc01768 encodes a MarR family transcriptional regulator, members of which usually serve roles in stress responses and neutralization or export of harmful compounds (30). Pagliai *et al.* reported that the protein product, named LdtR for L,D-transpeptidase Regulator, regulates its own gene transcription, an adjacent gene encoding the L,D-transpeptidase, LdtP, and several other genes encoding peptidoglycan-modifying enzymes and small molecule transporters in response to high osmotic stress (31, 32). Additionally, mutants lacking either LdtR or LdtP show reduced osmotic stress tolerance in *Liberibacter crescens* and *S. meliloti* strain 1021. We determined that the Δ*ldtR* mutant of *S. meliloti* strain RU11/001 exhibits similarly reduced osmotic stress tolerance in the presence of 0.45 M sucrose (Figure 3.1B).

The genes encoding bacterial flagella are transcribed such that the structural components of the basal body synthesized prior to the highly abundant flagellin proteins that comprise flagellar filaments. This quality control ensures that copious levels of filament protein are only produced once a functional basal body is present on which to build the filament structure. Therefore, to determine whether LdtR is involved in flagellar gene regulation, we compared the levels of the flagellin proteins for the wild type and the Δ*ldtR* strain by immunoblot analysis (Figure 3.1C). We found no difference in the flagellin levels between these strains indicating that LdtR is unlikely to influence motility at the transcriptional level and that the main axial flagellar structures required for filament synthesis are properly assembled in the Δ*ldtR* mutant. Altogether, these data suggest that balanced levels of LdtR are important for osmotic stress tolerance and motility but not production of flagella in *S. meliloti*.

Disruption of *orf23* or alteration of the TM1-coding region of *motA* restores motility to the Δ*ldtR* mutant

Motility assays of the Δ*ldtR* strain on soft agar swim plates revealed a uniquely robust tendency of this mutant to produce spontaneous suppressor mutations resulting in strongly restored motility (Figure 3.2A). Importantly, we tested two of the suppressor mutants for osmotic stress tolerance and found a very modest (if at all) improvement compared to the Δ*ldtR* parent strain on 0.45 M sucrose (Figure 3.2B) suggesting that although the suppressor mutations caused restored motility, the mutants likely retained substantial peptidoglycan defects. Whole genome sequencing of four suppressor mutants revealed that one strain had a mutation in the coding region of MotA corresponding to a G12S amino acid substitution in the first transmembrane domain (Table 3.1 and Figure 3.3A). The three remaining strains all had mutations in an uncharacterized gene, *SMc03026* (the 23rd gene in the flagellar regulon and referred to hereafter as *orf23*; Table 3.1), which is located in the contiguous flagellar regulon of the *S. meliloti* chromosome (Figure S3.1). Introduction of the *motA*$_{G12S}$ mutation or the Δ*orf23* mutation into the Δ*ldtR* mutant similarly restored motility to approximately 75% of the wild type (Figure 3.3B). Similar results were obtained for the Δ*ldtR* Δ*orf23 motA*$_{G12S}$ triple mutant indicating that the restorative effects of these mutations Δ*ldtR* strain are not additive. Notably, we found that spontaneous suppressor mutations also readily arise in *orf23* in an *Agrobacterium sp.* H13-3 Δ*ldtR* strain indicating that Orf23 and LdtR exert similar functions in these related alphaproteobacterial species (data not shown).

In an attempt to identify other Δ*ldtR* suppressor mutations, we isolated additional suppressor mutants. We introduced the pBS538 plasmid for ectopic expression of *orf23* into each mutant to eliminate the candidates with mutations in this gene from our screen. For 23 out of 24 mutants screened, the original swimming defect was observed (data not shown) indicating that disruption of the *orf23* gene is the primary cause for motility restoration to the Δ*ldtR* strain. Since flagellum assembly is unperturbed in the Δ*ldtR* strain (Figure 3.1C) and thus flagellar type-three secretion system (fT3SS) and axial components of the flagellum are clearly operational in terms of axial structure synthesis, our combined suppressor mutant results suggest that in the absence of LdtR, either stator function or torque transmission to the rotor is impaired by the presence of Orf23.

LdtR does not regulate Orf23

One possible explanation for the suppressor mutant data is that LdtR controls *orf23* gene transcription. However, this is unlikely because *orf23* is the last gene in a four-gene operon, which also codes for important flagellar rod and fT3SS components. Nonetheless, to determine whether LdtR is regulating Orf23 levels we performed immunoblot analysis with an Orf23-specific polyclonal antibody. As expected, we found no difference in the abundance of Orf23 in the Δ*ldtR* mutant compared to the wild type further indicating that LdtR does not regulate motility genes (Figure 3.4).

Orf23 contains a transmembrane domain near its N-terminus and resides mainly in the periplasm

To determine how the suppressor mutations in *orf23* improve motility of the Δ*ldtR* strain, we first investigated the cellular localization of Orf23. The signal peptide prediction server SignalP 6.0 (33) found no putative signal peptides in Orf23. Additionally, we detected Orf23 in *S. meliloti* wild type near its predicted molecular weight of 20.4 kDa indicating that the protein is unlikely to be cleaved by signal peptidases (Figure 3.4). Furthermore, the TMHMM server (34) predicted that Orf23 contains a short cytoplasmic domain (aa 1-25) followed by a transmembrane helix (aa 26-48) and a periplasmic domain (aa 49-183; Figure 3.5A). To experimentally validate these predictions, we employed the pKTop system, which drives production of a protein of interest fused at its C-terminus to *E. coli* alkaline phosphatase (AP, encoded by *phoA*) and the alpha subunit of β-galactosidase (LacZα) (35). If the C-terminus of Orf23 is located in the periplasm as predicted, PhoA will become activated and an *E. coli* DH5α

strain expressing the fusion protein will appear blue on indicator LB plates supplemented with the chromogenic alkaline phosphatase substrate X-Pho. However, if the C-terminus is located in the cytoplasm, AP will remain inactive and the bacterial growth will appear off-white. Bacteria possessing a positive control plasmid encoding AP-LacZα fused to the C-terminus of the outward-facing transmembrane domain of YmgF ($YmgF_{1-39}$) and unmodified pKTop negative control that encodes the cytoplasm-localized AP-LacZα fusion alone responded appropriately on indicator plates (Figure 3.5B). As predicted, bacteria producing the Orf23-AP-LacZα fusion protein produced blue colonies on X-Pho plates confirming that the C-terminal region of Orf23 is located in the periplasm.

Orf23 may possess a C-terminal β-sandwich domain similar to components of the type four pilus and type four secretion system

To investigate the putative structure of Orf23, we submitted its amino acid sequence to AlphaFold Collab (36). The results of this analysis suggest that the first 22 aa of Orf23 are disordered followed by an alpha helix comprised of aa 23-48, a long region with no predicted secondary structure from aa 50-127, and the remaining aa 128-183 are predicted to form a β-sandwich domain (Figure 3.6). The Δ*ldtR* suppressor mutant analysis identified three mutations that appear to cause a loss-of-function phenotype for Orf23 (Table 3.1). In two cases, disruption of *orf23* by frameshift mutation (Suppressor 1) or a transposon insertion (Suppressor 3) resulted in truncation of the Orf23 protein product by 16 aa or 79 aa, respectively, whereas the third mutation caused a single amino acid substitution (P163L). Notably, each of these mutations would have disruptive consequences for the putative β-sandwich domain.

We submitted the putative Orf23 structure predicted by AlphaFold to the DALI server to identify proteins with similar structures. The top hits were for different chains of the PilP protein from *Pseudomonas aeruginosa* (PDB ID: 2Y4Y) with an RMSD of 2.8 over 80 aa coverage. PilP is part of the type IV pilus (T4P) alignment complex that spans the periplasm connecting the inner membrane complex and cytoplasmic ATPase assembly to the outer membrane complex of T4P. Additionally, we submitted a query to the SWISS-MODEL server, which resulted in a top hit for the Dot/Icm type IV secretion system component DotF from *Legionella pneumophila* with an additional convincing hit for the *Neisseria meningitidis* PilP protein (Figure 3.6 and Table 3.2). DotF, along with DotG, is thought to form the periplasmic region of the TIVSS (37, 38).

Interestingly, both PilP and DotF form central rings in their respective macromolecular complexes.

The MotA$_{G12S}$ mutation is predicted to occur at the periphery of the MotA pentamer ring

To understand how the MotA$_{G12S}$ mutation restores motility to the Δ*ldtR* mutant, we performed homology modeling to map the putative location of the Gly12 residue of *S. meliloti* MotA using the recently solved *C. jejuni* MotA$_5$MotB$_2$ crystal structure (12) using the SWISS-MODEL server (Table 3.2). The G12S mutation is predicted to be positioned on the outside of the MotA pentamer ring about midway through TM1 of each monomer (Figure 3.7). Similar results were obtained when *S. meliloti* MotA was modeled to the recently solved *B. subtilis* MotA$_5$ structure (Table 3.2) (39). The high GMQE, QMEANDisCo scores and high coverage of these models suggest high confidence in the putative location of the affected MotA residue.

DISCUSSION

Multiple cellular pathways converge to influence flagellar motility in *S. meliloti* at the transcriptional level. However, in each of these cases, control over motility is exerted through modulation of *visNR* or *rem* gene expression. Examples include the succinoglycan pathway controlled by ExoR, ExoS, and ChvI, the quorum sensing system SinI and ExpR, and the exopolysaccharide, motility, and membrane stress regulators EmmABC, all of which negatively influence *visNR* transcription. In contrast, the plant symbiosis regulator CbrA, positively regulates *visNR*. Additionally, the exopolysaccharide regulator MucR controls motility by negative regulation of *rem* transcription (5).

It has previously been suggested that LdtR regulates motility in *S. meliloti* 1021 (40). In correlation with this notion, either loss of LdtR or its overproduction negatively impacts motility. However, in both circumstances, bacteria were found to exhibit altered cellular morphology: a short-cell phenotype was described for the Δ*ldtR* mutant while a strain that overexpressed *ldtR* was found to exhibit a branched-cell morphology (41). These phenotypes are likely linked to the abolished and enhanced activity of the peptidoglycan regulator LdtR, as it is directly linked to transcriptional control of peptidoglycan modification genes and stress responses (31, 40-44). Such disruptions in cell morphology are plausibly explained by disrupted peptidoglycan remodeling when LdtR levels are imbalanced, but it is unclear whether they are responsible for

the substantial loss of motility exhibited by *ldtR* mutants. Immunoblot analyses clearly show that LdtR does not regulate flagellum synthesis in *S. meliloti* (Figure 3.1C).

Our suppressor mutant data demonstrate that the Δ*ldtR* motility defects are overcome by alteration of the motor protein MotA or inactivation of Orf23. Since the Δ*ldtR* strain produces flagella, we hypothesize that altered peptidoglycan remodeling in the Δ*ldtR* strain severely disrupts rotor-stator interactions resulting in the observed motility defect. Notably, flagellin levels in the Δ*ldtR* strain are comparable to the wild type, which also implies that peptidoglycan remodeling necessary for production of the axial rod-hook-filament structure is not impeded. From this observation we infer that LdtR plays a role in mediating control of peptidoglycan remodeling necessary for 1) stator association with the peptidoglycan and/or 2) association of a stator alignment module with the sacculus.

The suppressor mutant analysis revealed a striking selective pressure to disrupt *orf23* in the Δ*ldtR* strain on swim plates (Table 3.1). Since Orf23 levels are comparable in wild type and Δ*ldtR* strains, we conclude that the presence of Orf23 is detrimental for flagellar motor function when peptidoglycan crosslinking is disrupted and propose that Orf23 may be involved in rotor-stator alignment in a peptidoglycan-dependent manner. Notably, motility of the Δ*orf23* single mutant is only slightly impaired, which indicates that the role of Orf23 in swimming motility is secondary and perhaps aimed towards fine-tuning of the rotor-stator arrangement to maximize power transfer.

We recently characterized the roles of *S. meliloti* FliL and its paralog MotF in stator function (Sobe *et al.* under review). FliL is required for stator function and perhaps recruitment of stator elements to the basal body while MotF appears to modulate the MotB proton plug. Both proteins were found to interact with one another as well as with both stator components, MotA and MotB. Since Orf23 contains a putative transmembrane domain and resides mostly in the periplasm (Figures 3.4 and 3.5), we predict that it interacts with other membrane-bound components of the flagellar motor by associating with stator components directly and/or indirectly through interactions with FliL and/or MotF. Future experiments aimed at identifying Orf23 interaction partners will include bacterial two-hybrid analysis and immobilized metal affinity

chromatography (IMAC) pull-down assays using Orf23 and each of these candidate interaction partners.

It was intriguing to find that the *motA*$_{G12S}$ mutation, which corresponds to the first transmembrane region (TM1) of MotA, affords the same motility restoration to the Δ*ldtR* mutant as does the deletion of *orf23* (Figure 3.3). Our homology modeling suggests that the Gly-12 is located on the outside of the MotA pentamer and a G12S mutation would likely alter interactions with the recently characterized *S. meliloti* MotF and FliL proteins that are hypothesized to surround stators much like a cage (Sobe *et al.* under review).

Protein structure predictions and homology modeling propose that the C-terminal region of Orf23 (aa 128-183) forms a β-sandwich domain similar to the C-terminal regions of the type IV pilus PilP proteins from *P. aeruginosa* (PDB ID: 2Y4Y) or *N. meningitidis* (PDB ID: 2IVW) and the Dot/Icm type IV secretion system protein DotF from *L. pneumophila* (PDB ID: 7MUC). Notably, PilP and DotF proteins form part of a tube/ring structure in their respective macromolecular machines as do essentially all components of the flagellum, pili, and secretion systems. Therefore, we can speculate with some confidence that Orf23 will likely associate with the motor as one or more rings. It will be interesting to determine with which other structures in the flagellum Orf23 interacts and whether it surrounds the rod to position stators appropriately for maximal torque generation. Additional flagellar motor structures beyond those produced by *E. coli* and *S. enterica* have been identified in the form of various disks and rings in *Vibrio spp.*, *C. jejuni*, *B. subtilis*, and *Borrelia burgdorferi* (45, 46). These are thought to serve stabilizing roles in their various motors due to increased demands such as higher velocity or sustained performance in high viscosity conditions. Thus, we anticipate that *S. meliloti* employs interesting structural diversity compared to other systems to meet its need to power through the soil environment.

We speculate that disruption of peptidoglycan crosslinking in the Δ*ldtR* mutant causes improper placement of the stators with respect to the rotor in an Orf23-dependent manner and that removal of Orf23 or deformation of MotA$_{TM1}$ with the substitution of Gly12 by a polar serine residue allows the formation of new contacts between MotA and the rotor component FliG. Both secondary mutations, however, provide less optimal contacts between the stator and rotor than is

observed for wild-type motors, which manifests as diminished swimming capacity. Notably, a small population (~5-10%) of the Δ*ldtR* strain in liquid culture retains high velocity swimming (data not shown) suggesting that LdtR-mediated control of peptidoglycan crosslinking is not absolutely required for motility but improves the probability that stator units will have appropriate binding sites in the sacculus to position the stators appropriately near the rotor. This small population could represent low-level regulatory heterogeneity of the peptidoglycan-modifying enzyme genes under control of LdtR by an alternative regulator.

Important experiments to complete this study will include stability analysis of Orf23 in deletion mutants lacking various motor components and vice versa to gauge the dependence of these proteins on one another. We will also investigate whether Orf23 is associated with peptidoglycan and, if so, does this occur directly or through interactions with the P-ring protein FlgI or some as yet unidentified component? We will quantify swimming velocities, the percentage of motile bacteria, and tethered cell rotation rates in various Δ*ldtR*, Δ*orf23*, and *motA* point mutants to better understand how these mutations impact swimming and motor performance. Analysis of these behaviors in different viscosities will help reveal possible roles for Orf23 maximizing torque under high-load conditions and perhaps as a "high-gear" in the speed-variable motor of *S. meliloti*. Additionally, experiments to analyze the Δ*orf23* strain under swarming conditions reveal a more pronounced phenotype and could strongly implicate Orf23 in torque generation. Cryo-electron tomography studies to determine the precise localization of Orf23, MotF, and FliL within the flagellar motor will yield exciting details regarding the structure of the speed-variable motor of *S. meliloti*.

MATERIALS AND METHODS

Strains and plasmids

Derivative strains of *E. coli* K-12 and BL21 (DE3), highly motile derivatives of *S. meliloti* MVII-1, and plasmids used in this study are described in Table 3.3.

Media and growth conditions

E. coli strains were routinely grown in lysogeny broth (LB; (47) at 37°C or 30°C supplemented with appropriate antibiotics at 100 µg/ml ampicillin (Ap) and 50 µg/ml kanamycin (Km). *S.*

meliloti strains were grown in tryptone-yeast extract-calcium chloride (TYC) broth supplemented with streptomycin (Sm) at 600 µg/ml at 30°C.

Swim plate assays

Stationary phase cultures were spot-plated (3 µl) on Bromfield swim plates (0.04% Bacto tryptone, 0.01% yeast extract, 0.01% $CaCl_2$, 0.3% agar) for 3-5 days at 30°C.

Osmotic stress assays

Stationary phase cultures were spot-plated (3 µl) on LB agar plates supplemented with 0.45 M sucrose and incubated for 3 days at 30°C.

Purification of recombinant proteins

The periplasmic domain of Orf23 (Orf23*) was expressed from pBSX1331 in *E. coli* ER2566 (Table 3.3) and purified by Intein-Mediated Purification with an Affinity Chitin-binding Tag (IMPACT™) as described by Mitchell and Lorsch (48). Cells were grown to an OD_{600} of 0.5-0.7 in LB broth at 37°C prior to induction of protein expression by addition of 0.3 mM isopropyl β-D-1-thiogalactopyranoside (IPTG) and incubation overnight at 16°C.

SDS-PAGE and immunoblotting

Aliquots (1 ml) of cultures grown in Bromfield overlay plates were harvested at 15k x g, all but ~15 µl of the supernatant removed, and resuspended in 15 µl Laemmli buffer. Samples were boiled for 10 min. For flagellin immunoblots, 15 µl culture was mixed directly with Laemmli buffer and boiled for 10 min. Samples were stored at -20°C for at least 2 hours prior to further processing. Immunoblot analyses were performed as previously described (49). Polyclonal anti-flagellin and anti-Orf23 crude sera were used at 1:10,000 and donkey anti-rabbit HRP secondary antibody (NA-934, Cytiva) was used at 1:1,000.

Membrane topology reporter assays

Membrane topology reporter assays used in this study employ a *phoA-lacZ*α transcriptional fusion to the 3' end of *orf23* in the pKTop plasmid to produce pBS1330 (35, 50). Strains with the positive control plasmid pBS1193 (producing $YmgF_{1-39}$-AP-LacZα) and negative control plasmid pKTop (producing AP-LacZα) plasmids were also used. Colonies of *E. coli* DH5α strains transformed with pKTop plasmids were streaked on LB agar supplemented with 1 mM

IPTG and 80 µg/ml 5-chloro-4-bromo-3-indolyl phosphate (X-Pho) (RPI, Mt Prospect, IL, USA) and incubated for 18 hours at 30°C.

ACKNOWLEDGEMENTS

We would like to thank Dr. Roderick Jensen for assistance with WGS analysis.

CONFLICT OF INTEREST

The authors declare no conflict of interest.

AUTHOR CONTRIBUTIONS

RCS and BES conceived and designed this study, performed experiments, and wrote the manuscript. DK performed osmotic stress assays and suppressor mutant swim ring analyses.

FUNDING INFORMATION

National Science Foundation, Grant/Award Number: MCB-1253234, MCB-1817652, and MCB-2128232 to BS**.**

REFERENCES

1. Galibert F, Finan TM, Long SR, Pühler A, Abola P, Ampe F, Barloy-Hubler F, Barnett MJ, Becker A, Boistard P. 2001. The composite genome of the legume symbiont Sinorhizobium meliloti. Science 293:668-672.
2. Morimoto YV, Minamino T. 2014. Structure and function of the bi-directional bacterial flagellar motor. Biomolecules 4:217-234.
3. Sourjik V, Muschler P, Scharf B, Schmitt R. 2000. VisN and VisR are global regulators of chemotaxis, flagellar, and motility genes in *Sinorhizobium* (*Rhizobium*) *meliloti*. Journal of Bacteriology 182:782-788.
4. Rotter C, Mühlbacher S, Salamon D, Schmitt R, Scharf B. 2006. Rem, a new transcriptional activator of motility and chemotaxis in *Sinorhizobium meliloti*. Journal of Bacteriology 188:6932-6942.
5. Scharf BE, Hynes MF, Alexandre GM. 2016. Chemotaxis signaling systems in model beneficial plant–bacteria associations. Plant molecular biology 90:549-559.
6. Johnson S, Furlong EJ, Deme JC, Nord AL, Caesar JJ, Chevance FF, Berry RM, Hughes KT, Lea SM. 2021. Molecular structure of the intact bacterial flagellar basal body. Nature Microbiology 6:712-721.
7. Kinoshita M, Furukawa Y, Uchiyama S, Imada K, Namba K, Minamino T. 2018. Insight into adaptive remodeling of the rotor ring complex of the bacterial flagellar motor. Biochemical and Biophysical Research Communications 496:12-17.
8. Sarkar MK, Paul K, Blair D. 2010. Chemotaxis signaling protein CheY binds to the rotor protein FliN to control the direction of flagellar rotation in *Escherichia coli*. Proceedings of the National Academy of Sciences 107:9370-9375.

9. Kaplan M, Ghosal D, Subramanian P, Oikonomou CM, Kjaer A, Pirbadian S, Ortega DR, Briegel A, El-Naggar MY, Jensen GJ. 2019. The presence and absence of periplasmic rings in bacterial flagellar motors correlates with stator type. Elife 8:e43487.
10. Berg HC. 2003. The rotary motor of bacterial flagella. Annual Review of Biochemistry 72.
11. Wadhwa N, Berg HC. 2021. Bacterial motility: machinery and mechanisms. Nature Reviews Microbiology:1-13.
12. Santiveri M, Roa-Eguiara A, Kühne C, Wadhwa N, Hu H, Berg HC, Erhardt M, Taylor NM. 2020. Structure and function of stator units of the bacterial flagellar motor. Cell 183:244-257. e16.
13. Hu H, Santiveri M, Wadhwa N, Berg HC, Erhardt M, Taylor NM. 2021. Structural basis of torque generation in the bi-directional bacterial flagellar motor. Trends in Biochemical Sciences.
14. Blair DF, Berg HC. 1990. The MotA protein of *E. coli* is a proton-conducting component of the flagellar motor. Cell 60:439-449.
15. Kojima S, Takao M, Almira G, Kawahara I, Sakuma M, Homma M, Kojima C, Imada K. 2018. The helix rearrangement in the periplasmic domain of the flagellar stator B subunit activates peptidoglycan binding and ion influx. Structure 26:590-598. e5.
16. Hosking ER, Vogt C, Bakker EP, Manson MD. 2006. The *Escherichia coli* MotAB proton channel unplugged. Journal of Molecular Biology 364:921-937.
17. De Mot R, Vanderleyden J. 1994. The C-terminal sequence conservation between OmpA-related outer membrane proteins and MotB suggests a common function in both gram-positive and gram-negative bacteria, possibly in the interaction of these domains with peptidoglycan. Molecular microbiology 12:333-336.
18. Deme JC, Johnson S, Vickery O, Aron A, Monkhouse H, Griffiths T, James RH, Berks BC, Coulton JW, Stansfeld PJ. 2020. Structures of the stator complex that drives rotation of the bacterial flagellum. Nature Microbiology 5:1553-1564.
19. Tachiyama S, Chan KL, Liu X, Hathroubi S, Peterson B, Khan MF, Ottemann KM, Liu J, Roujeinikova A. 2022. The flagellar motor protein FliL forms a scaffold of circumferentially positioned rings required for stator activation. Proceedings of the National Academy of Sciences 119.
20. Morimoto YV, Nakamura S, Kami-ike N, Namba K, Minamino T. 2010. Charged residues in the cytoplasmic loop of MotA are required for stator assembly into the bacterial flagellar motor. Molecular microbiology 78:1117-1129.
21. Kojima S, Imada K, Sakuma M, Sudo Y, Kojima C, Minamino T, Homma M, Namba K. 2009. Stator assembly and activation mechanism of the flagellar motor by the periplasmic region of MotB. Molecular microbiology 73:710-718.
22. Van Way SM, Hosking ER, Braun TF, Manson MD. 2000. Mot protein assembly into the bacterial flagellum: a model based on mutational analysis of the *motB* gene. Journal of molecular biology 297:7-24.
23. Zhu S, Takao M, Li N, Sakuma M, Nishino Y, Homma M, Kojima S, Imada K. 2014. Conformational change in the periplamic region of the flagellar stator coupled with the assembly around the rotor. Proceedings of the National Academy of Sciences 111:13523-13528.

24. Roujeinikova A. 2008. Crystal structure of the cell wall anchor domain of MotB, a stator component of the bacterial flagellar motor: implications for peptidoglycan recognition. Proceedings of the National Academy of Sciences 105:10348-10353.
25. Herlihey FA, Clarke AJ. 2016. Controlling autolysis during flagella insertion in Gram-negative bacteria, p 41-56, Protein Reviews. Springer.
26. Herlihey FA, Moynihan PJ, Clarke AJ. 2014. The essential protein for bacterial flagella formation FlgJ functions as a β-N-acetylglucosaminidase. Journal of biological chemistry 289:31029-31042.
27. García-Ramos M, de la Mora J, Ballado T, Camarena L, Dreyfus G. 2021. Modulation of the enzymatic activity of the flagellar lytic transglycosylase SltF by rod components and the scaffolding protein FlgJ in *Rhodobacter sphaeroides*. Journal of Bacteriology 203:e00372-21.
28. Roure S, Bonis M, Chaput C, Ecobichon C, Mattox A, Barrière C, Geldmacher N, Guadagnini S, Schmitt C, Prévost MC. 2012. Peptidoglycan maturation enzymes affect flagellar functionality in bacteria. Molecular microbiology 86:845-856.
29. Samsudin F, Ortiz-Suarez ML, Piggot TJ, Bond PJ, Khalid S. 2016. OmpA: a flexible clamp for bacterial cell wall attachment. Structure 24:2227-2235.
30. Deochand DK, Grove A. 2017. MarR family transcription factors: dynamic variations on a common scaffold. Critical reviews in biochemistry and molecular biology 52:595-613.
31. Loto F, Coyle JF, Padgett KA, Pagliai FA, Gardner CL, Lorca GL, Gonzalez CF. 2017. Functional characterization of LotP from *Liberibacter asiaticus*. Microbial Biotechnology 10:642-656.
32. Pagliai FA, Coyle JF, Kapoor S, Gonzalez CF, Lorca GL. 2017. LdtR is a master regulator of gene expression in Liberibacter asiaticus. Microb Biotechnol 10:896-909.
33. Teufel F, Almagro Armenteros JJ, Johansen AR, Gíslason MH, Pihl SI, Tsirigos KD, Winther O, Brunak S, von Heijne G, Nielsen H. 2022. SignalP 6.0 predicts all five types of signal peptides using protein language models. Nature biotechnology:1-3.
34. Krogh A, Larsson B, Von Heijne G, Sonnhammer EL. 2001. Predicting transmembrane protein topology with a hidden Markov model: application to complete genomes. Journal of molecular biology 305:567-580.
35. Karimova G, Ladant D. 2017. Defining membrane protein topology using *pho-lac* reporter fusions, p 129-142, Bacterial Protein Secretion Systems. Springer.
36. Jumper J, Evans R, Pritzel A, Green T, Figurnov M, Ronneberger O, Tunyasuvunakool K, Bates R, Zidek A, Potapenko A, Bridgland A, Meyer C, Kohl SAA, Ballard AJ, Cowie A, Romera-Paredes B, Nikolov S, Jain R, Adler J, Back T, Petersen S, Reiman D, Clancy E, Zielinski M, Steinegger M, Pacholska M, Berghammer T, Bodenstein S, Silver D, Vinyals O, Senior AW, Kavukcuoglu K, Kohli P, Hassabis D. 2021. Highly accurate protein structure prediction with AlphaFold. Nature 596:583-589.
37. Durie CL, Sheedlo MJ, Chung JM, Byrne BG, Su M, Knight T, Swanson M, Lacy DB, Ohi MD. 2020. Structural analysis of the Legionella pneumophila Dot/Icm type IV secretion system core complex. Elife 9:e59530.
38. Kubori T, Koike M, Bui XT, Higaki S, Aizawa S-I, Nagai H. 2014. Native structure of a type IV secretion system core complex essential for Legionella pathogenesis. Proceedings of the National Academy of Sciences 111:11804-11809.

39. Deme JC, Johnson S, Vickery O, Aron A, Monkhouse H, Griffiths T, James RH, Berks BC, Coulton JW, Stansfeld PJ, Lea SM. 2020. Structures of the stator complex that drives rotation of the bacterial flagellum. Nat Microbiol 5:1553-1564.
40. Pagliai FA, Coyle JF, Kapoor S, Gonzalez CF, Lorca GL. 2017. LdtR is a master regulator of gene expression in *Liberibacter asiaticus*. Microbial Biotechnology 10:896-909.
41. Barnett MJ, Solow-Cordero DE, Long SR. 2019. A high-throughput system to identify inhibitors of Candidatus *Liberibacter asiaticus* transcription regulators. Proceedings of the National Academy of Sciences 116:18009-18014.
42. Pagliai FA, Gardner CL, Bojilova L, Sarnegrim A, Tamayo C, Potts AH, Teplitski M, Folimonova SY, Gonzalez CF, Lorca GL. 2014. The transcriptional activator LdtR from 'Candidatus *Liberibacter asiaticus*' mediates osmotic stress tolerance. PLoS pathogens 10:e1004101.
43. Padgett-Pagliai KA, Pagliai FA, da Silva DR, Gardner CL, Lorca GL, Gonzalez CF. 2022. Osmotic stress induces long-term biofilm survival in Liberibacter crescens. BMC microbiology 22:1-16.
44. Coyle JF, Pagliai FA, Zhang D, Lorca GL, Gonzalez CF. 2018. Purification and partial characterization of LdtP, a cell envelope modifying enzyme in Liberibacter asiaticus. BMC microbiology 18:1-15.
45. Terashima H, Kawamoto A, Morimoto YV, Imada K, Minamino T. 2017. Structural differences in the bacterial flagellar motor among bacterial species. Biophysics and Physicobiology 14:191-198.
46. Minamino T, Imada K. 2015. The bacterial flagellar motor and its structural diversity. Trends in Microbiology 23:267-274.
47. Bertani G. 1951. Studies on lysogenesis I: the mode of phage liberation by lysogenic *Escherichia coli*. Journal of Bacteriology 62:293-300.
48. Mitchell SF, Lorsch JR. 2015. Protein affinity purification using intein/chitin binding protein tags, p 111-125, Methods in Enzymology, vol 559. Elsevier.
49. Zatakia HM, Arapov TD, Meier VM, Scharf BE. 2018. Cellular stoichiometry of methyl-accepting chemotaxis proteins in *Sinorhizobium meliloti*. Journal of bacteriology 200:e00614-17.
50. Karimova G, Robichon C, Ladant D. 2009. Characterization of YmgF, a 72-residue inner membrane protein that associates with the Escherichia coli cell division machinery. J Bacteriol 191:333-46.
51. Adler J. 1973. A method for measuring chemotaxis and use of the method to determine optimum conditions for chemotaxis by *Escherichia coli*. Microbiology 74:77-91.
52. Simon R, O'connell M, Labes M, Pühler A. 1986. Plasmid vectors for the genetic analysis and manipulation of rhizobia and other gram-negative bacteria. Methods in enzymology 118:640-659.
53. Pleier E, Schmitt R. 1991. Expression of two *Rhizobium meliloti* flagellin genes and their contribution to the complex filament structure. Journal of Bacteriology 173:2077-2085.
54. Kovach ME, Elzer PH, Hill DS, Robertson GT, Farris MA, Roop II RM, Peterson KM. 1995. Four new derivatives of the broad-host-range cloning vector pBBR1MCS, carrying different antibiotic-resistance cassettes. Gene 166:175-176.

55. Karimova G, Robichon C, Ladant D. 2009. Characterization of YmgF, a 72-residue inner membrane protein that associates with the *Escherichia coli* cell division machinery. Journal of Bacteriology 191:333-346.
56. Schäfer A, Tauch A, Jäger W, Kalinowski J, Thierbach G, Pühler A. 1994. Small mobilizable multi-purpose cloning vectors derived from the *Escherichia coli* plasmids pK18 and pK19: selection of defined deletions in the chromosome of *Corynebacterium glutamicum*. Gene 145:69-73.

TABLES

Table 3.1. Locations and effects of mutations identified in Δ*ldtR* suppressor mutants from *S. meliloti* RU11/001 and *Agrobacterium sp.* H13-3

Mutant ID (RU11/001 Δ*ldtR*)	**Mutation**	**Protein effect**
Suppressor 1	**orf23$_{G502-}$**	**Disruption of Gly168, loss of 16 aa**
Suppressor 2	**orf23$_{C464A}$**	**Orf23$_{P155L}$**
Suppressor 3	***orf23*::ISR21m**	**Disruption of Leu104, loss of 79 aa**
Suppressor 4	***motA*$_{G34A}$**	**MotA$_{G12S}$**

Table 3.2. Quality scores and similarity characteristics homology models obtained for *S. meliloti* Orf23 (aa 128-183) and MotA using the SWISS-MODEL server.

Hits for Orf23 (organism)	**PDB ID**	**GMQE**	**QMEANDisCo Global score**	**Sequence identity**	**Sequence similarity**	**Coverage**
DotF (*L. pneumophila*)	7MUC	0.67	0.61 ± 0.11	28.3%	35%	95%
PilP (*P. aeruginosa*)	2Y4Y	0.28	0.56 ± 0.12	27.3%	35%	59%
Hits for MotA (organism)						
MotA (*B. subtilis*)	6YSL	0.54	0.52 ± 0.05	20.7%	31%	91%
MotA (*C. jejuni*)	6YKM	0.55	0.57 ± 0.05	18.7%	30%	86%

Table 3.3. Bacterial strains and plasmids used in this study.

Strains	**Genotype**	**Reference**
Escherichia coli		
DH5α	F^- φ80*lac*ZΔM15 Δ(*lac*ZYA-*arg*F)U169 *rec*A1 *end*A1 *hsd*R17(r_K^-, m_K^+) *pho*A *sup*E44 λ^- *thi*-1 *gyr*A96 *rel*A1	(51)
ER2566	*Ion ompT lacZ::T7*	New England Biolabs
S17-1	*recA endA thi hsdR* RP4-2 Tc::Mu::Tn7 Tp^r Sm^r	(52)
Sinorhizobium meliloti		
BS244	Δ*ldtR* (Δ*SMc01768*)	This study
BS274	Δ*ldtR* Δ*orf23*	This study
BS278	$motA_{G12S}$	This study
BS279	Δ*orf23* $motA_{G12S}$	This study
BS280	Δ*ldtR* $motA_{G12S}$	This study
BS281	Δ*ldtR* Δ*orf23* $motA_{G12S}$	This study
RU11/001	Wild type, spontaneous Sm^r	(53)
RU11/552	Δ*orf23*	This study
RU11/555	Δ*rem*	(4)
Plasmid	**Description**	**Reference**
pBBR1MCS-2	Nm^r, Broad host-range expression vector	(54)
pBS502	Km^r, 560 bp HindIII/EcoRI PCR fragment containing Δ*ldtR*	This study

	cloned into pK18*mob sacB*	
pBS539	Km^r, 513 bp KpnI/XbaI PCR fragment containing *ldtR* cloned into pBBR1MCS-2	This study
pBS598	Km^r, 552 bp SpeI/HindIII PCR fragment containing *orf23* cloned into pBBR1MCS-2	This study
pBS601	Km^r, 519 bp HindIII/XbaI PCR fragment containing $motA_{G12S}$ cloned into pK18*mob sacB*	This study
pBS1193	Km^r, 117 bp PCR fragment containing *ymgF* fragment 1-117 (aa 1-39) cloned into pKTop	(55)
pBS1330	Km^r, 552 bp XbaI/SacI PCR fragment containing *orf23* cloned into pKTop	This study
pBS1331	Ap^r, 408 bp SapI/PstI PCR fragment containing *orf23** fragment 145-552 bps (aa 49-183) cloned into pTYB11	This study
pK18*mob sacB*	Km^r *lacZ mob sacB*	(56)
pKTop	Km^r, vector expressing dual reporter $PhoA_{22-472}/LacZ_{4-60}$, p15 ori	(55)
pRU2202	Km^r, 575 bp BamHI/HindIII PCR fragment containing Δ*orf23* cloned into pK18*mob sacB*	This study
pTYB11	Ap^r, Expression vector	New England Biolabs

FIGURES

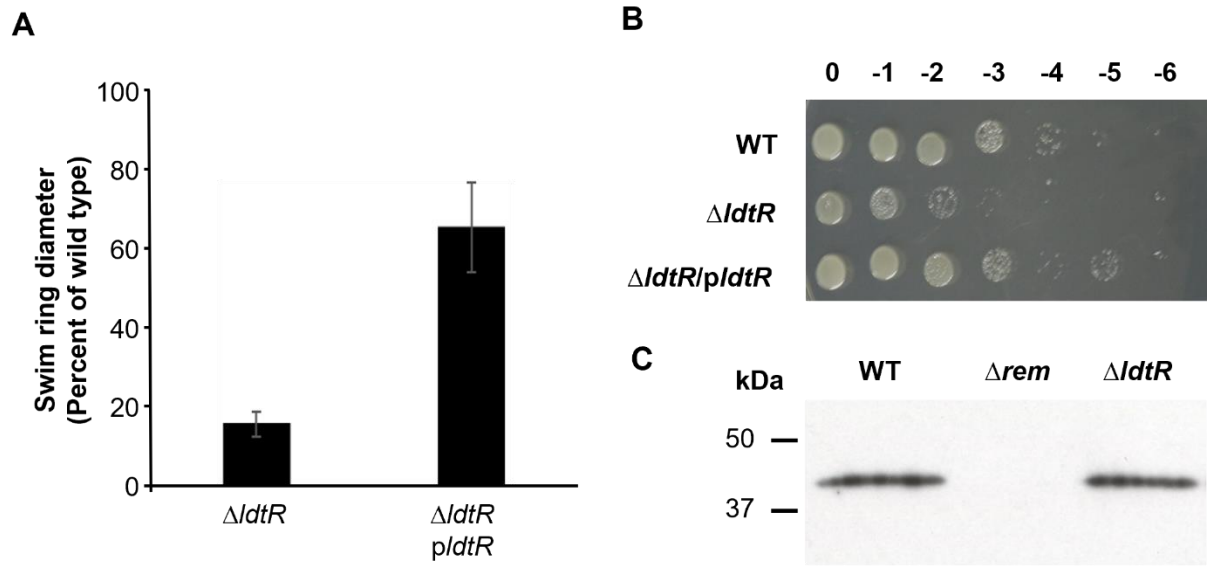

Figure 3.1. Investigation of the role of LdtR in motility and osmotic stress tolerance in *S. meliloti*. (A) Swim ring analysis and (B) osmotic stress tolerance assay of the Δ*ldtR* and complemented strain. For swim ring assays, stationary phase cultures (3 µl) were spot-plated onto swim plates and incubated at 30°C for five days. Shown are the averages and standard deviations of swim ring diameters for three independent experiments with three technical replicates each. (C) Anti-flagellin immunoblot analysis of wild type, Δ*rem* (negative control), and Δ*ldtR* strains.

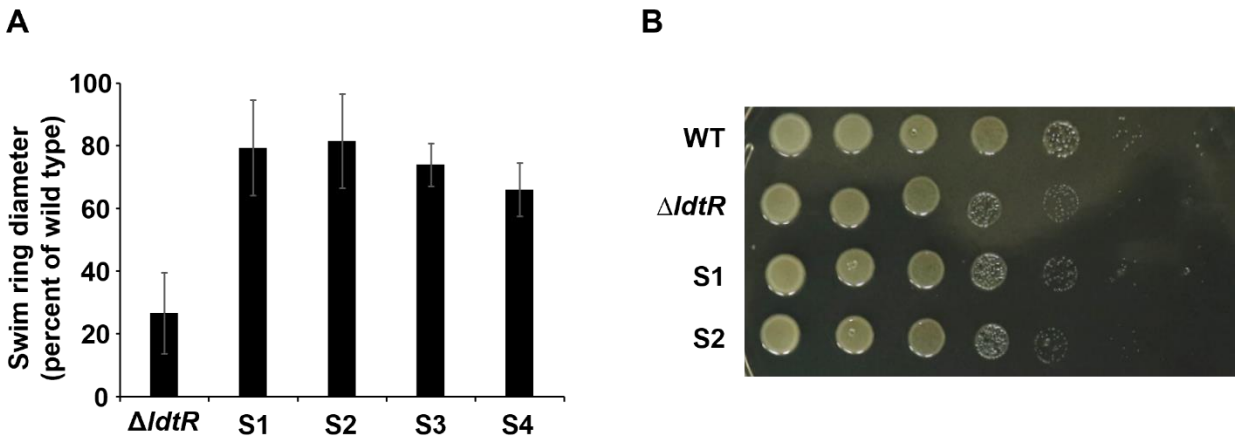

Figure 3.2. Analysis of swimming proficiency (A) and osmotic stress tolerance (B) of Δ*ldtR* suppressor (S) mutants.

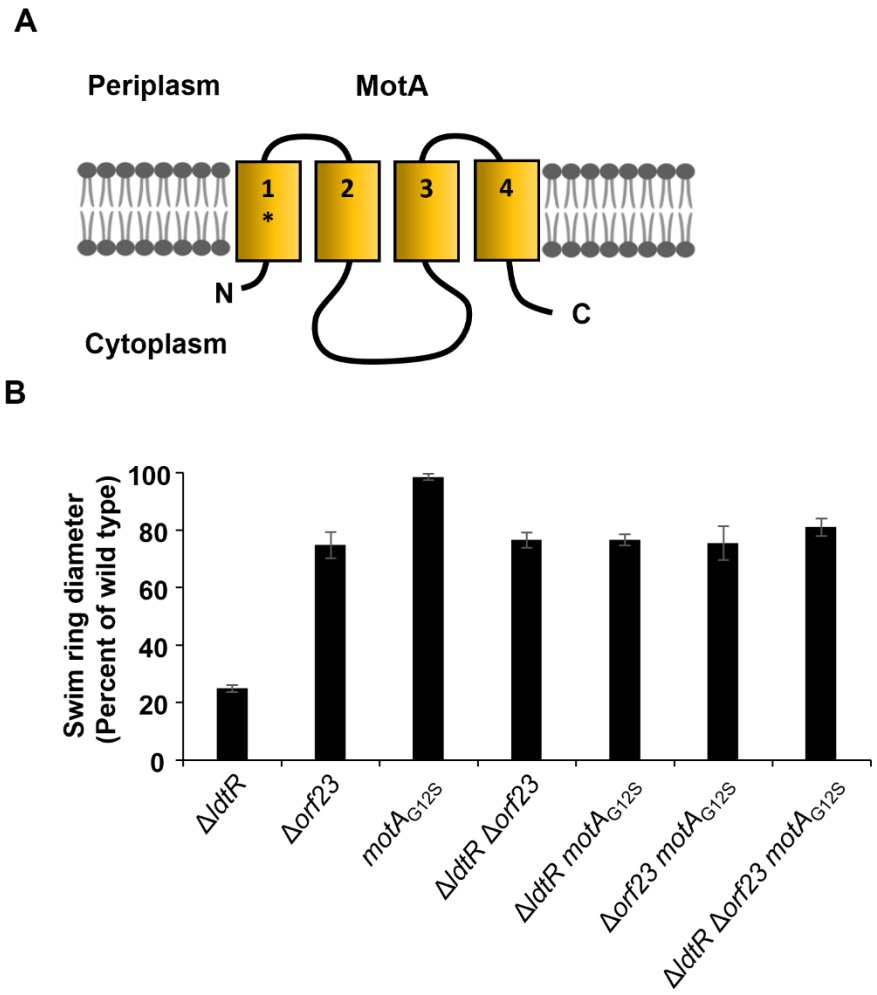

Figure 3.3. MotA topology (A) and swim ring analysis of Δ*ldtR* mutants (B). The TM domains of MotA are labelled and the approximate location of the G12 residue is shown as an asterisk. For swim ring analyses, shown are the averages and standard deviations of swim ring diameteres for three independent experiments with three technical replicates each.

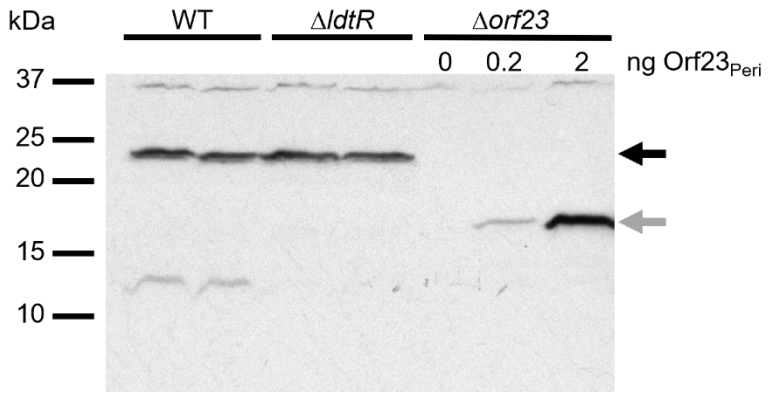

Figure 3.4. Immunoblot analysis of Orf23 levels in wild type and Δ*ldtR*. Black arrow indicates full-length Orf23 and the grey arrow indicates Orf23*.

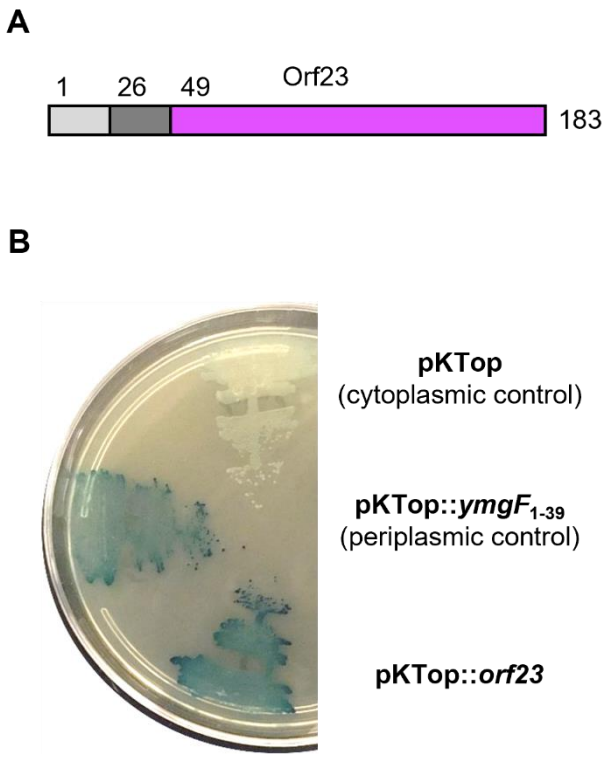

Figure 3.5. Membrane topology of Orf23. (A) A schematic showing the predicted topology of Orf23. Light grey, cytoplasmic domain; dark grey, transmembrane domain; pink, periplasmic domain. (B) Orf23 membrane topology analysis by alkaline phosphatase (AP) reporter assay. *E. coli* DH5α strains expressing unmodified AP (top) or AP fusion proteins with the periplasmic control $YmgF_{1-39}$ (middle) or with Orf23 (bottom) were incubated on LB agar plates supplemented with X-Pho overnight at 30°C. Blue growth indicates that localization of the C-terminus of the corresponding protein is in the periplasm.

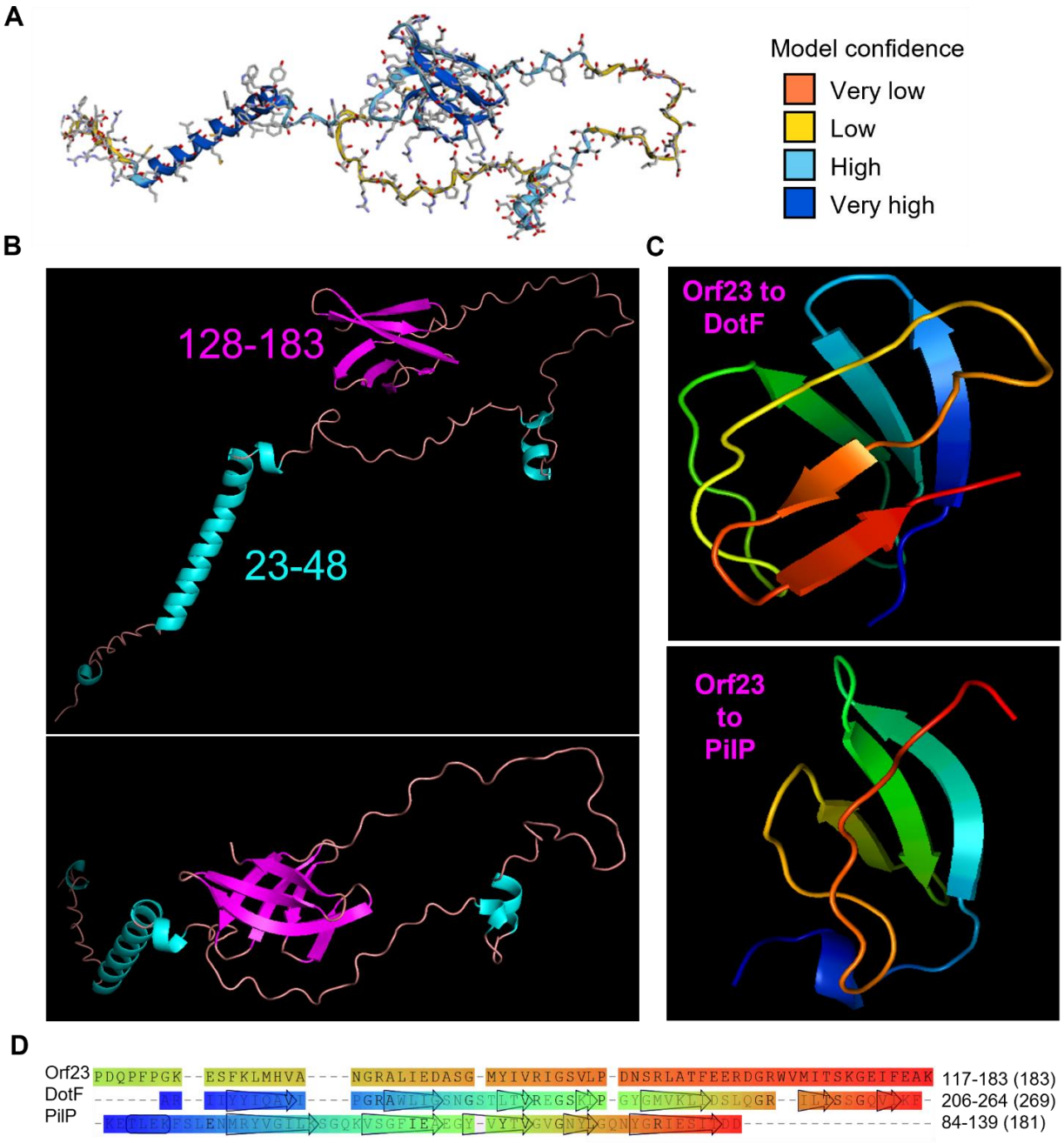
A
Model confidence
Very low
Low
High
Very high
B
128-183
23-48
C
Orf23 to DotF
Orf23 to PilP
D
Orf23
DotF
PilP
117-183 (183)
206-264 (269)
84-139 (181)

Figure 3.6. Protein structure prediction and homology modeling for Orf23. (A) AlphaFold prediction of Orf23 structure and (B) recolored rendering of the predicted Orf23 structure developed in PyMOL. (C) Homology models of the Orf23 C-terminal domain (aa 117-183) based on solved structures of DotF from *L. pneomophila* (top) and PilP from *N. meningitidis* (bottom) developed in SWISS-MODEL. (D) SWISS-MODEL multiple sequence alignment of Orf23 to DotF and PilP.

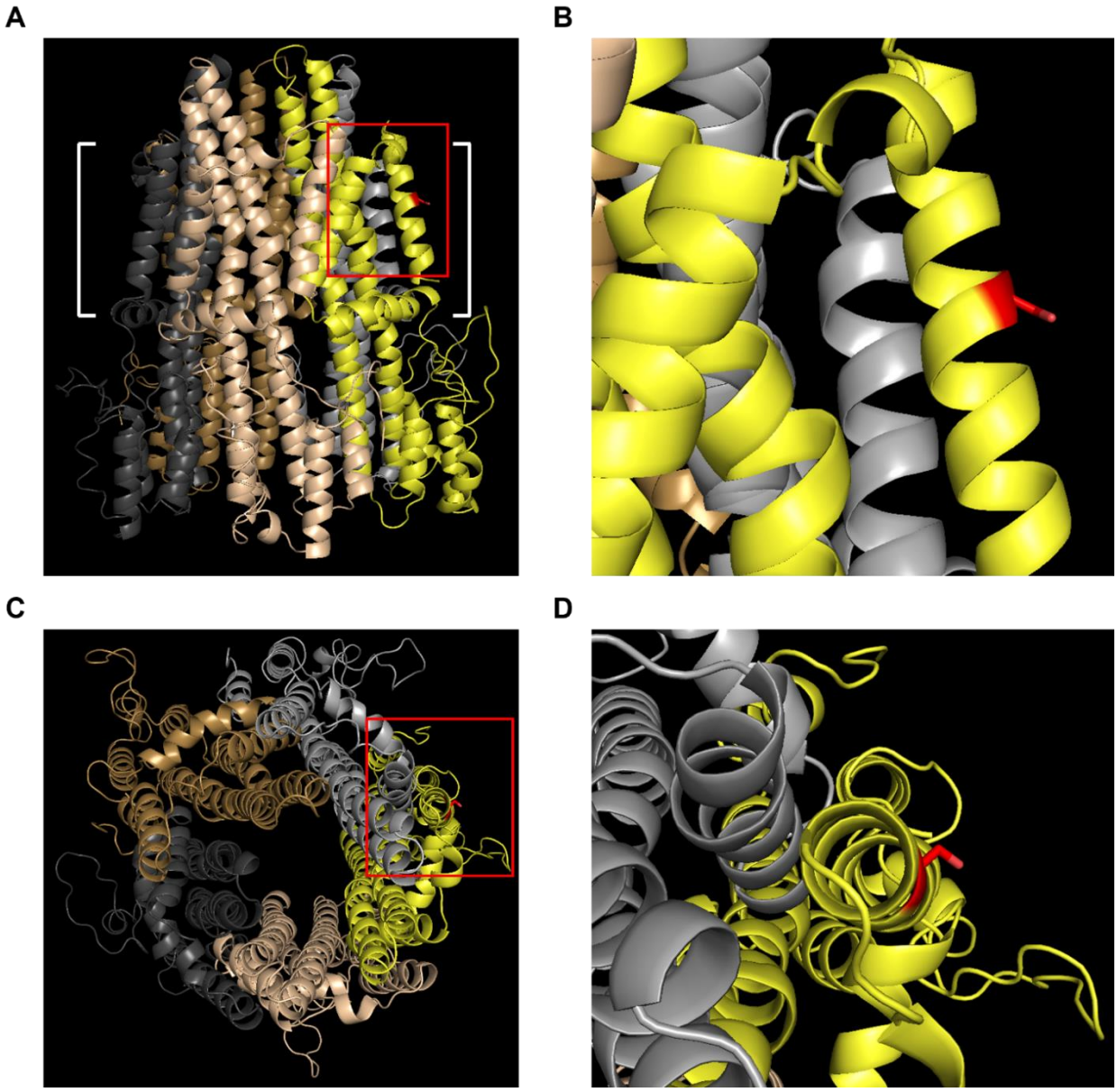

Figure 3.7. Homology modeling and identification of the location of the $MotA_{G12S}$ substitution in *S. meliloti* MotA. Side views (A and B) and top views (C and D) of the MotA pentamer showing the location of the G12S mutation in one MotA chain. In (A), the membrane-embedded region of the MotA pentamer is indicated by white brackets.

Chapter 4: Final Discussion

The bacterial flagellum is a wonderous and powerful nanomachine capable of propelling bacteria at extraordinary velocities. To put this into a relatable context, the world record for human swimming speed is held by Michael Phelps at 2.7 m/s. With a height of 1.9 m, Phelps achieves an average speed of about 1.4 body lengths per second (BL/s). Many flagellated bacteria including *Escherichia coli* and *Sinorhizobium meliloti* swim through liquid media with average velocities ranging between 25-40 μm/s and therefore, at about 2 μm long, these organisms swim at 13-20 BL/s. The fastest sea fish known to date are black marlin with body lengths of about 3.4 m. Top speeds have been recorded for these organisms at around of 36.7 m/s or 10.8 BL/s and thus reach comparable speeds achieved by *E. coli*. However, the average vibrio bacterium has been clocked darting through their medium with a burst velocity of over 400 μm/s or an astonishing 200 BL/s (1, 2). Thus, relative to their size, flagellated bacteria can achieve considerably greater speeds than other self-propelled swimming organisms known to humankind.

Added power and structural stabilization are of great benefit to bacteria attempting to explore soil environments, which are known to vary considerably in their viscosity depending on rainfall and irrigation in a particular habitat. It is therefore unsurprising that our investigations of the *S. meliloti* flagellar motor have revealed marked compositional differences compared to other bacteria characterized to date. Indeed, we expect to find more. It has been reported that the addition of *Rhizobia* selected for heightened motility as soil inoculants intended to boost plant yields exhibit a competitive advantage in host root colonization (3). Therefore, in efforts aimed to select for *Rhizobia* with improved plant-growth promoting properties, researchers would be wise to also select for heightened motility as manifested in increased torque generation and improved swarming capacity (4). It is intriguing to speculate how our knowledge of additional structures employed by the powerful flagellar motors of *S. meliloti* could be used to engineer other *Rhizobia* for improved swimming capacity in their soil environments, thus transforming these improvements to symbionts of other valuable plant hosts.

Experimental techniques that improve our understanding of flagellar motor function

For the characterization of new motor proteins identified in *S. meliloti,* the various behavioral assays used in Chapter 2 were highly valuable. Tethered cell analyses are particularly beneficial for understanding flagellar motor function in peritrichous bacteria, as it is important to observe

the behaviors of single flagellar motors to best explain the resulting influences of specific mutations on swimming behavior. Determination of swimming velocities and the fraction of motile bacteria in cell populations revealed that most cells in the Δ*motF* population are nonmotile and the remaining few swam slowly with erratic behavior. However, the swimming behavior only conveys the combined performance of flagellar motors but conceals the behavior of single motors. Our tethered cell behavioral analyses with the Δ*motF* mutants characterized in Chapter 2 revealed that erratic behavior of the remaining motile bacteria is explained well when considering that the activity of individual motors is similarly erratic. Tethered cell experiments were enlightening for the Δ*fliL* mutant as well, which appeared nonmotile on soft-agar plates and in liquid medium but was found to exhibit very low-level motor activity by the tethered cell assay. Thus, the various swimming and tethered cells analyse complement one another when elucidating the mechanisms of flagellar motor function.

Bacterial two-hybrid (BTH) analysis provides a fast and potentially high-throughput method to probe interactions between two proteins in a heterologous host. The BTH system was very useful in the work reported here for quickly probing for potential interactions between several different proteins with fusions at different locations on the proteins being tested, as shown in Chapter 2. However, BTH can sometimes provide nonspecific (false-positive) or undetectable (false-negative) results. It is therefore important to perform complementary biochemical experiments, such as *in vitro* chemical cross-linking and protein stability assays, which revealed interactions between the periplasmic regions of MotF and MotB as well as MotF with MotA and that MotF and FliL require each other for stability in the cell. We also showed by immunoblotting that LdtR is not required for production of flagellar motility proteins in Chapter 3. Additional informative approaches for characterizing interactions in the motor include an array of *in vivo* fluorescence microscopy techniques such as fluorescence resonance energy transfer (FRET) or fluorescence recovery after photobleaching (FRAP), both of which have provided a great deal of information regarding the localization dynamics and exchange of flagellar stator and rotor components (5-9).

Noncanonical components of the *S. meliloti* flagellar motor

S. meliloti is the first organism reported to employ both FliL and the FliL paralog, MotF, in the same flagellar motor. As described in Chapter 2, FliL appears to be required for initial stator recruitment and normal flagellation in *S. meliloti* whereas MotF is involved in control of proton flux by modulating the MotB proton plug. Our finding that the Δ*orf23* mutant exhibits reduced swimming capacity in soft agar swim plates suggests that Orf23 may be required for maximum swimming velocity and may therefore play a role as the "high-gear" in the speed-variable flagellar motor of *S. meliloti*. In fact, it appears to play a role in conferring maximum swimming velocity and its disengagement from stator assemblies (comprised of stator units MotAB, the putative stator recruitment protein FliL and putative proton plug modulator MotF) could be a requisite function to "downshift" the flagellar motor. It will be interesting to determine whether such "downshifting" results in reduced stator numbers assembled around the motor or reduced proton flow or a combination of the two. Tethered cell experiments to compare rotation rates of the Δ*orf23* strain to the wild type in media with varying degrees of viscosity will provide direct answers regarding the influence of Orf23 on torque generation. Analysis of the Δ*orf23* strain under swarming conditions may allow for the detection of a more pronounced phenotype as this mode of motility results in increased viscous drag on the bacterium and thus requires greater torque (10).

A protein BLAST search with the Orf23 amino acid sequence discovered its presence in only a very limited group of alphaproteobacteria and we are the first to report its role in the bacterial flagellar motor. Notably, suppressor mutations in the *orf23* gene were also rapidly produced int the Δ*ldtR* strain of the related *Agrobacterium sp.* H13-3 suggesting that the functional relationship of LdtR and Orf23 are similar in these organisms. This finding is unsurprising given that both organisms are inhabitants of the soil and will likely share several flagellum adaptations specific to this environment.

The identification of several additional components required for *S. meliloti* flagellar motor function suggests that these bacteria employ additional stabilizing structures required for swimming in the soil environment. We have observed that the absence of Orf23, MotF, FliL, or MotC exhibit a range of flagellar motility defects from only slightly diminished swimming speed to abolished motor function, respectively. Therefore, we are all but certain that these added

components form stabilizing structures similar to the flagellar outer membrane complex (FOMC) structure employed by *Vibrio spp.* As explained in Chapter 1, FOMC is comprised of additional outer membrane- and peptidoglycan-associated H- and T-rings, which interact with one another as well as with the L- and P-rings and are required to recruit stator components to the motor (11). It is quite possible that FliL, MotF, and MotC play important roles in stator recruitment to the motor because of the substantial defects in flagellar motor activity when these are lacking. Notably and in contrast to the *Vibrio* FOMC structural components, the various periplasmic discs and the P-ring decorations discovered in other diverse species (12), FliL, MotF, and Orf23 are all attached by transmembrane domains and are therefore clearly part of a distinctly different flavor of structures.

Structural studies greatly improve our understanding of the bacterial flagellar motor

One of the greatest strides in our ability to define precise locations of different proteins in the flagellar motor has come with the improvements in resolution derived from structural analyses permitted by cryo-electron tomography (cryo-ET) and cryo-electron microscopy (cryo-EM) coupled with subtomogram averaging. These techniques have bypassed the challenges inherent to the purification of very large assemblies of proteins and given that they provide a snapshot of the intact motor within the cell, even transient structures are being revealed such as the cytoplasmic rings involved in stator assembly and described in Chapter 1 (13). The massive influx of structural data provided by these techniques has greatly improved our understanding of the assembly and function of flagellar motor components. In particular, the determination of the $MotA_5MotB_2$ cryo-EM structures solved the long-standing question of how proton flow through stators is coupled to torque generation by interactions observed between MotA and FliG. This finding revealed an eloquent mechanism whereby proton flow through the stators drive rotation of the $MotA_5$ pentamer with respect to the fixed $MotB_2$ dimer to drive rotation of the rotor and entire axial flagellar assembly (14-16). Additionally, cryoEM and cryoET have recently made available a relatively large number of high-resolution structures, which have revealed great details of additional substructures found in the high-torque flagellar motors compared to those from enteric bacteria (12, 13, 17-26). Structural studies of the *S. meliloti* flagellar motor will be important to reveal the precise organization of FliL, MotF, Orf23, and the long-known but still poorly understood MotC.

Importance and modern applications of swimming bacteria

In addition to possessing remarkable power to drive motility, flagella are highly versatile structures with roles in surface and temperature sensing (27), adherence to surfaces and other cells (28), and host colonization for both bacterial symbionts and pathogens (28, 29) *Vibrio spp.* are very successful at persisting as motile bacteria in aquatic environments with relatively low nutrients in part due to their highly efficient motors and the relatively low energy costs of producing just one polar flagellum, which they use as a hybrid propellar and oar to efficiently form swarms around nutrients in their environments where nutrients may quickly become dissipated by currents (2, 30). Many bacterial pathogens including *V. cholerae, P. aeruginosa, Lysteria monocytogenes,* and others require motility for the initial steps that mediate the formation of biofilms, which cause major complications for human hosts during infection with these organisms and reduce the susceptibility of these organisms to host mediated clearance and antibiotic treatment (27, 31).

Bacterial motility and chemotaxis systems from diverse species have been refined through billions of years of selection to be suited best for the specific environments that they inhabit. Great success is being made to characterize these systems and leverage our knowledge thereof for various applications., Swarming *P. aeruginosa* show promise in bioremediation for their production of rhamnolipids used by the swarm to decrease surface tension and promote rapid migration across surfaces. It was determined that rhamnolipids enhance degradation of hydrocarbons and may therefore be used in the restoration of marine oil spills (10, 32).

Intriguingly, *S. putrefaciens* cells that have been genetically locked to employ their polar flagellar system are reported to escape entrapment between an agarose pad and a glass coverslip by eventually wrapping their flagellum in a spiral shape around the cell body to serve as rotating screw threads that allow the bacterium to escape axially outward from the trap (33). This type of resilience to entrapment would be very useful if bacteria were being selected or engineered to, for example, penetrate deep through grimy landfill or plastic waste to degrade the materials (34, 35). Hyperflagellated swarmer bacteria would conceivably also perform well at such tasks.

Research is underway to target flagellar motor function of pathogens such as *H.* pylori with proton pump inhibitors and to use the highly immunogenic flagellin components of *V. cholerae*

and *P. aeruginosa* for vaccine production (36). Additionally, efforts are being made to exploit *Salmonella spp.* and *E. coli* chemotaxis to colonize, deliver payloads to, and aid in necrosis of tumor tissues as a potential cancer therapy in humans (37-40).

As explained in Chapter 1, *Rhizobia* and their leguminous partners are excellent resources for maintaining cropland in a healthy condition, as a forage crop, and as a valuable source of nitrogen-rich fertilizers. These natural resources are environmentally friendly and financially attractive alternatives to the harmful synthetic fertilizers, which cause eutrophication of water resources from run-off, greenhouse effects, and acid rain (41). Flagellar motility and chemotaxis are critical for maximized colonization efficiency of alfalfa roots to promote growth of its alfalfa host.

Concluding remarks

The first part of the title of this dissertation is “The little engine that could” and the author must clarify that while an engine relies on the principals of combustion, motors are distinctly electric and require a flow of ions for power. Nonetheless, the flagellar motility and chemotaxis systems in bacteria are complex and astonishing. Although the flagellar core structure is highly conserved across bacterial genera, striking variation exists in the overall composition of flagellar motors described to date. Each of these has been subject to billions of years of selection and gradual evolution with distinctions in the types and magnitudes of selective pressures present in a particular environment. As a result, we have identified dramatic differences in the ligand specificities and adaption dynamics of the sensory systems and flagellar systems employed by diverse bacteria including *S. meliloti* in the soil environment. Clearly, different classes of motile bacteria will afford distinct types of advantages for various types of applications depending on the specific fuel requirements of their motors, whether the bacteria are fit to persist in the environment for a given application and depending on how the flagellar motors are adapted to function in that environment. However, bacteria have already performed remarkably in trials to help solve a variety of modern-day problems and as we continue putting them to the test to solve more, this author posits with certainty that flagellated bacteria with their little motors really could.

REFERENCES

1. Magariyama Y, Muramoto Y, Maekawa Y, Kawagishi I, Imae Y, Kudo S, Sugiyama S. 1994. Very fast flagellar rotation. Nature 371:752.
2. Mitchell JG, Pearson L, Bonazinga A, Dillon S, Khouri H, Paxinos R. 1995. Long lag times and high velocities in the motility of natural assemblages of marine bacteria. Applied and environmental microbiology 61:877-882.
3. Aroney ST, Poole PS, Sánchez-Cañizares C. 2021. Rhizobial chemotaxis and motility systems at work in the soil. Frontiers in Plant Science:1856.
4. Amaya-Gómez CV, Porcel M, Mesa-Garriga L, Gómez-Álvarez MI. 2020. A framework for the selection of plant growth-promoting rhizobacteria based on bacterial competence mechanisms. Applied and environmental microbiology 86:e00760-20.
5. Lin T-S, Zhu S, Kojima S, Homma M, Lo C-J. 2018. FliL association with flagellar stator in the sodium-driven Vibrio motor characterized by the fluorescent microscopy. Scientific reports 8:1-12.
6. Tusk SE, Delalez NJ, Berry RM. 2018. Subunit exchange in protein complexes. Journal of molecular biology 430:4557-4579.
7. Leake MC, Chandler JH, Wadhams GH, Bai F, Berry RM, Armitage JP. 2006. Stoichiometry and turnover in single, functioning membrane protein complexes. Nature 443:355.
8. Morimoto YV, Minamino T. 2017. Stoichiometry and Turnover of the Stator and Rotor, p 203-213, The Bacterial Flagellum. Springer.
9. Boehm A, Kaiser M, Li H, Spangler C, Kasper CA, Ackermann M, Kaever V, Sourjik V, Roth V, Jenal U. 2010. Second messenger-mediated adjustment of bacterial swimming velocity. Cell 141:107-116.
10. Yang A, Tang WS, Si T, Tang JX. 2017. Influence of physical effects on the swarming motility of Pseudomonas aeruginosa. Biophysical Journal 112:1462-1471.
11. Echazarreta MA, Klose KE. 2019. *Vibrio* flagellar synthesis. Frontiers in Cellular and Infection Microbiology 9:131.
12. Kaplan M, Ghosal D, Subramanian P, Oikonomou CM, Kjaer A, Pirbadian S, Ortega DR, Briegel A, El-Naggar MY, Jensen GJ. 2019. The presence and absence of periplasmic rings in bacterial flagellar motors correlates with stator type. Elife 8:e43487.
13. Kaplan M, Oikonomou CM, Wood CR, Chreifi G, Subramanian P, Ortega DR, Chang YW, Beeby M, Shaffer CL, Jensen GJ. 2022. Novel transient cytoplasmic rings stabilize assembling bacterial flagellar motors. The EMBO Journal:e109523.
14. Deme JC, Johnson S, Vickery O, Aron A, Monkhouse H, Griffiths T, James RH, Berks BC, Coulton JW, Stansfeld PJ. 2020. Structures of the stator complex that drives rotation of the bacterial flagellum. Nature Microbiology 5:1553-1564.
15. Hu H, Santiveri M, Wadhwa N, Berg HC, Erhardt M, Taylor NM. 2021. Structural basis of torque generation in the bi-directional bacterial flagellar motor. Trends in Biochemical Sciences.
16. Santiveri M, Roa-Eguiara A, Kühne C, Wadhwa N, Hu H, Berg HC, Erhardt M, Taylor NM. 2020. Structure and function of stator units of the bacterial flagellar motor. Cell 183:244-257. e16.
17. Minamino T, Imada K. 2015. The bacterial flagellar motor and its structural diversity. Trends in Microbiology 23:267-274.

18. Terashima H, Kawamoto A, Morimoto YV, Imada K, Minamino T. 2017. Structural differences in the bacterial flagellar motor among bacterial species. Biophysics and Physicobiology 14:191-198.
19. Imada K. 2018. Bacterial flagellar axial structure and its construction. Biophysical reviews 10:559-570.
20. Johnson S, Furlong EJ, Deme JC, Nord AL, Caesar JJ, Chevance FF, Berry RM, Hughes KT, Lea SM. 2021. Molecular structure of the intact bacterial flagellar basal body. Nature Microbiology 6:712-721.
21. Tachiyama S, Chan KL, Liu X, Hathroubi S, Peterson B, Khan MF, Ottemann KM, Liu J, Roujeinikova A. 2022. The flagellar motor protein FliL forms a scaffold of circumferentially positioned rings required for stator activation. Proc Natl Acad Sci U S A 119.
22. Beeby M, Ribardo DA, Brennan CA, Ruby EG, Jensen GJ, Hendrixson DR. 2016. Diverse high-torque bacterial flagellar motors assemble wider stator rings using a conserved protein scaffold. Proceedings of the National Academy of Sciences 113:E1917-E1926.
23. Chaban B, Coleman I, Beeby M. 2018. Evolution of higher torque in Campylobacter-type bacterial flagellar motors. Scientific Reports 8:1-11.
24. Rossmann FM, Beeby M. 2018. Insights into the evolution of bacterial flagellar motors from high-throughput in situ electron cryotomography and subtomogram averaging. Acta Crystallogr D Struct Biol 74:585-594.
25. Kaplan M, Sweredoski MJ, Rodrigues JP, Tocheva EI, Chang Y-W, Ortega DR, Beeby M, Jensen GJ. 2020. Bacterial flagellar motor PL-ring disassembly subcomplexes are widespread and ancient. Proceedings of the National Academy of Sciences 117:8941-8947.
26. Rossmann FM, Hug I, Sangermani M, Jenal U, Beeby M. 2020. *In situ* structure of the *Caulobacter crescentus* flagellar motor and visualization of binding of a CheY-homolog. Molecular Microbiology.
27. Mordue J, O'Boyle N, Gadegaard N, Roe AJ. 2021. The force awakens: The dark side of mechanosensing in bacterial pathogens. Cellular Signalling 78:109867.
28. Haiko J, Westerlund-Wikström B. 2013. The role of the bacterial flagellum in adhesion and virulence. Biology 2:1242-1267.
29. Poole P, Ramachandran V, Terpolilli J. 2018. Rhizobia: from saprophytes to endosymbionts. Nature Reviews Microbiology 16:291-303.
30. Xie L, Altindal T, Chattopadhyay S, Wu X-L. 2011. Bacterial flagellum as a propeller and as a rudder for efficient chemotaxis. Proceedings of the National Academy of Sciences 108:2246-2251.
31. Karatan E, Watnick P. 2009. Signals, regulatory networks, and materials that build and break bacterial biofilms. Microbiology and Molecular Biology Reviews 73:310-347.
32. Chen Q, Bao M, Fan X, Liang S, Sun P. 2013. Rhamnolipids enhance marine oil spill bioremediation in laboratory system. Marine pollution bulletin 71:269-275.
33. Kühn MJ, Schmidt FK, Eckhardt B, Thormann KM. 2017. Bacteria exploit a polymorphic instability of the flagellar filament to escape from traps. Proceedings of the National Academy of Sciences 114:6340-6345.
34. Asiandu AP, Wahyudi A, Sari SW. 2021. A review: plastics waste biodegradation using plastics-degrading bacteria. Journal of Environmental Treatment Techniques 9:148-157.

35. Puglisi E, Romaniello F, Galletti S, Boccaleri E, Frache A, Cocconcelli PS. 2019. Selective bacterial colonization processes on polyethylene waste samples in an abandoned landfill site. Scientific reports 9:1-13.
36. Josenhans C, Suerbaum S. 2002. The role of motility as a virulence factor in bacteria. International Journal of Medical Microbiology 291:605-614.
37. Karmakar R. 2021. State of the art of bacterial chemotaxis. Journal of Basic Microbiology 61:366-379.
38. Broadway KM, Scharf BE. 2019. Salmonella typhimurium as an anticancer therapy: recent advances and perspectives. Current Clinical Microbiology Reports 6:225-239.
39. Broadway KM, Suh S, Behkam B, Scharf BE. 2017. Optimizing the restored chemotactic behavior of anticancer agent Salmonella enterica serovar Typhimurium VNP20009. Journal of biotechnology 251:76-83.
40. Song J, Zhang Y, Zhang C, Du X, Guo Z, Kuang Y, Wang Y, Wu P, Zou K, Zou L. 2018. A microfluidic device for studying chemotaxis mechanism of bacterial cancer targeting. Scientific reports 8:1-9.
41. Liu C-W, Sung Y, Chen B-C, Lai H-Y. 2014. Effects of nitrogen fertilizers on the growth and nitrate content of lettuce (*Lactuca sativa* L.). International Journal of Environmental Research and Public Health 11:4427-4440.

Appendix A: Supplemental Material for Chapter 2

Table S2.1. Percent identity matrix of *S. meliloti* MotF compared to FliL from diverse bacterial species created in Clustal2.1.

	$MotF_{Sm}$	$FliL_{Sm}$	$FliL_{Rs}$	$FliL_{Cc}$	$FliL_{Va}$	$FliL_{Ec}$	$FliL_{St}$
*S.meliloti*_MotF	100						
*S.meliloti*_FliL	14	100					
*R.sphaeroides*_FliL	19	19	100				
*C.crescentus*_FliL	15	21	18	100			
*V.alginolyticus*_FliL	17	18	18	25	100		
*E.coli*_FliL	17	18	23	19	22	100	
*S.typhimurium*_FliL	17	19	25	19	23	77	100

Table S2.2. BACTH analysis of interactions between basal body proteins. Interacting pairs exhibited a range of red coloration and interpreted as no interaction (-, white), weak interaction (+, pale red), moderate interaction (++, red) and strong interaction (+++, intense red). ND, not determined. Data are representative of three separate experiments with at least two technical replicates each.

		pUT18C						
		MotF	MotA	MotB	FliF	FliG	FliL	Zip
pKT25	MotF	+++	+++	++	++	-	+++	-
	MotA	+++	+++	+(+)	-	-	+++	-
	MotB	++	++	ND	ND	ND	+	ND
	FliF	++	-	ND	-	-	++	-
	FliG	-	-	ND	-	+++	-	-
	FliL	+++	+++	++	++	+	+++	-
	Zip	-	-	ND	-	-	-	+++

Table S2.3. BACTH analysis of interactions between periplasmic regions (*) of MotF, MotB, and FliL and the periplasmic protein MotC. Interacting pairs exhibited a range of red coloration and interpreted as no interaction (-, white), weak interaction (+, pale red), moderate interaction (++, red) and strong interaction (+++, intense red). ND, not determined. Data are representative of three separate experiments with at least two technical replicates each.

		pUT18					**pUT18C**					
		MotF*	MotB*	MotC	FliL*	Empty	MotF*	MotB*	MotC	FliL*	ZIP	Empty
pKNT25	MotF*	-	-	-	-	-	+++	-	-	-	-	-
	MotB*	-	-	ND	-	-	-	+++	ND	-	-	-
	MotC	-	ND	ND	ND	-	-	ND	ND	ND	-	-
	FliL*	-	-	ND	-	-	-	-	ND	+	-	-
	Empty	-	-	-	-	-	-	-	-	-	-	-
pKT25	MotF*	+++	-	-	-	-	-	+	-	-	-	-
	MotB*	-	+++	ND	-	-	+	+++	ND	-	++‡	-
	MotC	-	ND	ND	ND		-	ND	ND	ND	-	-
	FliL*	-	-	ND	+	-	-	-	ND	+	-	-
	ZIP	-	-	-	-	-	-	+++‡	-	-	+++	ND
	Empty	-	-	-	-	-	-	-	-	-	ND	-

‡MotB*-Zip combinations resulted in nonspecific signal.

Table S2.4. Bacterial strains and plasmids used in this study.

Strains	Genotype	Reference
Escherichia coli		
BL21 (DE3)	F$^-$*omp*T *hsd*S$_B$ (r$_B^-$, m$_B^-$) *gal dcm* (DE3)	Novagen
DH5α	F$^-$ φ80*lac*ZΔM15 Δ(*lac*ZYA-*arg*F)U169 *rec*A1 *end*A1 *hsd*R17(r$_K^-$, m$_K^+$) *pho*A *sup*E44 λ$^-$ *thi*-1 *gyr*A96 *rel*A1	(1)
ER2566	*Ion ompT lacZ::T7*	New England Biolabs
S17-1	*recA endA thi hsdR* RP4-2 Tc::Mu::Tn7 Tp^r Sm^r	(2)
Sinorhizobium meliloti		
BS127	Δ*SMc03056*	This study
BS128	Δ*SMc03071*	This study
BS129	Δ*SMc03072*	This study
BS130	Δ*motF* (Δ*SMc03057*)	This study
BS239	Δ*motF motA*$_{Y248H}$	This study
BS240	*motA*$_{Y248H}$	This study
BS241	Δ*motF motA*$_{G136S}$	This study
BS242	*motA*$_{G136S}$	This study
BS300	Δ*motB*$_{plug}$ (amino acids 57-59)	This study
BS301	Δ*motF* Δ*motB*$_{plug}$	This study
BS302	Δ*fliL* Δ*motB*$_{plug}$	This study

BS303	Δ*fliL motA*$_{G136S}$	This study
BS304	*motB*$_{A64E}$	This study
BS305	Δ*motF motB*$_{A64E}$	This study
BS306	Δ*fliL motB*$_{A64E}$	This study
BS307	Δ*fliL motA*$_{Y248H}$	This study
BS309	*motB*$_{K60A}$	This study
BS310	Δ*motF motB*$_{K60A}$	This study
BS311	Δ*fliL motB*$_{K60A}$	This study
BS312	Δ*fliL* Δ*motF*	This study
RU11/001	Wild type, spontaneous Sm^r	(3)
RU11/011	Δ*flaA-D*, Km^r	(3)
RU11/211	Δ*motC*	(4)
RU11/218	Δ*motB*	(4)
RU11/308	Δ*cheY1*	(5)
RU11/553	Δ*motE*	(6)
RU11/802	Δ*motA*	(7)
RU11/827	Δ*fliL*	This study

Plasmid	**Description**	**Reference**
pBBR1MCS-2	Nm^r, Broad host-range expression vector	(8)
pBS54	Ap^r, PCR fragment containing *motB** cloned into pTYB11	This study
pBS56	Ap^r, 1,233 bp PCR fragment containing *motC*^{M} fragment 73-1305 (aa 25-434) cloned into pTYB11	This study

pBS62	Km^r, 685 bp EcoRI/HindIII PCR fragment containing Δ*fliL* cloned into pK18*mob sacB*	This study
pBS355	Km^r, 567 bp EcoRI/HindIII PCR fragment containing *motF* cloned into pBBR1MCS-2	This study
pBS357	Ap^r, 486 bp SapI/EcoRI PCR fragment containing *motF* bp 82-567 (MotF*, aa 28-188) cloned into pTYB11	This study
pBS638	Km^r, 492 bp HindIII/XbaI PCR fragment containing *fliL* cloned into pBBR1MCS-2	This study
pBS1193	Km^r, 117 bp PCR fragment containing *ymgF* fragment 1-117 (aa 1-39) cloned into pKTop	(9)
pBS1236	Km^r, 486 bp XbaI/SmaI PCR fragment containing *motF** fragment 85-564 bps (aa 29-188) cloned into pKNT25	This study
pBS1237	Km^r, 1257 bp XbaI/SmaI PCR fragment containing *motC** 76-1302 bps (aa 26-434) cloned into pKNT25	This study
pBS1238	Ap^r, 486 bp XbaI/SmaI PCR fragment containing *motF** fragment 85-564 bps (aa 29-188) cloned into pUT18	This study
pBS1239	Ap^r, 1257 bp XbaI/SmaI PCR fragment containing *motC** 76-1302 bps (aa 26-434) cloned into pUT18	This study
pBS1240	Km^r, 486 bp XbaI/SmaI PCR fragment containing *motF** fragment 85-564 bps (aa 29-188) cloned into	This study

	pKT25	
pBS1241	Ap^r, 486 bp XbaI/SmaI PCR fragment containing *motF** fragment 85-564 bps (aa 29-188) cloned into pUT18C	This study
pBS1242	Ap^r, 1257 bp XbaI/SmaI PCR fragment containing *motC** 76-1302 bps (aa 26-434) cloned into pUT18C	This study
pBS1243	Km^r, 1257 bp XbaI/SmaI PCR fragment containing *motC** 76-1302 bps (aa 26-434) cloned into pKT25	This study
pBS1263	Km^r, 876 bp XbaI/KpnI PCR fragment containing *motA* cloned into pKT25	This study
pBS1266	Km^r, 1,182 bp XbaI/KpnI PCR fragment containing *motB* cloned into pKT25	This study
pBS1267	Km^r, 1,671 bp XbaI/KpnI PCR fragment containing *fliF* cloned into pKT25	This study
pBS1268	Km^r, 1,038 bp XbaI/KpnI PCR fragment containing *fliG* cloned into pKT25	This study
pBS1269	Km^r, 489 bp XbaI/KpnI PCR fragment containing *fliL* cloned into pKT25	This study
pBS1270	Ap^r, 876 bp XbaI/KpnI PCR fragment containing *motA* cloned into pUT18C	This study
pBS1273	Ap^r, 1,182 bp XbaI/KpnI PCR fragment containing *motB* cloned into pUT18C	This study
pBS1274	Ap^r, 1,671 bp XbaI/KpnI PCR fragment containing	This study

	fliF cloned into pUT18C	
pBS1275	Ap^r, 1,038 bp XbaI/KpnI PCR fragment containing *fliG* cloned into pUT18C	This study
pBS1276	Ap^r, 489 bp XbaI/KpnI PCR fragment containing *fliL* cloned into pUT18C	This study
pBS1277	Km^r, 564 bp XbaI/SmaI PCR fragment containing *motF* cloned into pKT25	This study
pBS1278	Ap^r, 564 bp XbaI/SmaI PCR fragment containing *motF* cloned into pUT18C	This study
pBS1282	Km^r, 378 bp XbaI/KpnI PCR fragment containing *fliL** fragment 115-489 bps (aa 39-164) cloned into pKT25	This study
pBS1283	Km^r, 1,017 bp XbaI/KpnI PCR fragment containing *motB** fragment 169-1,182 bps (aa 57-394) cloned into pKT25	This study
pBS1284	Ap^r, 378 bp XbaI/KpnI PCR fragment containing *fliL** fragment 115-489 bps (aa 39-164) cloned into pUT18C	This study
pBS1285	Ap^r, 1,017 bp XbaI/KpnI PCR fragment containing *motB** fragment 169-1,182 bps (aa 57-394) cloned into pUT18C	This study
pBS1286	Ap^r, 378 bp SapI/SalI PCR fragment containing *fliL** fragment 115-489 bps (aa 39-164) cloned into	This study

	pTYB11	
pBS1292	Km^r, 378 bp XbaI/KpnI PCR fragment containing *fliL** fragment 115-489 bps (aa 39-164) cloned into pKNT25	This study
pBS1293	Km^r, 1,017 bp XbaI/KpnI PCR fragment containing *motB** fragment 169-1,182 bps (aa 57-394) cloned into pKNT25	This study
pBS1294	Ap^r, 378 bp XbaI/KpnI PCR fragment containing *fliL** fragment 115-489 bps (aa 39-164) cloned into pUT18	This study
pBS1295	Ap^r, 1,017 bp XbaI/KpnI PCR fragment containing *motB** fragment 169-1,182 bps (aa 57-394) cloned into pUT18	This study
pBS1296	Km^r, 402 bp XbaI/HindIII PCR fragment containing $motB_{K60A}$ cloned into pK18*mob sacB*	This study
pBS1297	Km^r, 402 bp XbaI/HindIII PCR fragment containing $motB_{A64E}$ cloned into pK18*mob sacB*	This study
pBS1298	Km^r, 363 bp XbaI/HindIII PCR fragment containing $motB_{\Delta plug}$ cloned into pK18*mob sacB*	This study
pBS1306	Ap^r, 876 bp BamHI/HindIII fragment containing *motA* cloned into MCS-I and 564 bp NdeI/EcoRV fragment containing motF cloned into MCS-II of pETDuet-1	This study
pBS1307	Ap^r, 489 bp BamHI/HindIII fragment containing *fliL* cloned into MCS-I and 564 bp NdeI/EcoRV fragment	This study

	containing motF cloned into MCS-II of pETDuet-1	
pBS1308	Ap^r, 906 bp BamHI/HindIII fragment containing *cheR* cloned into MCS-I and 564 bp NdeI/EcoRV fragment containing motF cloned into MCS-II of pETDuet-1	This study
pBS1311	Ap^r, 1,182 bp EcoRI/HindIII fragment containing *motB* cloned into MCS-I and 564 bp NdeI/EcoRV fragment containing motF cloned into MCS-II of pETDuet-1	This study
pBS1312	Ap^r, 1,671 bp BamHI/HindIII fragment containing *fliF* cloned into MCS-I and 564 bp NdeI/EcoRV fragment containing motF cloned into MCS-II of pETDuet-1	This study
pBS1313	Ap^r, 1,038 bp BamHI/HindIII fragment containing *fliG* cloned into MCS-I and 564 bp NdeI/EcoRV fragment containing motF cloned into MCS-II of pETDuet-1	This study
pBS1314	Ap^r, 1,302 bp BamHI/HindIII fragment containing *motC* cloned into MCS-I and 564 bp NdeI/EcoRV fragment containing motF cloned into MCS-II of pETDuet-1	This study
pBS1319	Km^r, 567 bp HindIII/BamHI fragment containing *motF* cloned into pKTop	This study
pBS1320	Km^r, 84 bp HindIII/BamHI fragment containing $motF_{1\text{-}28}$ cloned into pKTop	This study

pETDuet-1	Ap^r, Dual expression vector	Novagen
pK18*mob sacB*	Km^r *lacZ mob sacB*	(10)
pKNT25	Km^r, BACTH vector	(11)
pKT25	Km^r, BACTH vector	(11)
pKT25-zip	Km^r, BACTH positive control vector	(11)
pKTop	Km^r, vector expressing dual reporter $PhoA_{22-472}/LacZ_{4-60}$, p15 ori	(9)
pPHU236	Tc^r, Promoterless *lacZ* vector	(12)
pTYB11	Ap^r, Expression vector	New England Biolabs
pUT18	Ap^r, BACTH vector	(11)
pUT18C	Ap^r, BACTH vector	(11)
pUT18C-zip	Ap^r, BACTH positive control vector	(11)
pRU2274	Tc^r, 545 bp *Eco*RI/*Pst*I fragment containing the *flaA* promoter of *S. meliloti* in pPHU236	(13)

[a]Nomenclature is presented according to Bachmann (14) and Novick *et al*. (15). Ap^r, ampicillin resistance; Km^r, kanamycin resistance; Sm^r, streptomycin resistance; Tc^r, tetracycline resistance. *, periplasmic region

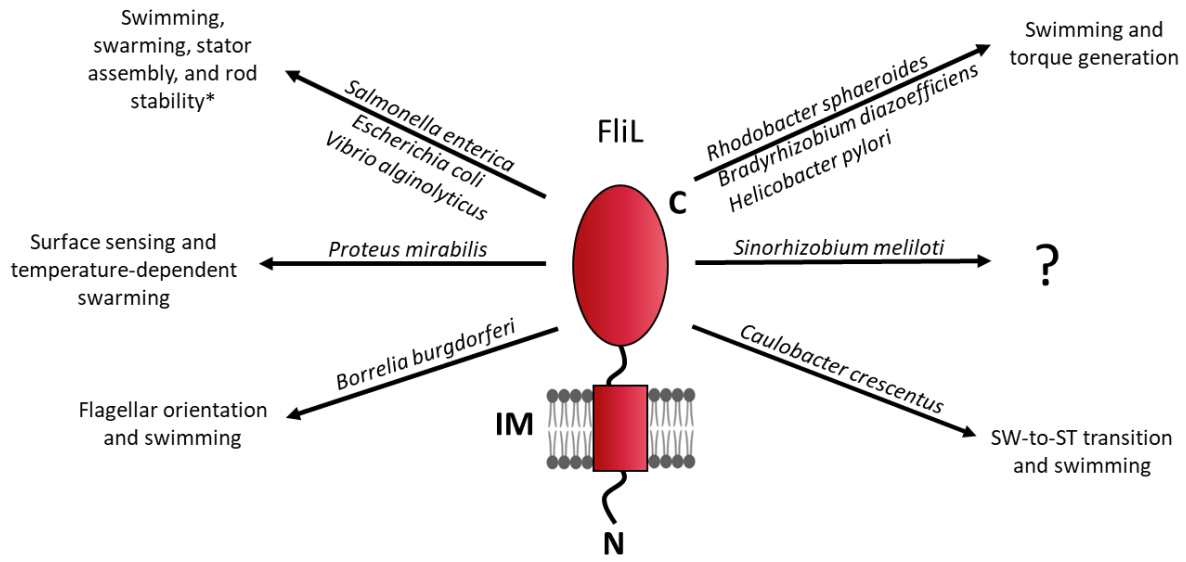

FIGURE S2.1. Functions of FliL in diverse bacterial species (16-37). *, FliL has only been implicated in rod stability for *S. enterica.*

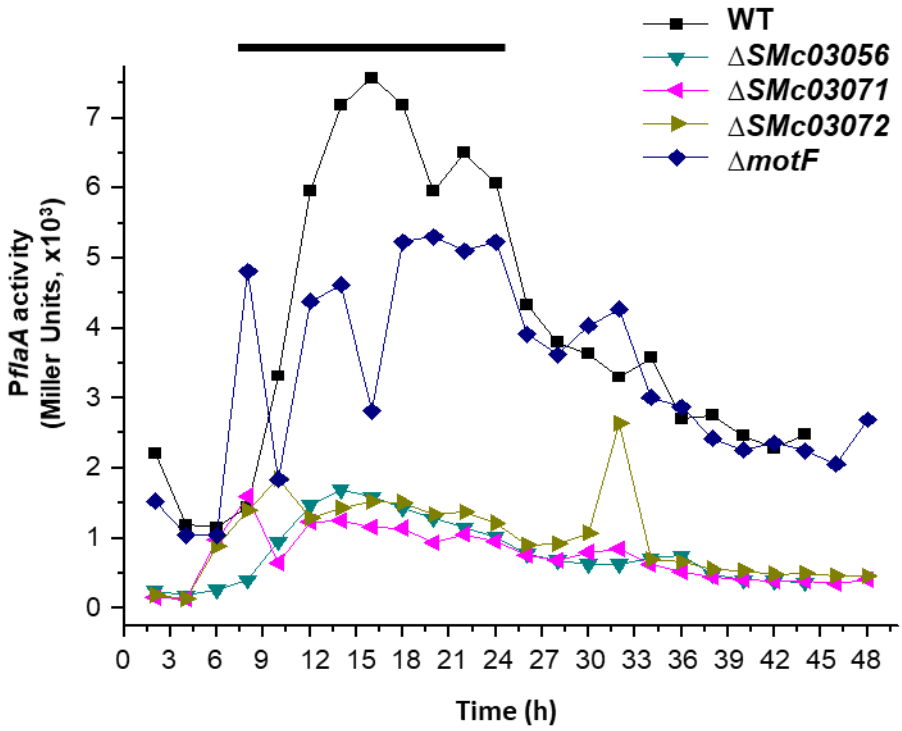

FIGURE S2.2. Effects of in-frame deletion mutations of *SMc03056*, *SMc03071*, *SMc03072*, and *SMc03057* (*motF*) on P*flaA* promoter activity compared to wild type (WT). P*flaA* promoter activity (in Miller units) was monitored by the P*flaA-lacZ* construct pRU2274 in each indicated strain. The black bar indicates the motility phase of growth.

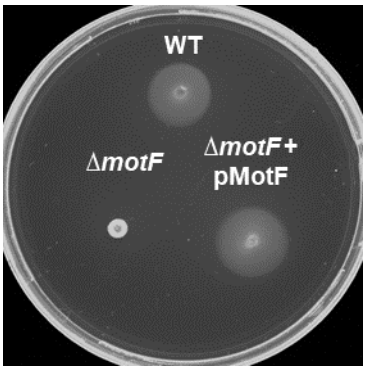

FIGURE S2.3. The swimming defect of Δ*motF* can be complemented by ectopic expression of *motF*.

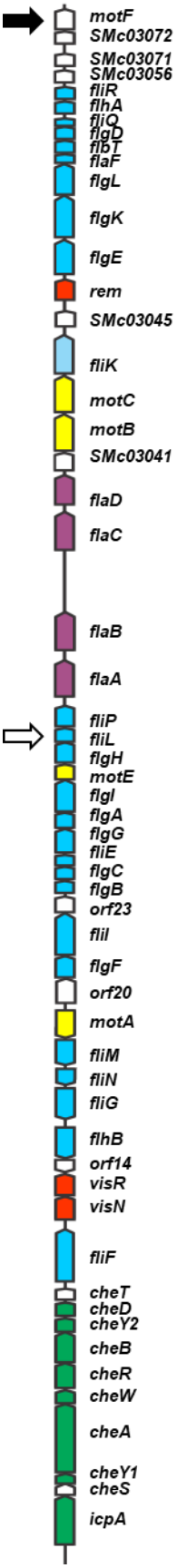
motF
SMc03072
SMc03071
SMc03056
fliR
flhA
fliQ
flgD
flbT
flaF
flgL
flgK
flgE
rem
SMc03045
fliK
motC
motB
SMc03041
flaD
flaC
flaB
flaA
fliP
fliL
flgH
motE
flgI
flgA
flgG
fliE
flgC
flgB
orf23
fliI
flgF
orf20
motA
fliM
fliN
fliG
flhB
orf14
visR
visN
fliF
cheT
cheD
cheY2
cheB
cheR
cheW
cheA
cheY1
cheS
icpA

FIGURE S2.4. The flagellar regulon in *S. meliloti*. The locations of *motF* and *fliL* are indicated with solid and empty arrows, respectively. Gene colors correspond to protein functional groups: green, chemotaxis; red, regulatory; blue, flagella structural; purple, flagellins; yellow, flagellar motor; white, unknown function prior to this study.

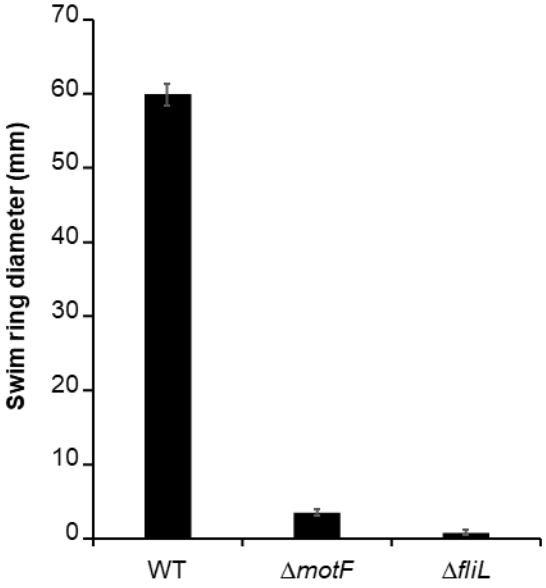

FIGURE S2.5. Quantitative swim ring analysis of Δ*motF* and Δ*fliL* mutants.

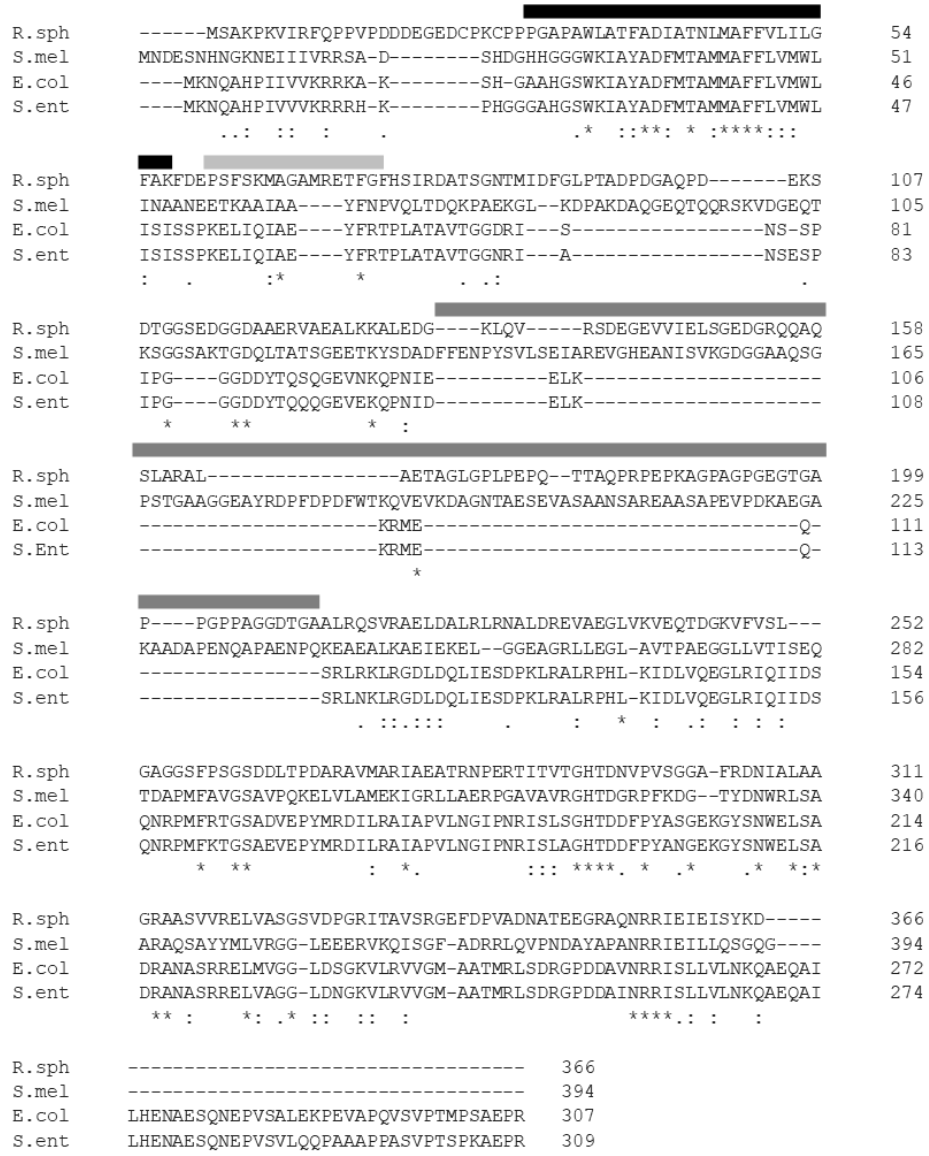

FIGURE S2.6. Clustal Omega multiple sequence alignment of MotB protein sequences. The MotB transmembrane domain is indicated by a black line and the plug region by a light grey line. The dark grey line indicates the large insertion in *S. meliloti* MotB.

Appendix B: Supplemental Material for Chapter 3

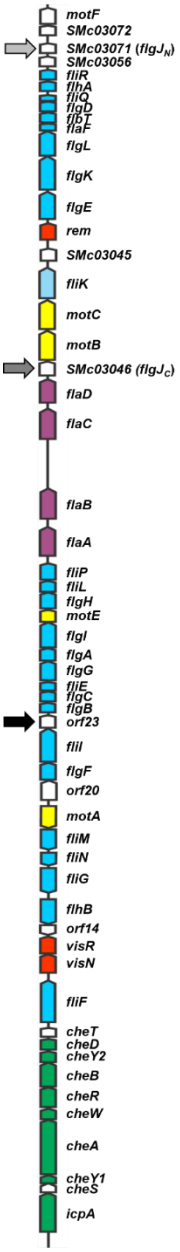

FIGURE S3.1. The *S. meliloti* flagellar regulon. The black arrow marks the location of *orf23*. Gene colors correspond to specific functional groups of the protein products: green, chemotaxis; blue, flagella structural; red, regulatory; yellow, flagellar motor; purple, flagellins; white, unknown function.

REFERENCES

1. Adler J. 1973. A method for measuring chemotaxis and use of the method to determine optimum conditions for chemotaxis by *Escherichia coli*. Microbiology 74:77-91.
2. Simon R, O'connell M, Labes M, Pühler A. 1986. Plasmid vectors for the genetic analysis and manipulation of rhizobia and other gram-negative bacteria. Methods in enzymology 118:640-659.
3. Pleier E, Schmitt R. 1991. Expression of two *Rhizobium meliloti* flagellin genes and their contribution to the complex filament structure. Journal of Bacteriology 173:2077-2085.
4. Platzer J, Sterr W, Hausmann M, Schmitt R. 1997. Three genes of a motility operon and their role in flagellar rotary speed variation in *Rhizobium meliloti*. Journal of Bacteriology 179:6391-6399.
5. Sourjik V, Schmitt R. 1996. Different roles of CheY1 and CheY2 in the chemotaxis of *Rhizobium meliloti*. Molecular Microbiology 22:427-436.
6. Eggenhofer E, Haslbeck M, Scharf B. 2004. MotE serves as a new chaperone specific for the periplasmic motility protein, MotC, in *Sinorhizobium meliloti*. Molecular Microbiology 52:701-712.
7. Sourjik V, Muschler P, Scharf B, Schmitt R. 2000. VisN and VisR are global regulators of chemotaxis, flagellar, and motility genes in *Sinorhizobium* (*Rhizobium*) *meliloti*. Journal of Bacteriology 182:782-788.
8. Kovach ME, Elzer PH, Hill DS, Robertson GT, Farris MA, Roop II RM, Peterson KM. 1995. Four new derivatives of the broad-host-range cloning vector pBBR1MCS, carrying different antibiotic-resistance cassettes. Gene 166:175-176.
9. Karimova G, Robichon C, Ladant D. 2009. Characterization of YmgF, a 72-residue inner membrane protein that associates with the *Escherichia coli* cell division machinery. Journal of Bacteriology 191:333-346.
10. Schäfer A, Tauch A, Jäger W, Kalinowski J, Thierbach G, Pühler A. 1994. Small mobilizable multi-purpose cloning vectors derived from the *Escherichia coli* plasmids pK18 and pK19: selection of defined deletions in the chromosome of *Corynebacterium glutamicum*. Gene 145:69-73.
11. Karimova G, Pidoux J, Ullmann A, Ladant D. 1998. A bacterial two-hybrid system based on a reconstituted signal transduction pathway. Proceedings of the National Academy of Sciences 95:5752-5756.
12. Hübner P, Willison J, Vignais P, Bickle T. 1991. Expression of regulatory nif genes in *Rhodobacter capsulatus*. Journal of Bacteriology 173:2993-2999.
13. Scharf B, Schuster-Wolff-Bühring H, Rachel R, Schmitt R. 2001. Mutational analysis of the *Rhizobium lupini* H13-3 and *Sinorhizobium meliloti* flagellin genes: Importance of flagellin A for flagellar filament structure and transcriptional regulation. Journal of Bacteriology 183:5334-5342.
14. Bachmann BJ. 1990. Linkage map of Escherichia coli K-8. Microbiological reviews 54:130-197.
15. Novick RP, Clowes RC, Cohen SN, Curtiss 3rd R, Datta N, Falkow S. 1976. Uniform nomenclature for bacterial plasmids: a proposal. Bacteriological reviews 40:168-189.
16. Tachiyama S, Chan KL, Liu X, Hathroubi S, Peterson B, Khan MF, Ottemann KM, Liu J, Roujeinikova A. 2022. The flagellar motor protein FliL forms a scaffold of

circumferentially positioned rings required for stator activation. Proceedings of the National Academy of Sciences 119.
17. Pecina A, Schwan M, Blagotinsek V, Rick T, Klüber P, Leonhard T, Bange G, Thormann KM. 2021. The stand-alone PilZ-domain protein MotL specifically regulates the activity of the secondary lateral flagellar system in *Shewanella putrefaciens*. Frontiers in microbiology 12:1160.
18. Mengucci F, Dardis C, Mongiardini EJ, Althabegoiti MJ, Partridge JD, Kojima S, Homma M, Quelas JI, Lodeiro AR. 2020. Characterization of FliL proteins in *Bradyrhizobium diazoefficiens*: lateral FliL supports swimming motility, and subpolar FliL modulates the lateral flagellar system. Journal of bacteriology 202.
19. Takekawa N, Isumi M, Terashima H, Zhu S, Nishino Y, Sakuma M, Kojima S, Homma M, Imada K. 2019. Structure of *Vibrio* FliL, a new stomatin-like protein that assists the bacterial flagellar motor function. mBio 10:e00292-19.
20. Lin T-S, Zhu S, Kojima S, Homma M, Lo C-J. 2018. FliL association with flagellar stator in the sodium-driven *Vibrio* motor characterized by the fluorescent microscopy. Scientific reports 8:1-12.
21. Kumar A, Isumi M, Sakuma M, Zhu S, Nishino Y, Onoue Y, Kojima S, Miyanoiri Y, Imada K, Homma M. 2017. Biochemical characterization of the flagellar stator-associated inner membrane protein FliL from *Vibrio alginolyticus*. The Journal of Biochemistry 161:331-337.
22. Chawla R, Ford KM, Lele PP. 2017. Torque, but not FliL, regulates mechanosensitive flagellar motor-function. Scientific reports 7:1-9.
23. Zhu S, Kumar A, Kojima S, Homma M. 2015. FliL associates with the stator to support torque generation of the sodium-driven polar flagellar motor of *Vibrio*. Molecular microbiology 98:101-110.
24. Partridge JD, Nieto V, Harshey RM. 2015. A new player at the flagellar motor: FliL controls both motor output and bias. MBio 6:e02367-14.
25. Lee Y-Y, Patellis J, Belas R. 2013. Activity of *Proteus mirabilis* FliL is viscosity dependent and requires extragenic DNA. Journal of bacteriology 195:823-832.
26. Fabela S, Domenzain C, De la Mora J, Osorio A, Ramirez-Cabrera V, Poggio S, Dreyfus G, Camarena L. 2013. A distant homologue of the FlgT protein interacts with MotB and FliL and is essential for flagellar rotation in *Rhodobacter sphaeroides*. Journal of Bacteriology 195:5285-5296.
27. Cusick K, Lee Y-Y, Youchak B, Belas R. 2012. Perturbation of FliL interferes with *Proteus mirabilis* swarmer cell gene expression and differentiation. Journal of bacteriology 194:437-447.
28. Motaleb MA, Pitzer JE, Sultan SZ, Liu J. 2011. A novel gene inactivation system reveals altered periplasmic flagellar orientation in a *Borrelia burgdorferi fliL* mutant. Journal of bacteriology 193:3324-3331.
29. Suaste-Olmos F, Domenzain C, Mireles-Rodríguez JC, Poggio S, Osorio A, Dreyfus G, Camarena L. 2010. The flagellar protein FliL is essential for swimming in *Rhodobacter sphaeroides*. Journal of Bacteriology 192:6230-6239.
30. Belas R, Horikawa E, Aizawa S-I, Suvanasuthi R. 2009. Genetic determinants of *Silicibacter* sp. TM1040 motility. Journal of Bacteriology 191:4502-4512.

31. Attmannspacher U, Scharf BE, Harshey RM. 2008. FliL is essential for swarming: motor rotation in absence of FliL fractures the flagellar rod in swarmer cells of *Salmonella enterica*. Molecular Microbiology 68:328-341.
32. Belas R, Suvanasuthi R. 2005. The ability of *Proteus mirabilis* to sense surfaces and regulate virulence gene expression involves FliL, a flagellar basal body protein. Journal of Bacteriology 187:6789-6803.
33. Segura A, Duque E, Hurtado A, Ramos JL. 2001. Mutations in genes involved in the flagellar export apparatus of the solvent-tolerant *Pseudomonas putida* DOT-T1E strain impair motility and lead to hypersensitivity to toluene shocks. Journal of Bacteriology 183:4127-4133.
34. Schoenhals GJ, Macnab RM. 1999. FliL is a membrane-associated component of the flagellar basal body of *Salmonella*. Microbiology 145:1769-1775.
35. Aldridge P, Jenal U. 1999. Cell cycle-dependent degradation of a flagellar motor component requires a novel-type response regulator. Molecular Microbiology 32:379-391.
36. Raha M, Sockett H, Macnab RM. 1994. Characterization of the fliL gene in the flagellar regulon of *Escherichia coli* and *Salmonella typhimurium*. Journal of Bacteriology 176:2308-2311.
37. Jenal U, White J, Shapiro L. 1994. *Caulobacter* flagellar function, but not assembly, requires FliL, a non-polarly localized membrane protein present in all cell types. Journal of molecular biology 243:227-244.